MODELING AND OPTIMIZATION OF GREEN SHIPPING SYSTEMS

YIDAN SHANGGUAN

PhD

The Hong Kong Polytechnic University

2026

The Hong Kong Polytechnic University

Department of Logistics and Maritime Studies

Modeling and Optimization of Green Shipping Systems

Yidan Shangguan

A thesis submitted in partial fulfilment of the

requirements for the degree of Doctor of Philosophy

October 2025

Certificate of Originality

I hereby declare that this thesis is my own work and that, to the best of my knowledge and belief, it reproduces no material previously published or written, nor material that has been accepted for the award of any other degree or diploma, except where due acknowledgement has been made in the text.

__________________________ (Signed)

Yidan Shangguan (Name of student)

Abstract

The maritime shipping sector plays a central role in global trade while simultaneously facing increasing pressure to reduce greenhouse gas emissions. In response, the field is seeing a rapid expansion of analytics- and optimization-driven approaches that integrate environmental considerations into operational decision making. This thesis focuses on the modeling and optimization of green shipping systems by examining carbon emission allocation mechanisms, carbon cost pass-through strategies under transshipment operations, and the operational management of dual-fuel vessels with methane slip concerns. All studies employ advanced mathematical optimization, informed by realistic network structures and regulatory contexts, to provide practical policy and managerial insights.

The first study addresses the inequality and inefficiency inherent in current carbon emission surcharge practices, which often apply uniform charges across diverse origin–destination (od) pairs and rely on self-reported emissions data. To improve the fairness and oversight of carbon emission allocation, we develop a bi-level programming model that captures the strategic interactions between governmental regulatory objectives and liner shipping companies' operational decisions. Three new carbon allocation metrics are introduced, integrating actual sailing distances, shortest sailing distances, and a convex combination termed harmonic distance. The findings demonstrate that shortest-distance-based allocation provides an equitable and socially optimal cost distribution, balancing government, industry, and consumer interests.

The second study extends the analysis to industry-driven carbon surcharge practices in networks with and without transshipment. A multi-route augmented network is constructed, and two od-link-based optimization models are proposed to examine how carbon allocation policies influence liner shipping companies' profit-maximizing decisions. Numerical experiments show that while carbon allocation has limited impact in networks without transshipment, it plays a critical role when transshipment is present. The results highlight the importance of selecting appropriate carbon allocation measures to avoid unintended cost distortions and profit losses under environmental regulation.

The third study investigates operational strategies for dual-fuel ships powered by liquefied natural gas (LNG), focusing on methane slip—unburned methane emissions that increase at lower sailing speeds and pose substantial climate risks. A nonlinear mixed-integer programming model is developed to jointly optimize fleet composition, sailing speed, and fuel usage decisions under carbon and methane taxation schemes. To ensure tractability, sailing times are discretized as proxies for speed, supported by theoretical validity and computational efficiency. The results indicate that explicitly accounting for methane slip can guide companies toward operational adjustments that mitigate both environmental impact and financial risk.

Collectively, this thesis demonstrates how integrating environmental considerations with optimization-based decision analytics can advance the development of green shipping systems. The methodologies and insights presented here support

the implementation of more equitable carbon policies, profitability-conscious fuel and fleet strategies, and climate-aligned maritime operations, providing practical guidance for regulators and shipping companies navigating the transition toward sustainable maritime logistics.

Keywords: carbon emission allocation; liner shipping; bi-level programming model; shortest sailing distance; od-link-based model; transshipment; dual-fuel ship; methane slip; nonlinear mixed-integer programming; time discretization.

Publications and Working Papers

Arising from the Thesis

- Tian, X., Shangguan, Y.*, Pang, K. W., Guo, Y., Lyu, M., Wang, S., Huang, G. Q., 2024. Carbon emission allocation policy making in liner shipping: A novel approach toward equitable and efficient maritime sustainability. Ocean & Coastal Management, 256, 107270.

- Shangguan, Y., Tian, X., Jin, Y., Wang, S, 2025. Optimizing carbon emission allocation for liner shipping companies. Computers & Industrial Engineering, 111348.

- Shangguan, Y., Tian, X., Pang, K. W., Wang, S., 2025. Optimizing dual-fuel ship operations considering methane slip. Transportation Research Part B: Methodological, 198, 103247.

Others

- Shangguan, Y., Tian, X., Pang, K. W., Ruan, Q., Jin, Y., Wang, S., 2024. Navigating the green shipping: Stochastic hydrogen hub deployment in inland waterways.Transportation Research Part D: Transport and Environment, 129, 104126.

- Shangguan, Y., Tian, X., Jin, S., Gao, K., Hu, X., Yi, W., Guo, Y., Wang, S., 2023. On the fundamental diagram for freeway traffic: Exploring the lower bound of the fitting error and correcting the generalized linear regression models. Mathematics, 11(16), 3460.

- Liu, Y., Shangguan, Y., Gao K., Jin S., Yi W., Wang, S. Integrated Network Design for E-scooters and Public Transit Systems. ASCE Journal of Transportation Engineering, forthcoming.

- Tian, X., Shangguan, Y.*, Wang, S. Multi-fuel operations for green container shipping. Submitted.

- Shangguan, Y., Song D., Wang, S. Carbon leakage under regional maritime decarbonization regulations: A cost-minimization perspective on firm behavior. Submitted.

- Shangguan, Y., Wu Y., Wang, S. Optimizing door-to-door service design in shipping: a multi-commodity flow formulation with a tailored benders decomposition approach. Submitted.

- Xu W., Guo W., Gao K., Yang C., Shangguan Y., Yin Y., Yan W., Jin S. Echelon utilization of retired electric bus batteries: economic and environmental potential. Submitted.

Acknowledgments

As I began to organize and write this thesis, I found myself not only reviewing my past research, but also reflecting on the journey I have undertaken since the beginning of my doctoral study. Looking forward, I may still consider myself a beginner; yet, looking back, I realize that I have already walked a meaningful and unforgettable path.

First and foremost, I would like to express my deepest gratitude to my supervisor, Prof. Shuaian (Hans) Wang. I am sincerely thankful for the opportunity he offered me to pursue a PhD, especially at a time when I was uncertain about my direction. This opportunity has enabled me to experience a life I could not have envisioned before. Prof. Wang has been a true mentor and guide in my academic growth. His ability to explain complex concepts through clear and vivid examples has helped me understand many ideas that initially seemed difficult and abstract. From the fundamental question of why we build mathematical models, to the precise use of notation, to the creative formulation of models and rigorous derivation of theoretical properties, his guidance has profoundly shaped my research mindset. Whenever I encountered difficulties, he responded with patience and unwavering support. Such support not only assisted me academically, but also reassured me that although research may be challenging, I have never been alone. It has been a source of strength that encouraged me to persist through every setback.

I am also deeply grateful to Prof. Dongping Song, whom I had the pleasure of working with during my exchange at the University of Liverpool. His deep understanding of the practical operations of the shipping industry guided me to approach research questions from real-world perspectives. Under his mentorship, research felt like solving an engaging and meaningful puzzle. Each discovery of a new pattern or property brought a sense of joy and motivation that reminded me why research matters. His care and kindness in daily life also made me feel at home even when I was far away from my own. I believe he will always remain both a mentor and a friend to me.

I would also like to thank the senior colleagues and mentors who supported and guided me throughout my PhD journey, especially Dr. Xuecheng (Simon) Tian. His rigorous academic attitude and persistent work ethic have constantly encouraged me to move forward. I am equally grateful to my friends. As one of them once said, we are not only friends, but also companions in battle. Their companionship and encouragement have made this journey far less lonely and far more meaningful.

Finally, I would like to express my heartfelt appreciation to my family. Thank you to my parents and grandparents for their unconditional love and support. And thank you to my cat, Liuyi, for the quiet companionship. Thank you all for walking with me through this journey—may we continue to move forward together, with love.

And lastly, I would like to thank myself—for not giving up, and for continuing to try. To the future me: Be brave, be strong, and be happy.

Contents

Certificate of Originality i

Abstract iv

Publications and Working Papers vi

Acknowledgements viii

1 Introduction 1

1.1 Background 1

1.2 Thesis Outline 3

2 Carbon Allocation Policy Making in Liner Shipping 6

2.1 Introduction 6

2.2 Literature Review 12

2.3 Problem Description 14

2.3.1 Interests of the three stakeholders 14

2.3.2 Carbon allocation methods per TEU per od pair 16

2.3.3 Assumptions 22

2.4 Mathematical Model 23

2.5 Solution Approach 28
2.5.1 Model conversion 28
2.5.2 Algorithm 32
2.6 Case Study 33
2.6.1 Parameter settings 33
2.6.2 Results 37
2.6.3 Robustness tests 38
2.7 Conclusions 47

3 Optimizing Carbon Allocation for Liner Shipping Companies 49

3.1 Introduction 49
3.2 Literature Review 53
3.3 Problem Description 55
3.3.1 Shipping network 55
3.3.2 Carbon emission allocation method 60
3.3.3 Illustrative Example 62
3.4 Model Formulation 65
3.4.1 Carbon allocation model without transshipment 65
3.4.2 Carbon allocation model with transshipment 68
3.5 Solution Approach 71
3.5.1 Discretization of the volume of accepted cargoes 72
3.5.2 Big-M reformulation 73
3.5.3 Sub-model for the carbon emission allocation model without considering transshipment 74

3.5.4 Sub-model for the carbon emission allocation model considering transshipment . . . 75

3.5.5 Algorithm . . . 76

3.6 Case Study . . . 77

3.6.1 Parameter settings . . . 77

3.6.2 Results . . . 79

3.7 Robustness Tests . . . 82

3.7.1 Parameter settings for the synthetic shipping network . . . 83

3.7.2 The impact of demand variations . . . 84

3.7.3 The impact of customers' maximum acceptable carbon emission allocation . . . 85

3.8 Conclusions . . . 87

4 Optimizing Dual-Fuel Ship Operations with Methane Slip 88

4.1 Introduction . . . 88

4.2 Literature Review . . . 94

4.3 Problem Formulation . . . 96

4.4 Solution Method . . . 102

4.4.1 A preliminary model transformation . . . 102

4.4.2 An advanced model reformulation based on the duel-fuel usage strategy . . . 105

4.4.3 Time discretization . . . 114

4.4.4 Theoretical analysis for Model M4 . . . 117

4.5 Computational Experiments . . . 118

4.5.1 Experimental settings . . . 119

4.5.2 Results 121
4.5.3 Sensitivity analyses 122
4.5.4 The effect of methane slip 125
4.5.5 The Performance of the Proposed Solution Method 129
4.5.6 The effectiveness of the dual-fuel usage strategy 131
4.6 Conclusions 132

5 Conclusions and Future Research Directions 135

5.1 Conclusions 135
5.2 Future Research Directions 137

References 155

List of Figures

2.1 Illustration of Example 2.3. 20
2.2 Relationship between demand and carbon allocation. 23
2.3 Objective function values for different maximum carbon emissions. 40
2.4 Objective function values for different J. 41

3.1 Original shipping routes. 56
3.2 New shipping routes based on splitting nodes. 57
3.3 The augmented shipping network with source and sink nodes. . . 58
3.4 An example of the shortest sailing distance and the traveling distance. 61
3.5 Optimal objective function values under different h. 65
3.6 Additional arcs for transshipment. 69
3.7 Visualization of COSCO shipping lines. 79
3.8 Synthetic shipping network. 83
3.9 The impact of demand variation on the objective function value when $x_{od}^{\max} = 100$, where the red boxes indicate the optimal h for each line. 84

3.10 The impact of $x_{od}^{\max}$ on the objective function value when $a = b = c = 10,000$, where the red boxes indicate the optimal h for each line. 86

4.1 The relationship between total costs and the time sailing 1 nm for VLSFO and LNG two types of fuel. 108

4.2 Tangent segment for costs of two types of fuel. 109

4.3 Four possible relationships between t_{min}, t_{max}, t_1, and t_2. 110

4.4 COSCO shipping lines. 120

4.5 Total objective function values and solution times under different discretization precisions. 122

4.6 The costs of the two types of fuel ignoring the methane slip problem. 127

4.7 The intersection speed and the range between t_1 and t_2 under different values of β. 132

4.8 The costs of two types of fuel when $\beta = 1.28$. 132

List of Tables

2.1 Notations 24

2.2 Shortest sailing distances between physical ports (nautical miles). 35

2.3 Demand (q_{od}) between physical ports (TEU). 35

2.4 Transportation price (USD/TEU). 36

2.5 Penalty costs (USD/TEU). 36

2.6 Speed v_i^{hr} and fuel consumption $\delta_{hri}^{\text{cons}}$ for each leg. 37

2.7 The cargoes y_{od}^{hr} transported per od pair. 38

2.8 The carbon emissions distributed per od pair x_{od}^{hr}. 38

2.9 Outcomes for different maximum carbon emissions $x_{od}^{\max}$. 40

2.10 Outcomes for different J. 42

2.11 Demands proportional to the shortest sailing distance (nautical miles). 43

2.12 Speed v_i^{hr} and fuel consumption $\delta_{hri}^{\text{cons}}$ for each leg. 44

2.13 The cargoes y_{od}^{hr} transported per od pair. 44

2.14 The carbon emissions distributed per od pair x_{od}^{hr}. 44

2.15 Demands inversely proportional to the shortest sailing distance. . . 45

2.16 Speed v_i^{hr} and fuel consumption $\delta_{hri}^{\text{cons}}$ for each leg. 45

2.17 The cargoes y_{od}^{hr} transported per od pair. 46

2.18 The carbon emissions distributed per od pair x_{od}^{hr}. 46

3.1 Information of three COSCO Shipping lines. 79

3.2 Physical ports corresponding to nodes in the augmented shipping network. 80

3.3 Comparison of solutions for models in Section 3.4.1 and Section 3.4.2 81

3.4 Objective function values for sub-models under different h 82

3.5 Demands q_{od} in synthetic network (TEUs) 84

4.1 Ports of call of each shipping line. 120

4.2 Total lengths of four types of segments for each route (nm). 120

4.3 Number of ships and sailing times (speeds) for four types of segments across all routes. 121

4.4 Total objective function values and sailing speeds for type-2 and type-4 segments under different numbers of ships. 124

4.5 Total objective function values and corresponding detailed information under different numbers of ships. 126

4.6 Impact of carbon emission fee on total objective function value and sailing speeds. 127

4.7 Impact of β on the optimal objective for the methane slip issue. . . 128

4.8 Relative gaps between the objective function values of models M4 and E.1 under various values methane slip coefficient. 128

4.9 Relative gaps between the objective function values of models M4 and E.1 under various values of the methane slip coefficient after exchanging the distances between type-1 and type-2 segments with those of type-3 and type-4. 129

4.10 Comparison of the results of different solution methods. 130

Chapter 1

Introduction

1.1 Background

Maritime shipping plays a vital role in global trade, transporting approximately 90% of the world's cargo volume and widely recognized as the most energy-efficient mode of large-scale freight transportation (Zhen et al., 2019, 2024). Despite its efficiency advantages, the shipping industry remains a major source of environmental pollution. It is responsible for 15% of global nitrogen oxide (NO_X) emissions, 13% of sulfur dioxide (SO_X) emissions, and about 2.7% of carbon dioxide (CO_2) emissions from human activities (Wang et al., 2022). As global climate and air quality concerns intensify, the decarbonization of maritime transportation has become increasingly urgent.

To mitigate these environmental impacts, multiple regulatory measures have been introduced by international and regional authorities. Since January 1, 2015, the International Maritime Organization (IMO) and regional regulators have established four Emission Control Areas (ECAs)—the Baltic Sea, North Sea, North

America, and U.S. Caribbean—where ships must use fuels with sulfur content no higher than 0.1% or adopt equivalent emission-reducing technologies (Wang et al., 2021). The Mediterranean Sea will become the fifth ECA in May 2025, enforcing the same sulfur limit (IMO, 2022). Beyond ECAs, the IMO has also lowered the global sulfur cap from 3.50% to 0.50% for ships operating in non-ECA regions, leading to the widespread use of very low-sulfur fuel oil (VLSFO), which typically contains 0.45%–0.50% sulfur (Tan et al., 2022).

In addition to sulfur regulations, the European Union (EU) has implemented the Maritime Emissions Trading System (METS) effective January 1, 2024, which requires vessels of 5,000 gross tonnage and above calling at EU ports to pay for greenhouse gas emissions (European Commission, 2022). Under this system, 50% of emissions are charged for voyages between EU and non-EU ports, and 100% for voyages between EU ports. Moreover, the EU has introduced a renewable fuel mandate requiring that at least 2% of marine fuel consumption must come from renewable sources (Wang et al., 2023a).

These increasingly strict green policies significantly influence the operational strategies of shipping companies, affecting decisions related to fleet deployment, sailing speed, fuel type selection, and logistics network design.

Against this regulatory backdrop, this thesis examines the optimization challenges arising under environmental policies from both governmental and industry perspectives. From the government's standpoint, the objective is to design carbon and emissions management policies that effectively monitor and reduce total emissions. From the shipping companies' standpoint, the challenge lies in maximizing operational profitability while complying with these environmental regulations. Although both perspectives concern the same set of policies, their goals and constraints differ, leading to different interpretations and strategic responses.

Therefore, this thesis aims to provide analytical and optimization-based insights that can (i) support governments in designing more equitable and effective green regulatory mechanisms, and (ii) guide shipping companies in developing profit-maximizing operational strategies under environmental constraints. Through these dual perspectives, we seek to contribute to the advancement of sustainable and economically viable maritime logistics.

1.2 Thesis Outline

This thesis comprises three studies that collectively examine the modeling and optimization of green shipping systems from both governmental and industry perspectives. The studies are organized as follows:

- **Study 1: Carbon Allocation Policy Making in Liner Shipping**[1]

  Chapter 2 examines carbon emission allocation policies from the perspective of government. Current industry practices often impose uniform carbon emission surcharges across heterogeneous origin−destination (od) pairs and rely heavily on self-reported emission data, resulting in fairness and efficiency concerns. To address these issues, this chapter develops a bi-level programming model that captures the strategic interactions between governmental regulatory objectives and liner shipping companies' operational decisions. Three carbon allocation metrics are proposed—based on actual sailing distance, shortest sailing distance, and a convex combination termed harmonic distance. The results demonstrate

[1]Tian, X., Shangguan, Y.*, Pang, K. W., Guo, Y., Lyu, M., Wang, S., Huang, G. Q., 2024. Carbon emission allocation policy making in liner shipping: A novel approach toward equitable and efficient maritime sustainability. Ocean & Coastal Management, 256, 107270.

that the allocation based on shortest sailing distance provides a socially optimal and equitable cost distribution, balancing the interests of governments, shipping companies, and consumers.

- **Study 2: Optimizing Carbon Allocation for Liner Shipping Companies**[2]

  Chapter 3 shifts to the industry perspective and analyzes carbon surcharge practices under network structures with and without transshipment. A multi-route augmented shipping network is constructed, and two od-link-based optimization models are developed to assess how different carbon allocation policies influence profit-maximizing decisions by liner shipping companies. Numerical experiments reveal that while carbon allocation policies have limited impact in networks without transshipment, they play a critical role when transshipment is present. These findings underscore the importance of selecting appropriate allocation schemes to prevent cost distortions and profit reductions under environmental regulation.

- **Study 3: Optimizing Dual-Fuel Ship Operations with Methane Slip**[3]

  Chapter 4 investigates operational decision-making for dual-fuel container ships powered by liquefied natural gas (LNG), with a particular focus on methane slip —unburned methane emissions that increase at low sailing speeds and pose significant climate challenges. This chapter formulates a nonlinear mixed-integer programming model to jointly optimize fleet composition, sailing speed, and fuel usage under combined carbon and methane taxation mechanisms. To ensure computational tractability, sailing time is discretized as a proxy for speed,

[2]Shangguan, Y., Tian, X., Jin, Y., Wang, S, 2025. Optimizing carbon emission allocation for liner shipping companies. Computers & Industrial Engineering, 111348.

[3]Shangguan, Y., Tian, X., Pang, K. W., Wang, S., 2025. Optimizing dual-fuel ship operations considering methane slip. Transportation Research Part B: Methodological, 198, 103247.

supported by theoretical justification and numerical performance. The results show that explicitly accounting for methane slip can guide shipping companies toward operating strategies that reduce environmental impacts while mitigating potential financial risks.

At last, Chapter 5 concludes the thesis and discusses several future research directions.

Chapter 2

Carbon Allocation Policy Making in Liner Shipping

2.1 Introduction

Maritime shipping, which is responsible for carrying 90% of global trade, is recognized as the most energy-efficient mode of cargo transportation(Tan et al., 2021; Li et al., 2022; Useche, 2023; Zhou et al., 2024). Despite its pivotal role in global trade, maritime transport predominantly depends on burning fossil fuels, contributing to nearly 3% of global annual carbon dioxide emissions (IMO, 2020). This emission level surpasses that of Japan, which ranks as the fifth highest carbon-emitting country (Tay and Konovessis, 2023). The IMO aimed to reduce the carbon intensity of international shipping by at least 40% by 2023, and it intends to reduce total annual greenhouse gas emissions by a minimum of 50% by 2050 from a 2008 baseline (IMO, 2020; Romano and Yang, 2021; Gössling et al., 2021; Wang and Guo, 2024).

The cap-and-trade (C&T) system requires regulated entities (such as shipping companies) to maintain their carbon emission levels within specified CEAs, with regulators (e.g., the government) establishing the CEAs to cap total emissions (Stavins, 1995; Mao et al., 2024). In the C&T system, companies are charged based on their CEAs. Regulated entities, such as shipping companies, that emit less than their allocated allowances have the option to sell their surplus, whereas those exceeding their allowances must procure additional ones (Hong et al., 2017). Therefore, the C&T system promotes cost-effective and operationally feasible emission reductions (Armstrong, 2013; Garcia et al., 2021; Wu et al., 2022b). Concurrently, shipping companies have begun to factor these carbon emission costs into their overall transportation expenses, thereby influencing consumer demand for shipping services (Liao et al., 2015; Xue et al., 2024).

In this system, the setting of CEAs is crucial. Based on the objectives of carbon reduction, the regulator establishes the value of CEAs. Once these allowances are set, shipping companies operate their fleets and conduct other operational activities accordingly. However, shipping companies typically do not bear the costs of potential carbon emissions fees themselves; instead, they calculate the carbon emissions for each route, and then add an additional surcharge to the transportation cost. The carbon allocation method is central to this process, as it not only enables the government to monitor the carbon footprint but also serves as the basis for shipping companies to apply additional carbon emission fees. To manage carbon emissions effectively and impose a reasonable carbon emission fee, an efficient and equitable allocation method is essential. Here, "efficient" refers to that with the allocation method implemented, the government can effectively monitor the carbon footprints and reduce social costs. "Equitable" indicates that the method can allocate carbon emission based on od pairs, rather than disregarding the differences between od pairs and applying a uniform price for a certain shipping route.

Some leading liner shipping companies, such as MSC and Maersk, plan to implement carbon emission surcharges in 2024, with the charges determined by trade region and cargo types (Maersk, 2023a). They allocate carbon emissions for each twenty-foot equivalent unit (TEU) container by treating the carbon allocation per TEU across a broad trade region uniformly, without accounting for the disparities between different loading and unloading ports. Therefore, the surcharges are uniform regardless of the different distances between different od pairs, a system that lacks efficiency and equity. Taking Maersk as an example, transporting containers on a trade route such as the “Far East to North Europe” route incurs a fixed surcharge of 27 euros per TEU, even though this trade covers multiple port pairs with different distances (Maersk, 2023a). This standard fee fails to capture the true differences in carbon allocation associated with different loading and unloading ports, potentially leading to potentially inequitable cost allocations and swaying customer preferences towards higher-emission transport methods such as rail, thereby reducing demand for shipping. From a regulatory standpoint, this uniform approach complicates the government’s ability to accurately monitor the carbon footprint of shipping activities. Without precise data on emissions based on actual distances traveled, it becomes challenging for governments to set appropriate CEAs and effectively control overall emissions.

Considering the inequality of carbon emission surcharges levied by shipping companies, this study is motivated to consider how overall carbon emissions should be allocated to all transported containers per TEU per od pair using an equitable approach. Furthermore, the current C&T system relies on self-reported data from shipping companies to make carbon allocation decisions, which involves the risks of potential under-reporting by shipping companies and inaccuracies in the carbon allocation results. Therefore, this study investigates how to proactively allocate carbon emissions per TEU per od pair from the perspective of the government with the aim of minimizing social costs, which include the operating costs of ships, carbon emission costs, and the penalty costs of unshipped cargoes due to the introduction of carbon emission surcharges levied by shipping companies. Through this more detailed allocation method, the government can effectively monitor emissions for each od pair, facilitate stricter control of emissions, and set feasible CEAs. By adopting this method, customers are charged emission fees based on the shortest sailing distances between od pairs, ensuring an equitable system. This approach is likely to reduce the inclination for customers to opt for other, more carbon-intensive modes of transportation due to high costs. Ultimately, this more granular method of carbon allocation helps in achieving a more equitable distribution of carbon costs and controlling the overall emissions by aligning economic incentives with environmental goals.

From this more detailed method, the government can monitor the emission for each od pair, easily control the emission, and set the feasible CEAs. The customer just need afford the od related emission fee, much more equitiable, thus, can reduce the amount of cargos forced to use other, more carbon-emission modes of transportation due to high cost.

Carbon emissions are intrinsically linked to fuel consumption (Shangguan et al., 2024), which is significantly influenced by the traveling distance of cargoes. Consequently, the allocation of carbon emissions per TEU per od pair is always presumed to be correlated with its traveling distance. Furthermore, using the traveling distance to measure the carbon emissions per TEU per od pair aligns with the industrial practice (Wagenborg, 2023). However, our analysis identifies a potential flaw in relying solely on the actual traveling distance for carbon allocation. Interestingly, this approach inadvertently favors circuitous routes for some od pairs, thereby introducing potential inequities. To rectify this issue and establish a fairer allocation system, we consider the shortest sailing distance per od pair as a basis for carbon allocation per TEU. As the shortest sailing distance may not accurately reflect the sailing realities of shipping routes, we propose a "harmonic distance" metric to take into account both equity and operational characteristics. This innovative metric is a combination of both the actual traveling distance and the shortest sailing distance, with these two distances serving as special cases of the harmonic distance.

To ascertain the most effective carbon allocation method that aligns with the interests of both government and shipping companies, we establish a bi-level programming model. Compared to other modeling approaches, our bi-level programming approach is capable of reflecting the interactions of multiple parties influenced by the carbon emission allocation policy and facilitates the derivation of outcomes that are beneficial for both governments and shipping companies, making it more applicable to real-world policy implementation. In the upper-level model, we optimize the carbon allocation policy making from the perspective of the government with the aim of minimizing the total social costs associated with shipping activities. In the lower-level model, we consider the optimal responsive operational decisions of shipping companies under a given policy. Through this sophisticated modeling approach, we can identify a socially optimal carbon allocation method that considers the diverse needs and constraints of all stakeholders involved in the liner shipping industry.

Our *contributions* can be summarized as follows. First, we introduce four carbon allocation methods per TEU per od pair. These methods are designed to accurately allocate carbon emissions for each TEU across different od pairs, enhancing the accuracy and equality of carbon footprint tracking. Second, we develop a bi-level programming model to identify the optimal carbon allocation policy, which integrates the perspectives of the government, shipping companies, and customers. The primary objective of this model is to minimize the total social costs given a set of carbon allocation methods. The total social costs include the environmental costs and operational expenses of shipping companies. Our model facilitates a balanced approach to carbon management, aiming to achieve both environmental sustainability and economic efficiency. Third, through comprehensive experiments, we demonstrate the effectiveness of using the shortest sailing distance for carbon allocation. This method proves to be straightforward, route-independent, and equitable, balancing the interests of the government and shipping companies by providing a fair basis for emissions allocation. Notably, this approach diverges from current industrial practices, which often rely on actual distances traveled for emission calculations (Wagenborg, 2023). Therefore, our findings offer valuable insights and practical recommendations for refining carbon emission allocation methods in the liner shipping industry.

The remainder of this chapter is organized as follows. Section 2.2 reviews the related research. Section 2.3 describes the research problem. Section 2.4 presents the mathematical model with nonlinearity and Section 2.5 demonstrates how to linearize the original model and introduces the solution algorithm. Section 2.6 presents our case study and robustness tests. Section 2.7 concludes the study.

2.2 Literature Review

Our work is related to the literature on emission trading systems, which have received considerable attention from researchers. Lee et al. (2013) assessed the quantitative impacts of a maritime carbon tax on the global economy. Huang et al. (2013) introduced a marine emission trading scheme, examining its effects on the annual profits and emissions of container ships through speed reduction strategies. Cullinane and Cullinane (2013) provided an overview of the existing policy framework for shipping carbon emissions, stating that a synergistic approach combining policy measures and technological innovations could more effectively facilitate reductions in ship emissions than current policies. Guo et al. (2020) explored the dynamics between increased abatement investments and emissions reduction through a decision-making model. Furthermore, Zhu et al. (2023) analyzed strategies for and outcomes of CEAs within a C&T framework among shipping firms. Liu et al. (2023) investigate the effects of carbon tax policies on carbon emission reduction technologies, taking into account both port and liner companies. Furthermore, the EU Emissions Trading System uses the pass-through costs of CEAs as a mechanism to regulate carbon emissions (Carratù et al., 2020). In this system, the method of allocating CEAs allocation directly influences both the costs of carbon emissions and the overall effectiveness of the C&T system. Collectively, these studies have highlighted the diverse impacts of an emission trading system, ranging from economic implications to emissions mitigation and the efficacy of CEAs. In addition to their economic impacts, emission trading systems remain a viable tool for carbon emission control.

With the introduction of carbon emission control strategies, many studies have focused on the responsive operations of shipping companies. Kim et al. (2014) investigated the optimization of ship speeds on predetermined routes, considering the need to reduce carbon emissions and fuel consumption. Wang and Chen (2017) analyzed the impact of CEAs on strategies for ship refueling, speed, and deployment. Zhu et al. (2018) addressed fleet planning challenges under the uncertainty of CEA with a multi-stage stochastic integer programming model, whereas Wan et al. (2018) emphasized the importance of differentiating the allocation of CEAs based on ship types and sizes due to their distinct emission profiles. Cheaitou and Cariou (2019) proposed a multi-objective model to determine the optimal sailing speed that balances environmental impacts with profitability, and Xin et al. (2019) designed an integer programming model for the eco-friendly scheduling of shuttle tanker fleets to minimize operational costs. Recently, Zhu et al. (2023) examined the strategies and performance of CEA allocation within the C&T system among shipping companies. However, all of the abovementioned studies have focused on the responsive operations of shipping companies under the assigned CEAs. To the best of our knowledge, only one study has proposed further methods for allocating assigned CEAs to each shipping service from the perspective of shipping companies. Specifically, Sun et al. (2022) used a mixed-integer linear programming model to facilitate CEA allocation for liner shipping companies under an emission permit set by the government and reallocated the permit system to every shipping route accurately. However, this study was conducted from the perspective of shipping companies and thus did not account for the dynamic interactions between regulatory decisions and the responses of shipping companies throughout the CEA allocation process. Therefore, the study ignored the overall societal benefits of carbon allocation per shipping route. Furthermore, Sun et al. (2022) did not provide a comprehensive and persuasive method of carbon allocation that accounted for the carbon footprint per TEU per od pair. The absence of a reliable and precise method of carbon allocation allows shipping companies to independently estimate carbon emissions and pass on carbon costs to customers based on self-defined rules to preserve their profitability. Moreover, this gap presents challenges for government in monitoring carbon emissions, complicating the development of future steps for effective carbon control.

2.3 Problem Description

In this section, we first outline the interests of the three key stakeholders involved in the carbon allocation process (Section 2.3.1), namely the government, shipping companies, and customers. Then, for each od pair (Section 2.3.2), we propose several methods for calculating carbon emissions per TEU. Finally, Section 2.3.3 presents the main assumptions underlying our model.

2.3.1 Interests of the three stakeholders

In the process of carbon allocation, we consider the interests of three primary stakeholders: the regulator (e.g., the government), the regulated entities (e.g., shipping companies), and consumers. The government's role is to formulate a carbon allocation policy aimed at minimizing social costs or maximizing social benefits. The policy must consider the social impact of its implementation, including the costs associated with carbon emissions, the operational expenses of the shipping companies, and the influence of the policy on customer demand. Conversely, shipping companies focus on maximizing profits under a given governmental CEA policy, using strategies such as designing optimal shipping routes and fleet deployment. Customers, as the end users, have transportation demands that are closely linked to the costs of transportation services. Increases in transportation costs can lead to significant reductions in demand (Clark et al., 2004).

We assume that the overall transportation costs are increased when the government imposes carbon emission fees based on carbon allocation results per TEU per od pair. Subsequently, shipping companies pass on these costs onto customers through carbon emission surcharges. Hence, the policy-making of the government and the strategic responses of the shipping companies influence the transportation costs, which, in turn, affect customer demand. This interconnected relationship underscores the complexity of developing and implementing effective carbon allocation strategies in the liner shipping industry in a socially optimal manner.

The optimization objectives for the three key stakeholders are summarized as follows. The government's objective is to minimize the total social costs. Such costs have several components: the costs associated with carbon emissions, the operating costs incurred by the shipping companies, and the costs of cargo rejection by customers due to carbon emission surcharges. Notably, shipping can be rejected as a means of transporting cargo because customers consider the costs excessive following the introduction of carbon emission surcharges. When cargoes are not transported by shipping, the demand does not vanish but shifts to other transportation modes, such as rail, which may seem less expensive but are more costly from an environmental and social perspective, thus increasing the overall costs to society. For a shipping company, the optimization objective subject to a given policy, is to maximize the shipping profit, which is calculated by subtracting fuel costs and operating expenses from the shipping company's revenue. The customer's objective is to minimize transportation costs, which include carbon emission surcharges.

2.3.2 Carbon allocation methods per TEU per od pair

Assuming that a liner shipping company services a set of ports, referred to as **N**, ships are scheduled to visit these ports in a specific sequence with a weekly frequency (Meng et al., 2014). This scheduling results in various routes, denoted as r ($r \in \mathbf{R}$). Each port visited on a given route r is identified as a port of call i, with $\mathbf{I}_r$ representing the set of all such ports of call on route r. We assume that within a complete journey, each port in **N** is visited exactly once, ensuring that $|\mathbf{I}_r| = |\mathbf{N}|$. The distance from port of call $i-1$ to port of call i ($i \in \mathbf{I}_r$) on route r is expressed as L_i^r; the associated carbon emissions for this distance are denoted as c_i^r. Consequently, the cumulative carbon emissions for route r are calculated as $c^r = \sum_{i \in \mathbf{I}_r} c_i^r$.

The number of containers (measured in TEUs) transported weekly from origin port o to destination port d on route r is represented by y_{od}^r ($o, d \in \mathbf{N},\ o \neq d$). The quantity of containers Q_i^r from port of call $i-1$ to port of call i ($i \in \mathbf{I}_r$) is calculated as $Q_i^r = \sum_{o \in \mathbf{N}} \sum_{d \in \mathbf{N} \setminus \{o\}} \rho_{od}^{ri} y_{od}^r$, where ρ_{od}^{ri} indicates whether the od pair utilizes shipping leg i ($i \in \mathbf{I}_r$) on route r ($r \in \mathbf{R}$). The set $\mathbf{I}'_r$ comprises shipping legs on route r ($r \in \mathbf{R}$) with a non-zero TEU count:

$$\mathbf{I}'_r = \{i \in \mathbf{I}_r \mid Q_i^r > 0\}. \tag{2.1}$$

The government attempts to design an equitable policy to allocate c^r ($r \in \mathbf{R}$) for the total TEUs $Q^r = \sum_{o \in \mathbf{N}} \sum_{d \in \mathbf{N} \setminus \{o\}} y_{od}^r$. The allocation per TEU per od pair on route r ($r \in \mathbf{R}$), denoted as x_{od}^r, should satisfy the following conditions: (i) The allocation of carbon emissions x_{od}^r for any od pair must be non-negative, i.e., $x_{od}^r \geq 0 (r \in \mathbf{R},\ o, d \in \mathbf{N},\ o \neq d)$; and (ii) The total carbon emission allocation is the sum of carbon emissions for all TEUs across all od pairs on the route, formulated as $c^r = \sum_{o \in \mathbf{N}} \sum_{d \in \mathbf{N} \setminus \{o\}} y_{od}^r x_{od}^r (r \in \mathbf{R})$. Given the above introduction, we next present four methods for allocating carbon emissions per TEU per od pair.

(1) **Traditional method**

The traditional method distributes the total carbon emissions generated along a shipping route evenly across each TEU, disregarding the differences in distance between od pairs.

The carbon emission allocation x_{od}^r can be initially computed by dividing the carbon emissions c_i^r on shipping leg i ($i \in \mathbf{I}_r$) by the cargo volume Q_i^r, shown as follows:

$$x_{od}^r = \sum_{i \in \mathbf{I}_r'} \frac{c_i^r}{Q_i^r} \rho_{od}^{ri}, r \in \mathbf{R},\ o, d \in \mathbf{N},\ o \neq d. \tag{2.2}$$

However, this method is simplistic, as demonstrated by the following two examples.

Example 2.1 *Consider a shipping route with two physical ports* ($|\mathbf{N}| = 2$). *A shipment comprising a batch of cargoes is transported from port* 1 *to port* 2*, with* $y_{12}^1 = 10$*, after which the ship returns empty with* $y_{21}^1 = 0$*. The carbon emissions generated by the ship equal* 50 *tons for each leg, denoted as* $c_1^1 = c_2^1 = 50$ *tons. Given this case,* $\mathbf{I}_r' = \{1\}$*, and the carbon emission allocation* x_{12}^1 *is calculated as* $x_{12}^1 = \sum_{i \in \mathbf{I}_r'} c_i^r \rho_{od}^{ri} / Q_i^r = 5$ *tons, and* $x_{21}^1 = 0$ *tons. However, this calculation method overlooks the carbon emissions from the return voyage* ($c_2^1 = 50$ *tons*)*. Although no cargo is carried on the return voyage, the carbon* *emissions generated on the return voyage should be factored into the carbon allocation for containers on the first leg. By doing so, the corrected carbon allocation for the shipment becomes* $x_{12}^1 = 10$ *tons, ensuring that the total emissions* $x_{12}^1 \times 10 + x_{21}^1 \times 0 = \ 100$ *tons are fully allocated.*

Example 2.2 *Following Example 2.1, suppose that on the return voyage from port* 2 *to port* 1*, the ship transports only one TEU* ($y_{21}^1 = 1$)*. The initial calculation method yields a carbon emission allocation of* $x_{21}^1 = 50$ *tons for this TEU, which lacks fairness and practicality.*

In the examples provided, it is evident that the traditional method for carbon emission allocations x_{od}^r does not deliver equitable allocations. Specifically, in Example 2.1, the methodology undervalues the carbon emissions of the empty return leg by omitting the return voyage from the calculation, even though its emissions are a direct consequence of transporting cargoes. In contrast, Example 2.2 highlights the method's propensity to allocate excessive carbon emissions to legs with low container volumes. To address these disparities, this study proposes two new carbon allocation methods.

(2) **Allocating carbon emissions per TEU by traveling distance**

For a given route r ($r \in \mathbf{R}$), the traveling distance for containers from physical port o to d is denoted as $l_{od}^r = \sum_{i \in \mathbf{I}_r} \rho_{od}^{ri} L_i^r, (r \in \mathbf{R},\ o, d \in \mathbf{N},\ o \neq d)$. The carbon allocation for each od pair is determined by the actual traveling distance and the cargo volume as follows:

$$x_{od}^r = l_{od}^r \frac{c^r}{\sum_{o' \in \mathbf{N}} \sum_{d' \in \mathbf{N} \setminus \{o'\}} y_{o'd'}^r l_{o'd'}^r}, r \in \mathbf{R},\ o, d \in \mathbf{N},\ o \neq d. \qquad (2.3)$$

Applying this formula to Example 2.1 yields $x_{12}^1 = l_{12}^1 \frac{c_1^1+c_2^1}{y_{12}^1 l_{12}^1 + y_{21}^1 l_{21}^1} = 10 \times \frac{50+50}{10\times10+0} =$ 10tons, and $x_{21}^1 = l_{21}^1 \frac{c_1^1+c_2^1}{y_{12}^1 l_{12}^1 + y_{21}^1 l_{21}^1} = 10$ tons, maintaining the total carbon emissions at 100 tons for the route. In Example 2.2, the total carbon emissions are $x_{12}^1 \times 10 + x_{21}^1 \times 0 = 100$ tons. Applying this formula yields $x_{12}^1 = l_{12}^1 \frac{c_1^1+c_2^1}{y_{12}^1 l_{12}^1 + y_{21}^1 l_{21}^1} = 10 \times \frac{50+50}{10\times10+1\times10} \approx 9.1$ tons. This adjustment ensures a balanced carbon allocation across each TEU for every od pair, mitigating the illogical outcomes observed from application of the traditional method.

However, the dependency on l_{od}^r introduces challenges, particularly when route detours increase the traveling distance, potentially skewing the fairness of the allocation. We illustrate this phenomenon using the following example.

Example 2.3 *Consider a shipping route with three physical ports, denoted as* $|\mathbf{N}| = 3$*, where the route follows the sequence* $1 \to 2 \to 3 \to 1$*, as shown in Figure 2.1. The shortest sailing distances between consecutive ports are uniformly* 10*, which equal to the lengths of each of the three shipping legs, i.e.,* $L_1^1 = L_2^1 = L_3^1 = 10$*. Assume that there is an equal cargo volume from port* 1 *to port* 2 *and from port* 1 *to port* 3*, i.e.,* $y_{12}^1 = y_{13}^1 = 10$*, and identical carbon emissions* $c_1^1 = c_2^1 = c_3^1 = 50$ *tons for each leg. The traveling distances of the two shipping services are* $l_{12}^1 = 10$ *and* $l_{13}^1 = 20$*. The carbon allocation formula* $x_{od}^r = l_{od}^r \frac{c^r}{\sum_{o'\in\mathbf{N}}\sum_{d'\in\mathbf{N}\setminus\{o'\}} y_{o'd'}^r l_{o'd'}^r}$ *yields* $x_{12}^1 = l_{12}^1 \frac{c_1^1+c_2^1+c_3^1}{y_{12}^1 l_{12}^1 + y_{13}^1 l_{13}^1} = 10 \times \frac{50+50+50}{10\times10+10\times20} =$ 5 *tons, and* $x_{13}^1 = l_{13}^1 \frac{c_1^1+c_2^1+c_3^1}{y_{12}^1 l_{12}^1 + y_{13}^1 l_{13}^1} = 20 \times \frac{50+50+50}{10\times10+10\times20} = 10$ *tons. This discrepancy arises even though the shortest sailing distances between ports* 1–2 *and ports* 1–3 *are identical. The detour for the od pair* 1–3 *significantly distorts the carbon allocation outcome, leading to an inequitable distribution for the containers involved.*

(3) **Allocating container carbon emissions by the shortest sailing distance**

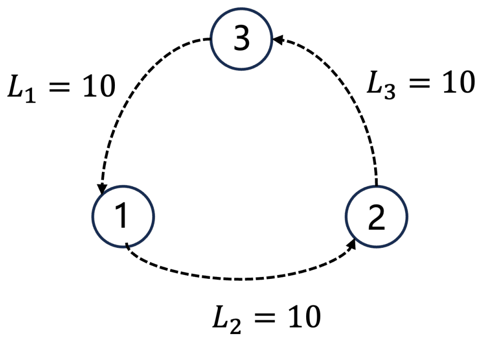

Figure 2.1: Illustration of Example 2.3.

We use l'_{od} to denote the minimal sailing distance per od pair. Using l'_{od}, the carbon allocation is redefined as follows:

$$x^{r'}_{od} = l'_{od} \times \frac{c^r}{\sum_{o' \in \mathbf{N}} \sum_{d' \in \mathbf{N} \setminus \{o'\}} y^r_{o'd'} l'_{o'd'}}, r \in \mathbf{R},\ o, d \in \mathbf{N},\ o \neq d. \tag{2.4}$$

Although the carbon allocation scheme calculated based on the shortest sailing distance per od pair may not accurately reflect the actual traveling distance, it offers a more equitable allocation of carbon emissions than alternative methods. Following Example 2.2, the recalculated shortest sailing distances are denoted as $l^{1'}_{12} = l^{1'}_{13} = 10$. This leads to an equitable carbon allocation outcome for each od pair, i.e., $x^1_{12} = l^{1'}_{12} \frac{c_1+c_2+c_3}{y^1_{12} l^{1'}_{12} + y^1_{13} l^{1'}_{13}} = 10 \times \frac{50+50+50}{10\times10+10\times10} = 7.5$ tons, and $x^1_{13} = l^{1'}_{13} \frac{c_1+c_2+c_3}{y^1_{12} l^{1'}_{12} + y^1_{13} l^{1'}_{13}} = 10 \times \frac{50+50+50}{10\times10+10\times10} = 7.5$ tons. Consequently, when the shortest sailing distances of several od pairs are identical, the carbon allocation results are consistent, thereby ensuring equity.

The carbon allocation method based on the traveling distances of od pairs meticulously captures the nuances of realistic shipping routes. Conversely, the carbon allocation approach based on the shortest sailing distances of od pairs aims to distribute carbon emissions more equitably. Thus, this study addresses the following pivotal research question regarding the superiority of the previous two carbon allocation schemes designed per TEU per od pair: *Which carbon allocation method is more effective: the method based on traveling distance or the method based on the shortest sailing distance per od pair?*

Motivated by the different characteristics of these two methods, we combine them and propose the concept of *harmonic distance*, which is of increased complexity and presents regulatory and operational challenges.

(4) **Allocating container carbon emissions based on the harmonic distance**

We first define a harmonic factor $h \in [0, 1]$, which controls the degree of consideration given to the traveling and shortest sailing distances. The harmonic factor h is assigned a value within the range $[0, 1]$. Instead of finding a definite precise h, this paper discretizes $[0, 1]$ into several policy candidates, which constitute the set **H** ($h \in \mathbf{H}$). This harmonic distance is represented as follows:

$$\hat{l}_{od}^{rh} = h \times l_{od}^{r} + (1 - h) l'_{od}. \tag{2.5}$$

Subsequently, the carbon allocation for each od pair is computed using this harmonic distance as follows:

$$x_{od}^{hr} = \hat{l}_{od}^{hr} \times \frac{c^{hr}}{\sum_{o' \in \mathbf{N}} \sum_{d' \in \mathbf{N} \setminus \{o'\}} y_{o'd'}^{hr} \hat{l}_{o'd'}^{hr}}, r \in \mathbf{R},\ o, d \in \mathbf{N},\ o \neq d,\ h \in \mathbf{H}. \tag{2.6}$$

It is obvious that when $h = 1$, the carbon allocation is calculated based solely on the traveling distance per od pair, reflective of the actual shipping route. Conversely, when $h = 0$, the allocation relies entirely on the shortest sailing distance per od pair, aiming for an equitable distribution. For $h \in (0, 1)$, the scheme employs a convex combination approach, blending the two methods. This approach allows for a nuanced carbon allocation that considers both the operational realities and the equity requirement. However, because this method requires determination of the optimal h, its adoption as a governmental policy framework is contingent on its demonstrable benefits over singular allocation methods.

2.3.3 Assumptions

Before we introduce the mathematical model, we outline the assumptions on which our analysis is based: (i) There is an adequate supply of ships to meet all the shipping company's demand. (ii) A physical port cannot be visited multiple times within a single voyage. (iii) There is only one ship type on a given shipping route. (iv) Transportation costs comprise base freight rates (BFR) and surcharges. The primary component, BFR, is associated with port-to-port transportation (De Oliveira, 2014). Shipping surcharges represent additional fees charged by maritime transport providers beyond the BFR, such as the bunker adjustment factor (BAF) and the terminal handling charge (THC) for the ports of origin and destination. Leading shipping companies incorporate the carbon emission cost into the shipping surcharges, maintaining uniform charges across the same trade region for each TEU (Maersk, 2023a).

However, our allocation method, calculated per TEU per od pair, associates the carbon emission cost with port-to-port transportation and includes it in the BFR. The determination of the BFR can be influenced by numerous factors, such as economies of scale and cargo prices. When the BFR (including the carbon emission cost) increases, demand decreases (Jugović et al., 2015). For simplicity, we assume that the demand from port o to port d ($o, d \in \mathbf{N},\ o \neq d$) under the specified policy h on route r, denoted as q_{od}^{hr}, has a linear relationship in the carbon allocation scheme x_{od}^{hr}. As shown in Figure 2.2, when the carbon allocation of the od pair from port o to port d ($o, d \in \mathbf{N},\ o \neq d$) is 0, the demand for cargo transport is q_{od}; when the carbon allocation of the od pair is between 0 and $x_{od}^{\max}$ (which is the maximum allowable carbon emissions for each TEU per od pair and is assumed to be known), the demand for cargo transport is $q_{od}^{hr} = q_{od} - \frac{q_{od}}{x_{od}^{\max}} x_{od}^{hr}$; and when the carbon allocation per od pair reaches $x_{od}^{\max}$, the demand for cargo transport is zero. If the relationship between demand q_{od}^{hr} and carbon allocation x_{od}^{hr} is non-linear, for example, $q_{od}^{hr} = q_{od} - \frac{q_{od}}{x_{od}^{\max}} (x_{od}^{hr})^2$, this non-linear relationship can be effectively handled by commercial solvers such as CPLEX and Gurobi.

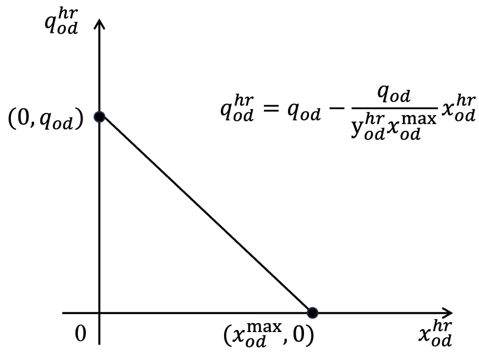

Figure 2.2: Relationship between demand and carbon allocation.

2.4 Mathematical Model

Before presenting the model, the notations employed are detailed in Table 2.1. To allocate carbon emissions in a socially optimal manner, we formulate a bi-level programming model. The upper-level model solves the regulatory decision-

Table 2.1: Notations

Sets and indices	
N	Set of physical ports, indexed by o and d.
R	Set of candidate shipping routes, indexed by r.
I_r	Set of ports of call (or legs) on ship route r, indexed by i; $\lvert I_r\rvert = \lvert\mathbf{N}\rvert$.
H	Set of harmonic factors, indexed by h.
Parameters	
G	Capacity of the ship.
L_i^r	Sailing distance from port of call $i-1$ to port of call i on route r, $i \in I_r$, $r \in \mathbf{R}$.
e	Carbon emissions per unit of fuel consumption.
θ	Unit carbon emission cost.
f^{fuel}	Fuel cost per unit.
q_{od}	Demand for cargo transportation from port o to port d, $o, d \in \mathbf{N}, o \neq d$.
q_{od}^{hr}	Cargo demand on route r under harmonic factor h, $r \in \mathbf{R}, h \in \mathbf{H}, o, d \in \mathbf{N}, o \neq d$.
f_{od}	Transportation price per TEU from port o to port d, $o, d \in \mathbf{N}, o \neq d$.
l_{od}^r	Traveling distance from port o to d on route r, $o, d \in \mathbf{N}, o \neq d, r \in \mathbf{R}$.
l_{od}'	Shortest sailing distance from port o to d, $o, d \in \mathbf{N}, o \neq d$.
p^{od}	Unit penalty cost per TEU for untransported cargo, $o, d \in \mathbf{N}, o \neq d$.
$x_{od}^{\max}$	Maximum allowable carbon emissions per TEU from port o to d, $o, d \in \mathbf{N}, o \neq d$.
$v_{\min}$	Minimum speed required for ship sailing.
$v_{\max}$	Maximum speed allowed for ship sailing.

making challenges faced by the regulator (e.g., the government). The lower-level model addresses the decisions encountered by the regulated entity (e.g., a shipping company) given a specified upper-level policy. The objective of the upper-level model is to minimize the total social costs associated with shipping activities from the perspective of the government. This objective considers the optimal solutions derived from the lower-level model under a given policy (harmonic factor) h. We use $\dot{u}^{hr}$, $\dot{y}_{od}^{hr}$, $\dot{m}^{hr}$, and $\dot{x}_{od}^{hr}$ to denote the optimal solutions derived from the lower-level model.

c_0	Fixed parameter for the relationship between fuel consumption and speed.
c^{oper}	Fixed operation cost for each ship per week.
T	Total docking time of a ship completing a full voyage on route r, $r \in \mathbf{R}$.
M	A very large number.
Decision variables	
ω_h	Binary variable: $\omega_h = 1$ if harmonic factor h is selected; 0 otherwise, $h \in \mathbf{H}$.
u^{hr}	Binary variable: $u^{hr} = 1$ if route r is chosen for operation under harmonic factor h; 0 otherwise, $h \in \mathbf{H}, r \in \mathbf{R}$.
$\hat{l}_{od}^{hr}$	Harmonic distance from port o to d on route r, $o, d \in \mathbf{N}, o \neq d, r \in \mathbf{R}, h \in \mathbf{H}$.
ρ_{od}^{ri}	Binary variable: $\rho_{od}^{ri} = 1$ if transportation from o to d on route r engages leg i; 0 otherwise, $r \in \mathbf{R}, i \in I_r, o, d \in \mathbf{N}, o \neq d$.
y_{od}^{hr}	Number of cargoes delivered from o to d on route r under harmonic factor h, $h \in \mathbf{H}, r \in \mathbf{R}, o, d \in \mathbf{N}, o \neq d$.
m^{hr}	Number of ships deployed on route r under harmonic factor h, $h \in \mathbf{H}, r \in \mathbf{R}$.
x_{od}^{hr}	Carbon allocation per TEU from o to d on route r under harmonic factor h, $h \in \mathbf{H}, r \in \mathbf{R}, o, d \in \mathbf{N}, o \neq d$.
v_i^{hr}	Sailing speed for leg i on route r under harmonic factor h, $i \in I_r, h \in \mathbf{H}, r \in \mathbf{R}$.
$\delta_{hri}^{\text{cons}}$	Fuel consumption for leg i on route r under harmonic factor h, $i \in I_r, r \in \mathbf{R}$.
c^{hr}	Total carbon emissions for completing a full voyage on route r under harmonic factor h, $r \in \mathbf{R}, h \in \mathbf{H}$.

The upper-level model can be expressed as follows:

$$
\begin{aligned}
[\text{UL}] \quad \min_{\omega_h,\, u^{hr}} \sum_{h\in\mathbf{H}} \omega_h \sum_{r\in\mathbf{R}} \dot{u}^{hr} \Bigg(& \sum_{o\in\mathbf{N}} \sum_{d\in\mathbf{N}\setminus\{o\}} p^{od}(q_{od} - \dot{y}_{od}^{hr}) + c^{\text{oper}} \dot{m}^{hr} \\
& + \sum_{i\in I_r} f^{\text{fuel}} \dot{\delta}_{hri}^{\text{cons}} + \sum_{o\in\mathbf{N}} \sum_{d\in\mathbf{N}\setminus\{o\}} \theta\, \dot{y}_{od}^{hr} \dot{x}_{od}^{hr} \Bigg)
\end{aligned}
\tag{2.7}
$$

subject to

$$\sum_{h\in\mathbf{H}} \omega_h = 1, \tag{2.8}$$

$$\omega_h \in \{0,1\}, \forall h \in \mathbf{H}. \tag{2.9}$$

Objective function (2.7) includes four terms, where $\sum_{o\in\mathbf{N}} \sum_{d\in\mathbf{N}\setminus\{o\}} p^{od}(q_{od} - \dot{y}_{od}^{hr})$ represents the penalty costs of unshipped cargoes, $c^{\text{oper}}\dot{m}^{hr}$ represents the operating costs of all ships, $\sum_{i\in I_r} f^{\text{fuel}}\dot{\delta}_{hri}^{\text{cons}}$ represents the fuel costs, and $\sum_{o\in\mathbf{N}} \sum_{d\in\mathbf{N}\setminus\{o\}} \theta \dot{y}_{od}^{hr} \dot{x}_{od}^{hr}$ represents the carbon emission costs.

Given a policy h, the lower-level model aims to maximize the interests of the shipping company, which are established as follows:

$$[\text{LL}^h] \max_{u^{hr},\, y_{od}^{hr},\, m^{hr}} \sum_{r\in\mathbf{R}} u^{hr} \left(\sum_{o\in\mathbf{N}} \sum_{d\in\mathbf{N}\setminus\{o\}} f_{od} y_{od}^{hr} - c^{\text{oper}} m^{hr} - \sum_{i\in I_r} f^{\text{fuel}} \delta_{hri}^{\text{cons}} \right) \tag{2.10}$$

subject to

$$\sum_{r\in\mathbf{R}} u^{hr} = 1 \tag{2.11}$$

$$\sum_{o\in\mathbf{N}} \sum_{d\in\mathbf{N}\setminus\{o\}} \rho_{od}^{ri} y_{od}^{hr} \le G, \forall r \in \mathbf{R},\, i \in I_r \tag{2.12}$$

$$\left(\sum_{i\in\mathbf{I}_r}\frac{L_i^r}{v_i^{hr}}+T\right)u^{hr}\leq 168m^{hr},\forall r\in\mathbf{R} \tag{2.13}$$

$$v_{\text{min}}\leq v_i^{hr}\leq v_{\text{max}},\forall r\in\mathbf{R},\ i\in\mathbf{I}_r \tag{2.14}$$

$$\delta_{hri}^{\text{cons}}=c_0L_i^r(v_i^{hr})^2,\forall r\in\mathbf{R},\ i\in\mathbf{I}_r \tag{2.15}$$

$$\hat{l}_{od}^{rh}=\sum_{r\in\mathbf{R}}u^{hr}\left[h\times l_{od}^r+(1-h)\times l_{od}'\right],\forall o,d\in\mathbf{N},\ o\neq d \tag{2.16}$$

$$x_{od}^{hr}=\frac{\hat{l}_{od}^{hr}c^{hr}}{\sum_{o'\in\mathbf{N}}\sum_{d'\in\mathbf{N}\setminus\{o'\}}y_{o'd'}^{hr}\hat{l}_{o'd'}^{hr}},\forall r\in\mathbf{R},\ o,d\in\mathbf{N},\ o\neq d \tag{2.17}$$

$$c^{hr}=\sum_{i\in\mathbf{I}_r}e\,\delta_{hri}^{\text{cons}},\forall r\in\mathbf{R} \tag{2.18}$$

$$x_{od}^{hr}\leq x_{od}^{\text{max}}u^{hr},\forall o,d\in\mathbf{N},\ o\neq d,\ \forall r\in\mathbf{R} \tag{2.19}$$

$$y_{od}^{hr}\leq\left(q_{od}-\frac{q_{od}}{x_{od}^{\text{max}}}x_{od}^{hr}\right)u^{hr},\forall o,d\in\mathbf{N},\ o\neq d,\ \forall r\in\mathbf{R} \tag{2.20}$$

$$u^{hr}\in\{0,1\},\forall r\in\mathbf{R},\ o,d\in\mathbf{N},\ o\neq d \tag{2.21}$$

$$m^{hr}\in\mathbb{N}^+,\forall r\in\mathbf{R} \tag{2.22}$$

$$x_{od}^{hr}\geq 0,\forall r\in\mathbf{R},\ o,d\in\mathbf{N},\ o\neq d \tag{2.23}$$

$$y_{od}^{hr}\geq 0,\forall r\in\mathbf{R},\ o,d\in\mathbf{N},\ o\neq d \tag{2.24}$$

$$v_i^{hr}\geq 0,\forall r\in\mathbf{R},\ i\in\mathbf{I}_r \tag{2.25}$$

$$\delta_{hri}^{\text{cons}}\geq 0,\forall r\in\mathbf{R},\ i\in\mathbf{I}_r \tag{2.26}$$

$$c^{hr}\geq 0,\forall r\in\mathbf{R}. \tag{2.27}$$

Objective function (2.10) includes three terms, where $\sum_{o\in\mathbf{N}}\sum_{d\in\mathbf{N}\setminus\{o\}}f_{od}y_{od}^{hr}$ represents the transportation revenue earned by the shipping company, $c^{\text{oper}}m^{hr}$ represents the operating costs of the shipping company, and $\sum_{i\in\mathbf{I}_r} f^{\text{fuel}}\delta^{\text{cons}}_{hri}$ represents the total fuel costs. Constraint (2.11) requires the shipping company to choose only one route for operation. Constraint (2.12) requires that for each shipping leg, the cargoes transported on the leg cannot surpass the ship's maximum capacity. Constraint (2.13) calculates the required number of ships so that each port of call on a route is visited weekly. Constraint (2.14) imposes speed requirements for ships sailing. Fuel consumption, the calculation of harmonic distance, the carbon allocation for each od pair, and the total carbon emissions are expressed in Constraints (2.15)–(2.18), respectively. Constraint (2.19) ensures that the carbon allocation x^{hr}_{od} per od pair remains below customers' maximum acceptable level. Constraint (2.20) requires that the volume of cargo transported per od pair y^{hr}_{od} cannot exceed the actual cargo demand, influenced by the carbon allocation scheme $q_{od} - \frac{q_{od}}{x^{\max}_{od}} x^{hr}_{od}$. Constraints (2.21)– (2.22) define the binary, integer, and non-negative variables, respectively.

2.5 Solution Approach

In this section, we create a new converted model by transforming the nonlinear terms presented in the original model to simplify the solution process. Subsequently, a corresponding algorithm is developed to solve the new model.

2.5.1 Model conversion

The model $\mathbf{LL}^h$ ($h \in \mathbf{H}$) described in Section 2.4 incorporates several nonlinear terms, specifically within Constraints (2.15) and (2.17). To facilitate the solving of the model, we develop reformulation methods to linearize the speed-related and carbon allocation terms appearing in Constraints (2.15) and (2.17), respectively.

(1) **Conversion of speed related terms**

Constraints (2.15) have nonlinear terms because of the squared terms related to shipping speeds. To solve them, we define $\mu_i^{hr} = 1/v_i^{hr}$, and Constraints (2.13)–(2.15) can be transformed into

$$\sum_{i \in \mathbf{I}_r} L_i^r \mu_i^{hr} + T \leq 168 m^{hr}, \forall r \in \mathbf{R} \tag{2.28}$$

$$\frac{1}{v_{\text{max}}} \leq \mu_i^{hr} \leq \frac{1}{v_{\text{min}}}, \forall r \in \mathbf{R},\ i \in \mathbf{I}_r \tag{2.29}$$

$$\delta_{hri}^{\text{cons}} (\mu_i^{hr})^2 = c_0 L_i^r, \forall r \in \mathbf{R},\ i \in \mathbf{I}_r. \tag{2.30}$$

Furthermore, considering that the lower-level model aims at maximizing profit, we can replace Constraints (2.30) with the following constraints:

$$\frac{\delta_{hri}^{\text{cons}} (\mu_i^{hr})^2}{c_0 L_i^r} \geq 1, \forall r \in \mathbf{R},\ i \in \mathbf{I}_r. \tag{2.31}$$

By taking the square root of both sides of Constraints (2.31), they are further transformed into

$$\left(\frac{\delta_{hri}^{\text{cons}}}{c_0 L_i^r} \right)^{1/2} (\mu_i^{hr}) \geq 1, \forall r \in \mathbf{R},\ i \in \mathbf{I}_r. \tag{2.32}$$

Regarding Constraints (2.32), they can be represented by a series of hyperbolic constraints (Du et al., 2011), shown as follows:

$$\frac{\delta_{hri}^{\text{cons}}}{c_0 L_i^r} \geq \omega_{i1}^2, \omega_{i1} \mu_i^{hr} \geq 1, \frac{\delta_{hri}^{\text{cons}}}{c_0 L_i^r},\ \mu_i^{hr},\ \omega_{i1} \geq 0, \forall r \in \mathbf{R},\ i \in \mathbf{I}_r. \tag{2.33}$$

where ω_{i1} represents the newly introduced decision variable. A hyperbolic inequality of the form $v_2 v_3 \geq v_1^2$, $v_1, v_2, v_3 \geq 0$ can be reformulated as a second-order cone programming (SOCP) constraint. The constraint can be rewritten as $v_2 + v_3 \geq \|(2v_1, v_2 - v_3)\|_2$, where $\|\cdot\|_2$ denotes the Euclidean norm. Thus, hyperbolic inequalities (2.33) can be further represented by a group of SOCP constraints as follows:

$$\frac{\delta^{\text{cons}}_{hri}}{c_0 L_i^r} + 1 \geq \left\| \left(2\omega_{i1}, \frac{\delta^{\text{cons}}_{hri}}{c_0 L_i^r} - 1 \right) \right\|_2,$$
$$\omega_{i1} + \mu_i^{hr} \geq \|(2, \omega_{i1} - \mu_i^{hr})\|_2,$$
$$\frac{\delta^{\text{cons}}_{hri}}{c_0 L_i^r},\ \mu_i^{hr},\ \omega_{i1} \geq 0, \forall r \in \mathbf{R},\ i \in \mathbf{I}_r.$$

We use SOCP to solve specific nonlinear structures. This approach simplifies the solution process for our model.

(2) **Conversion of carbon allocation terms**

Constraints (2.17) can be written as follows:

$$x_{od}^{hr} \sum_{o' \in \mathbf{N}} \sum_{d' \in \mathbf{N} \setminus \{o'\}} y_{o'd'}^{hr} \hat{l}_{o'd'}^{hr} = \hat{l}_{od}^{hr} c^{hr}, \forall r \in \mathbf{R},\ o, d \in \mathbf{N},\ o \neq d. \tag{2.34}$$

where the term $x_{od}^{hr} \sum_{o' \in \mathbf{N}} \sum_{d' \in \mathbf{N} \setminus \{o'\}} y_{o'd'}^{hr} \hat{l}_{o'd'}^{hr}$ is a product of two decision variables and is thus nonlinear. To solve this issue, we first fix h ($h \in \mathbf{H}$) and r ($r \in \mathbf{R}$) for analytical simplicity. We then approximate the upper and lower bounds for $\sum_{o' \in \mathbf{N}} \sum_{d' \in \mathbf{N} \setminus \{o'\}} y_{o'd'}^{hr} \hat{l}_{o'd'}^{hr}$ under the given h and r, and then discretize the original model into several subproblems given the obtained upper and lower bounds of $\sum_{o' \in \mathbf{N}} \sum_{d' \in \mathbf{N} \setminus \{o'\}} y_{o'd'}^{hr} \hat{l}_{o'd'}^{hr}$, which are then solved sequentially.

In detail, for a given h ($h \in \mathbf{H}$) and r ($r \in \mathbf{R}$), the upper bound of $\sum_{o' \in \mathbf{N}} \sum_{d' \in \mathbf{N} \setminus \{o'\}} y_{o'd'}^{hr} \hat{l}_{o'd'}^{hr}$

can be obtained by solving the following model:

$$[\text{UB}(h,r)] \quad UB^{hr} = \max \sum_{o' \in \mathbf{N}} \sum_{d' \in \mathbf{N} \setminus \{o'\}} y^{hr}_{o'd'} \hat{l}^{hr}_{o'd'} \tag{2.35}$$

subject to Constraints (2.12), (2.24) and

$$\sum_{r \in \mathbf{R}} u^{hr} y^{hr}_{o'd'} \leq q_{od}, \forall o, d \in \mathbf{N},\ o \neq d. \tag{2.36}$$

Identifying an appropriate lower bound for $\sum_{o' \in \mathbf{N}} \sum_{d' \in \mathbf{N} \setminus \{o'\}} y^{hr}_{o'd'} \hat{l}^{hr}_{o'd'}$ presents considerable difficulties because of the uncertainty relating to y^{hr}_{od}. However, from a practical perspective, assuming that each route transports at least one TEU, the lower bound can be expressed as $LB^{hr} = \min \sum_{o' \in \mathbf{N}} \sum_{d' \in \mathbf{N} \setminus \{o'\}} 1 \times \hat{l}^{hr}_{o'd'} = \min \sum_{o' \in \mathbf{N}} \sum_{d' \in \mathbf{N} \setminus \{o'\}} \hat{l}^{hr}_{o'd'}$. Given that the minimum value of $\sum_{o' \in \mathbf{N}} \sum_{d' \in \mathbf{N} \setminus \{o'\}} \hat{l}^{hr}_{o'd'}$ is at least one, we can define the lower bound as $LB^{hr} = 1$.

We discretize the interval $[1, UB^{hr}]$ into J segments evenly, resulting in a total of J subproblems. In the jth subproblem, $\sum_{o' \in \mathbf{N}} \sum_{d' \in \mathbf{N} \setminus \{o'\}} y^{hr}_{o'd'} \hat{l}^{hr}_{o'd'}$ is bounded as $[lb_j,\ ub_j]$, where lb_j and ub_j denote the lower and upper bounds of the jth segment, respectively. For the jth subproblem, we introduce the following two constraints to establish upper and lower bounds for $\sum_{o' \in \mathbf{N}} \sum_{d' \in \mathbf{N} \setminus \{o'\}} y^{hr}_{o'd'} \hat{l}^{hr}_{o'd'}$:

$$\sum_{o' \in \mathbf{N}} \sum_{d' \in \mathbf{N} \setminus \{o'\}} y^{hr}_{o'd'} \hat{l}^{hr}_{o'd'} \geq lb_j, \forall j = 1, \ldots, J \tag{2.37}$$

$$\sum_{o' \in \mathbf{N}} \sum_{d' \in \mathbf{N} \setminus \{o'\}} y^{hr}_{o'd'} \hat{l}^{hr}_{o'd'} \leq ub_j, \forall j = 1, \ldots, J. \tag{2.38}$$

Concurrently, we use the value of the lower bound in the jth segment lb_j to approximate the value of x^{hr}_{od} in the jth subproblem. As a result, in the jth subproblem,

x_{od}^{hr} can be calculated as follows:

$$x_{od}^{hr} = \frac{\hat{l}_{od}^{hr} c^{hr}}{lb_j}, \forall o, d \in \mathbf{N},\ o \neq d. \tag{2.39}$$

Concurrently, Constraints (2.28), (2.29), and (2.30) are utilized to replace the original nonlinear Constraints (2.14), (2.15), and (2.16), respectively, for the jth subproblem. For a given h and r, the transformed lower-level model (LL_j^{hr}) for the jth subproblem is finally as follows:

$$[\mathrm{LL}_j^{hr}] \quad \max \sum_{r \in \mathbf{R}} u^{hr} \left(\sum_{o \in \mathbf{N}} \sum_{d \in \mathbf{N} \setminus \{o\}} f_{od} y_{od}^{hr} - c^{\text{oper}} m^{hr} - \sum_{i \in I_r} f^{\text{fuel}} \delta_{hri}^{\text{cons}} \right) \tag{2.40}$$

subject to Constraints (2.12), (2.18)–(2.29), (2.34), and (2.37)–(2.39).

2.5.2 Algorithm

Based on our proposed conversion procedures, Algorithm 2.1 outlines the solution process. We define the following solutions: w_h represents the selection of the harmonic factor; and $\dot{u}^{hr}$, $\dot{Y}_{od}^{hr}$, $\dot{m}^{hr}$, $\dot{X}_{od}^{hr}$, $\dot{v}_i^{hr}$, $\dot{\delta}_{hri}^{\text{cons}}$, and $\dot{c}^{hr}$ denote the optimal solutions of the lower-level model LL^h for a given h ($h \in \mathbf{H}$). Specifically, for route r under the harmonic factor h, $\dot{u}^{hr}$ indicates the binary selection of the shipping route; $\dot{Y}_{od}^{hr}$ denotes the matrix of the optimal number of cargoes delivered; $\dot{m}^{hr}$ represents the optimal number of ships; $\dot{X}_{od}^{hr}$ denotes the matrix of the optimal carbon allocation per TEU per OD pair; $\dot{v}_i^{hr}$ specifies the optimal sailing speed for leg i; $\dot{\delta}_{hri}^{\text{cons}}$ denotes the optimal fuel consumption for leg i; and $\dot{c}^{hr}$ represents the total carbon emissions. The overall solving procedure is outlined in Algorithm 2.1.

Based on the linearized model, our proposed Algorithm 2.1 iteratively examines each candidate policy h ($h \in \mathbf{H}$) and each candidate route r ($r \in \mathbf{R}$). Under a given combination of h and r, we discretize $\sum_{o'\in\mathbf{N}}\sum_{d'\in\mathbf{N}\setminus\{o'\}} y^{hr}_{o'd'}\hat{l}^{hr}_{o'd'}$ into J segments, resulting in a total of J subproblems, each denoted by LL^{hr}_j ($j \in \{1,\ldots,J\}$). By evaluating all of the optimal objective function values obtained from LL^{hr}_j ($j \in \{1,\ldots,J\}$), we determine the optimal solution of the lower-level model under the given h and the corresponding objective function value of the upper-level model. Finally, by comparing all of the resulting objective function values of the upper-level model with different h ($h \in \mathbf{H}$), we determine the optimal policy.

2.6 Case Study

In this section, we first introduce the parameter settings for our case study. Next, we present the optimal solution for the case study. Finally, we conduct robustness tests to verify the effectiveness of our proposed carbon allocation methods.

2.6.1 Parameter settings

In this study, we focus on ports situated within the northeastern, northern, and Shandong regions of China that are integrated into its domestic trade circuits (Zhonggu Logistics). The selected ports include Yingkou (YIK), Qinhuangdao (QHD), Tianjin (TSN), Yantai (YNT), Weihai (WEH), and Dalian (DLC). We document the shortest sailing distances between these specified ports (HiFleet), as shown in Table 2.2. In addition, the weekly demands between physical ports are presented in Table 2.3.

The capacity of the ships (G) is assumed to be 5,000 TEUs (Wang et al., 2021).

Algorithm 2.1 Solution procedure for the bi-level model

Input: Candidate policies $h \in \mathbf{H}$, routes $r \in \mathbf{R}$, ports $\mathbf{N}$, segment number J.
Output: Optimal upper-level policy $\dot{w}_h$ and lower-level solutions $\big(\dot{u}^{hr}, \dot{Y}_{od}^{hr}, \dot{m}^{hr}, \dot{X}_{od}^{hr}, \dot{v}_i^{hr}, \dot{\delta}_{hri}^{\text{cons}}, \dot{c}^{hr}\big)$.

Define the optimal solution for the upper-level model: $\dot{w}_h$.
Define the optimal objective function value for the upper-level model: ul.
Initialization: $ul \leftarrow \infty$.
for $h \in \mathbf{H}$ **do**
    Set $w_h \leftarrow 1$.
    Initialize the optimal solution for LL^h: $\big(\dot{u}^{hr}, \dot{Y}_{od}^{hr}, \dot{m}^{hr}, \dot{X}_{od}^{hr}, \dot{v}_i^{hr}, \dot{\delta}_{hri}^{\text{cons}}, \dot{c}^{hr}\big)$.
    Define the optimal objective function value for $\mathbf{LL}^h$: ll^h.
    Initialization: $ll^h \leftarrow 0$.
    for $r \in \mathbf{R}$ **do**
        Set $u^{hr} \leftarrow 1$.
        Solve model UB(h, r) to obtain the upper bound of $\sum_{o' \in \mathbf{N}} \sum_{d' \in \mathbf{N} \setminus \{o'\}} y_{o'd'}^{hr} \, \hat{l}_{o'd'}^{hr}$, i.e., UB^{hr}.
        The lower bound is $LB^{hr} \leftarrow \min \sum_{o' \in \mathbf{N}} \sum_{d' \in \mathbf{N} \setminus \{o'\}} \hat{l}_{o'd'}^{hr}$.
        Divide UB^{hr} and LB^{hr} into J groups with even interval: $\Delta \leftarrow \left\lceil \dfrac{UB^{hr} - LB^{hr}}{J} \right\rceil$.
        for $j = 1, \ldots, J$ **do**
            Set $lb_j \leftarrow LB^{hr} + (j-1) \times \Delta$.
            Set $ub_j \leftarrow lb_j + \Delta$.
            Solve the approximate model LL_j^{hr}.
            Obtain the current solution $\big(Y_{od}^{hr}, m^{hr}, X_{od}^{hr}, v_i^{hr}, \delta_{hri}^{\text{cons}}, c^{hr}\big)$.
            if current objective value of the lower-level model $> ll^h$ **then**
                Update the optimal solution $\big(\dot{u}^{hr}, \dot{Y}_{od}^{hr}, \dot{m}^{hr}, \dot{X}_{od}^{hr}, \dot{v}_i^{hr}, \dot{\delta}_{hri}^{\text{cons}}, \dot{c}^{hr}\big)$.
                Update the optimal objective function value ll^h.
            end if
        end for
    end for
    Compute the current objective function value for the upper-level model.
    if the current upper-level objective value $< ul$ **then**
        Update the optimal solution $\dot{w}_h$.
        Update the optimal objective function value ul.
    end if
end for

Table 2.2: Shortest sailing distances between physical ports (nautical miles).

	YIK	QHD	TSN	YNT	WEH	DLC
YIK	0	141	246	218	255	194
QHD	141	0	145	172	209	143
TSN	246	145	0	197	246	200
YNT	218	172	197	0	63	89
WEH	255	209	246	63	0	109
DLC	194	143	200	89	109	0

Table 2.3: Demand (q_{od}) between physical ports (TEU).

	YIK	QHD	TSN	YNT	WEH	DLC
YIK	0	500	2,000	1,600	1,800	1,000
QHD	500	0	800	600	1,000	1,200
TSN	2,000	800	0	1,200	1,500	2,000
YNT	1,600	600	1,200	0	200	300
WEH	1,800	1,000	1,500	200	0	1,400
DLC	1,000	1,200	2,000	300	1,400	0

The conversion rate of fuel consumption and emissions e is set to 3.15 (Offshore Energy, 2022). The costs per unit of carbon allowance (θ) at 47.31 USD/ton. The costs per unit of fuel consumed by a ship f^{fuel} are approximately 600 USD/ton (Wang et al., 2023a). The maximum and minimum sailing speeds (v_{min} and v_{max}) are set to 8 and 22 knots, respectively (Wang et al., 2015; Zhen et al., 2020). We set the coefficient c_0 at 0.00085 (Wang and Meng, 2012). The weekly operational costs (c^{oper}) are assumed to be 180,000 USD (Alharbi et al., 2015; Zhen et al., 2019). We also assume that ships dock at each physical port for 24 hours (Wu et al., 2022b), and the total docking time is $T = 24 \times 10 = 240$ hours. Furthermore, we assume that shipping prices are mainly affected by the shortest sailing distance, and the shipping price per TEU (f_{od}) per od pair is shown in Table 2.4.

Containers that are not shipped will be transferred to alternative transportation

Table 2.4: Transportation price (USD/TEU).

	YIK	QHD	TSN	YNT	WEH	DLC
YIK	0	300	500	500	500	300
QHD	300	0	300	300	500	300
TSN	500	300	0	300	500	500
YNT	500	300	300	0	100	100
WEH	500	500	500	100	0	200
DLC	300	300	500	100	200	0

modes that are more costly in terms of both fees and carbon emissions, such as rail transportation. Therefore, the penalty per TEU should be greater than the unit shipping price. Accordingly, we set the penalty costs p^{od} to be three times the unit shipping price, as shown in Table 2.5.

Table 2.5: Penalty costs (USD/TEU).

	YIK	QHD	TSN	YNT	WEH	DLC
YIK	0	900	1,500	1,500	1,500	900
QHD	900	0	900	900	1,500	900
TSN	1,500	900	0	900	1,500	1,500
YNT	1,500	900	900	0	300	300
WEH	1,500	1,500	1,500	300	0	600
DLC	900	900	1,500	300	600	0

Based on the parameters established, we aim to determine the value of the maximum allowable carbon emissions $x_{od}^{\max}$. Given that the average shortest sailing distances and demand are approximately 150 nm and 1,000 TEU, respectively, and assuming an average speed of about 10 knots, we calculate the corresponding parameters as follows:

$$\delta_{hri}^{\text{cons}} = c_0 L_i^r (v_i^{hr})^2 = 0.00085 \times 150 \times 10^2 = 12.75 \text{ tons}$$

$$c^{hr} = \sum_{i \in \mathbf{I}_r} e\, \delta^{\text{cons}}_{hri} = 3.15 \times 12.75 \times 5 = 200.8125 \text{ tons}$$

$$x^{hr}_{od} = \frac{\hat{l}^{hr}_{od} c^{hr}}{\sum_{o' \in N} \sum_{d' \in N \setminus \{o'\}} y^{hr}_{o'd'} \hat{l}^{hr}_{o'd'}} = \frac{200.8125 \times 150}{1000 \times 150 \times 5} \approx 0.04016 \text{ tons.}$$

Assuming that customers, compared with the other two stakeholder groups, are more tolerant of carbon emissions, we set the maximum allowable carbon emissions $x^{\max}_{od}$ at 1 ton per TEU per od pair, which is larger than 0.04. Later, we conduct sensitivity studies of these parameters to expand the analysis in Section 2.6.3.

2.6.2 Results

Based on the given parameters and employing an interval of $J = 100$ for the algorithm, the computation time is approximately 4,303 seconds. The outcomes are as follows: the optimal policy, $h^* = 0$, indicates that we should use the shortest sailing distance as the basis for carbon allocation per TEU, and the resulting optimal objective function value for the upper-level model is 17,387,727 USD. For the $LL^{(h^*)}$ model, the objective function value is 7,510,308.155 USD; total carbon emissions are $c^{hr} = 444.6322$ tons; the optimal shipping route is delineated as "YIK $\to$ QHD $\to$ YNT $\to$ WEH $\to$ TSN $\to$ DLC;" the fleet size is $m^{hr} = 3$; the shipping route spans six legs; and the speed v^{hr}_i and fuel consumption $\delta^{\text{cons}}_{hri}$ for each leg are specified in Table 2.6.

Table 2.6: Speed v^{hr}_i and fuel consumption $\delta^{\text{cons}}_{hri}$ for each leg.

	1	2	3	4	5	6
v^{hr}_i (knots)	8.59	8.56	8.56	8.56	8.56	8.58
$\delta^{\text{cons}}_{hri}$ (tons)	8.84	14.64	15.32	19.25	31.71	51.40

The cargo transported per od pair y^{hr}_{od} is shown in Table 2.7. The carbon emissions distributed per od pair x_{od}^{hr} are shown in Table 2.8. It is evident that od pairs with larger cargo volumes are allocated correspondingly larger carbon emissions than those with smaller cargo volumes. Interestingly, there are allocations of carbon emissions for some od pairs even in the absence of a cargo volume. This occurs because ships may transit through these od pairs while navigating along their routes, thereby incurring carbon emissions.

Table 2.7: The cargoes y_{od}^{hr} transported per od pair.

$d\backslash o$	YIK	QHD	TSN	YNT	WEH	DLC
YIK	0	0	410	931	1,684	0
QHD	0	0	413	582	979	0
TSN	306	414	0	207	1,458	1,975
YNT	981	582	0	0	193	0
WEH	1,738	979	1,458	193	0	0
DLC	0	0	1,975	0	0	0

Table 2.8: The carbon emissions distributed per od pair x_{od}^{hr}.

$d\backslash o$	YIK	QHD	TSN	YNT	WEH	DLC
YIK	0.000	0.020	0.030	0.036	0.034	0.027
QHD	0.020	0.000	0.024	0.029	0.020	0.020
TSN	0.030	0.024	0.000	0.009	0.027	0.012
YNT	0.036	0.029	0.009	0.000	0.034	0.015
WEH	0.034	0.020	0.027	0.034	0.000	0.028
DLC	0.027	0.020	0.012	0.015	0.028	0.000

2.6.3 Robustness tests

To validate the findings of this study, we conduct robustness tests to examine the impact of parameter variations on the carbon allocation outcomes. These tests specifically focus on several critical parameters: the maximum carbon emissions

$x_{od}^{\max}$ that are acceptable to customers, the discretization interval J used in the algorithm, and variations in demand levels.

(1) **The maximum carbon emissions $x_{od}^{\max}$ acceptable to customers**

We only vary the value of $x_{od}^{\max}$ while maintaining all other parameters at the values specified in Section 2.6.1. The outcomes for different values of $x_{od}^{\max}$ are listed in Table 2.9. As $x_{od}^{\max}$ increases, the number of ships m^{hr} remains constant, and the value of h is largely unaffected.

Notably, the value of the optimal total carbon emissions c^{hr} (tons) becomes more pronounced when $x_{od}^{\max} = 0.2$. This distinction arises because the optimal route shifts to "YIK $\rightarrow$ QHD $\rightarrow$ WEH $\rightarrow$ YNT $\rightarrow$ TSN $\rightarrow$ DLC" at $x_{od}^{\max} = 0.2$, as opposed to the other route of $x_{od}^{\max}$, "YIK $\rightarrow$ QHD $\rightarrow$ YNT $\rightarrow$ WEH $\rightarrow$ TSN $\rightarrow$ DLC." The alteration in optimal routes explains the discrepancy in total carbon emissions: the magnitude of the maximum acceptable carbon emissions does not directly influence the actual total carbon emissions.

For the upper-level model, the objective is to minimize the total social costs; conversely, for the LL^h model, the objective is to maximize shipping profit. As shown in Figure 2.3, when $x_{od}^{\max}$ increases, the optimal objective function value for the UL model decreases, indicating a reduction in costs, whereas the optimal objective function value for the LL^h model increases, suggesting enhanced profitability. This indicates that both the shipping company and the government gain additional benefits, allowing the shipping company to achieve greater profits and the government to secure enhanced social welfare than under alternative scenarios. Notably, the crossover point in Figure 3 is not meaningful since the measurement units for the UL and LL^h models differ; they do not actually intersect in practice.

(2) **The discretization interval J used in the algorithm**

Table 2.9: Outcomes for different maximum carbon emissions $x_{od}^{\max}$.

$x_{od}^{\max}$	Objective function value of upper-level model	h^*	Optimal objective function value of LL^h (USD)	Optimal total carbon emissions c^{hr}	Optimal number of ships m^{hr}	Optimal shipping route
0.2	18,085,529.19	0	7,265,885.943	376.50	3	YIK → QHD → WEH → YNT → TSN → DLC
0.4	17,601,727.48	0	7,412,908.114	444.63	3	YIK → QHD → YNT → WEH → TSN → DLC
0.6	17,481,739.12	0	7,468,108.387	444.63	3	YIK → QHD → YNT → WEH → TSN → DLC
0.8	17,423,728.33	0	7,494,307.434	444.64	3	YIK → QHD → YNT → WEH → TSN → DLC
1.0	17,387,727.00	0	7,510,308.155	444.63	3	YIK → QHD → YNT → WEH → TSN → DLC
2.0	17,319,726.63	0	7,541,909.194	444.63	3	YIK → QHD → YNT → WEH → TSN → DLC
3.0	17,295,727.56	0	7,553,108.114	444.63	3	YIK → QHD → YNT → WEH → TSN → DLC
4.0	17,285,728.61	0.1	7,557,707.434	444.64	3	YIK → QHD → YNT → WEH → TSN → DLC
5.0	17,277,727.68	0	7,560,908.114	444.63	3	YIK → QHD → YNT → WEH → TSN → DLC

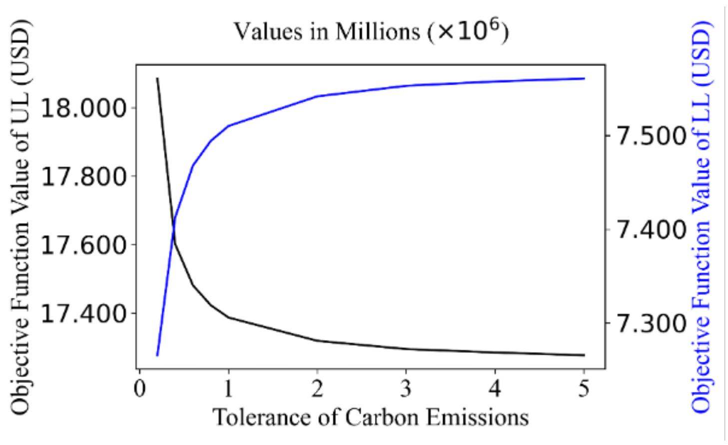

Figure 2.3: Objective function values for different maximum carbon emissions.

Now, we vary only the value of J, maintaining all other parameters at the values specified in Section 2.6.1. The results of different values of J are illustrated in Figure 2.4 and Table 2.10. As the value of J increases, the optimal objective function value for the UL model exhibits a decreasing trend, whereas that for the optimal objective function value for the LL^h model shows an increasing trend. This pattern suggests that as J increases, the approximation solution progressively converges toward the optimal solution, enabling the government to achieve the maximum social benefit (the minimum total costs) and the shipping company to realize the maximum profit.

However, beyond the value of 50, the optimization of the objective function does not yield more significant increased benefits. Thus, a value of $J = 50$ is identified as the threshold beyond which no substantial gains are observed, suggesting that this value provides a sufficiently satisfactory solution for our models.

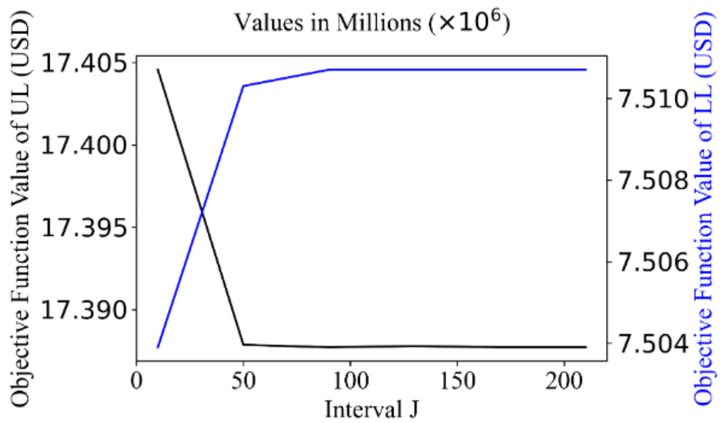

Figure 2.4: Objective function values for different J.

(3) **Demand levels**

In Section 2.6.2, the solution of h predominantly remains at 0, indicating a preference for the carbon allocation scheme that utilizes the shortest sailing dis-

Table 2.10: Outcomes for different J.

$x_{od}^{\max}$	Objective function value of upper-level model	h^*	Optimal objective function value of LL^h (USD)	Optimal total carbon emissions c^{hr}	Optimal number of ships m^{hr}	Optimal shipping route
10	17,404,569.0	0	7,503,908.15	444.632189	3	YIK $\rightarrow$ QHD $\rightarrow$ YNT $\rightarrow$ WEH $\rightarrow$ TSN $\rightarrow$ DLC
50	17,387,875.5	0	7,510,308.27	444.631591	3	YIK $\rightarrow$ QHD $\rightarrow$ YNT $\rightarrow$ WEH $\rightarrow$ TSN $\rightarrow$ DLC
90	17,387,727.9	0	7,510,708.11	444.632399	3	YIK $\rightarrow$ QHD $\rightarrow$ YNT $\rightarrow$ WEH $\rightarrow$ TSN $\rightarrow$ DLC
130	17,387,799.0	0	7,510,708.12	444.626733	3	YIK $\rightarrow$ QHD $\rightarrow$ YNT $\rightarrow$ WEH $\rightarrow$ TSN $\rightarrow$ DLC
170	17,387,728.5	0	7,510,708.13	444.632319	3	YIK $\rightarrow$ QHD $\rightarrow$ YNT $\rightarrow$ WEH $\rightarrow$ TSN $\rightarrow$ DLC
210	17,387,727.5	0	7,510,708.11	444.632399	3	YIK $\rightarrow$ QHD $\rightarrow$ YNT $\rightarrow$ WEH $\rightarrow$ TSN $\rightarrow$ DLC

tance per od pair as the optimal strategy. To further assess the validity of adopting $h = 0$ across various demand scenarios, this chapter conducts a numerical analysis. This analysis uses the case data from Section 2.6.1, with modifications to the demand levels per od pair.

The parameter h serves as a bridge between the traveling distance and the shortest sailing distance. When the shortest sailing distance per od pair is extensive and the transportation demand is low, it is more feasible to meet the demand through alternative ports rather than direct transportation. In such cases, employing the traveling distance for the carbon emission allocation (i.e., $h = 1$) is appropriate. Conversely, when the shortest sailing distance for an od pair is significant and the corresponding transportation demand is high, adopting the shortest sailing route for long-distance demand becomes more economical. That is, utilizing the shortest sailing distance for carbon emission allocation (i.e., $h = 0$) is justified. Therefore, the following experiments consider two cases. We first consider Case A, in which the amount of demand exhibits a positive linear relationship with the shortest sailing distance per od pair. In this context, an increase in the shortest sailing distance leads to an increase in demand. The demand values utilized for the numerical test are shown in Table 2.11.

Table 2.11: Demands proportional to the shortest sailing distance (nautical miles).

$d\backslash o$	YIK	QHD	TSN	YNT	WEH	DLC
YIK	0	1,410	2,460	2,180	2,550	1,940
QHD	1,410	0	1,450	1,720	2,090	1,430
TSN	2,460	1,450	0	1,970	2,460	2,000
YNT	2,180	1,720	1,970	0	630	890
WEH	2,550	2,090	2,460	630	0	1,090
DLC	1,940	1,430	2,000	890	1,090	0

Based on the given parameters and employing an interval of $J = 100$ for the algorithm, the solution time is approximately 3962 seconds. The results are as follows: the optimal policy $h^* = 0$, indicates that we should use the shortest sailing distance as the basis for carbon allocations per TEU, and the resulting optimal objective function value for the upper-level model is 32,545,638.03 USD. For the LL^{h^*} model, the objective function value is 9,174,901.188 USD; total carbon emissions are $c^{hr} = 763.8688$ tons; the optimal shipping route is delineated as "YIK $\rightarrow$ YNT $\rightarrow$ QHD $\rightarrow$ WEH $\rightarrow$ DLC $\rightarrow$ TSN;" the requisite fleet size is indicated by $m^{hr} = 4$; the shipping route spans six legs; and the speed v_i^{hr} and fuel consumption $\delta_{hri}^{\text{cons}}$ for each leg are specified in Table 2.12. The cargoes transported per od pair y_{od}^{hr} are shown in Table 2.13. The carbon emissions distributed per od pair x_{od}^{hr} are shown in Table 2.14.

Table 2.12: Speed v_i^{hr} and fuel consumption $\delta_{hri}^{\text{cons}}$ for each leg.

	1	2	3	4	5	6
v_i^{hr} (knots)	8.71	8.71	8.71	8.71	8.71	8.71
δ_{hri}^{cons} (tons)	38.62	24.55	40.43	29.36	42.13	67.42

Table 2.13: The cargoes y_{od}^{hr} transported per od pair.

$d\backslash o$	YIK	QHD	TSN	YNT	WEH	DLC
YIK	0	0	80	2,065	256	0
QHD	0	0	0	1,697	2,005	0
TSN	293	0	0	0	2,386	1,941
YNT	2,065	1,697	0	0	594	0
WEH	469	2,005	2,386	168	0	0
DLC	0	0	1,941	0	0	0

Table 2.14: The carbon emissions distributed per od pair x_{od}^{hr}.

$d\backslash o$	YIK	QHD	TSN	YNT	WEH	DLC
YIK	0.000	0.045	0.029	0.052	0.050	0.040
QHD	0.045	0.000	0.035	0.013	0.040	0.018
TSN	0.029	0.035	0.000	0.043	0.030	0.029
YNT	0.052	0.013	0.043	0.000	0.050	0.022
WEH	0.050	0.040	0.030	0.050	0.000	0.041
DLC	0.040	0.018	0.029	0.022	0.041	0.000

We also consider Case B, where the amount of demand exhibits a negative linear relationship with the shortest sailing distance per od pair. This implies that an increase in the shortest sailing distance results in a decrease in demand. The specific demands used for the numerical analysis are shown in Table 2.15.

Table 2.15: Demands inversely proportional to the shortest sailing distance.

$d\backslash o$	YIK	QHD	TSN	YNT	WEH	DLC
YIK	0	3,546	2,033	2,294	1,961	2,577
QHD	3,546	0	3,448	2,907	2,392	3,497
TSN	2,033	3,448	0	2,538	2,033	2,500
YNT	2,294	2,907	2,538	0	7,937	5,618
WEH	1,961	2,392	2,033	7,937	0	4,587
DLC	2,577	3,497	2,500	5,618	4,587	0

Based on the given parameters and employing an interval of $J = 100$ for the algorithm, the solving time is approximately 3,465 seconds. The results are as follows. The optimal policy is $h^* = 0.2$, and the resulting optimal objective function value for the upper-level model is 55,752,795.29 USD. For the LL^{h^*} model, the objective function value is 10,154,201.31 USD; total carbon emissions are $c^{hr} = 763.8688$ tons; the optimal shipping route is delineated as "YIK→YNT→QHD→WEH →DLC→TSN;" the requisite fleet size is indicated by $m^{hr} = 4$; the shipping route spans six legs; and the speed v_i^{hr} and fuel consumption $\delta_{hri}^{\text{cons}}$ for each leg are specified in Table 2.16. The cargoes transported per od pair y_{od}^{hr} are shown in Table 2.17. The carbon emissions distributed per od pair x_{od}^{hr} are shown in Table 2.18.

Table 2.16: Speed v_i^{hr} and fuel consumption $\delta_{hri}^{\text{cons}}$ for each leg.

	1	2	3	4	5	6
v_i^{hr} (knots)	8.71	8.71	8.71	8.71	8.71	8.71
$\delta_{hri}^{\text{cons}}$ (tons)	38.62	24.55	40.43	29.36	42.13	67.42

Table 2.17: The cargoes y_{od}^{hr} transported per od pair.

$d\backslash o$	YIK	QHD	TSN	YNT	WEH	DLC
YIK	0	0	8	517	1299	0
QHD	0	0	433	2858	2303	121
TSN	0	449	0	0	1978	2419
YNT	835	2858	0	0	0	0
WEH	1625	2303	1978	0	0	0
DLC	0	106	2419	0	651	0

Table 2.18: The carbon emissions distributed per od pair x_{od}^{hr}.

$d\backslash o$	YIK	QHD	TSN	YNT	WEH	DLC
YIK	0.000	0.028	0.025	0.042	0.048	0.048
QHD	0.028	0.000	0.022	0.017	0.037	0.031
TSN	0.025	0.022	0.000	0.027	0.027	0.032
YNT	0.042	0.017	0.027	0.000	0.032	0.023
WEH	0.048	0.037	0.027	0.032	0.000	0.026
DLC	0.048	0.031	0.032	0.023	0.026	0.000

By analyzing the results of the two cases, the optimal values of h^* are 0 and 0.2, for Cases A and B, respectively. These values lead to identical routing choices, total carbon emissions produced on these routes, and the number of ships deployed. The value of h^* significantly influences the acceptable freight demand values y_{od}^{hr} in the two cases. However, this variation does not affect the total carbon emissions or the strategies used by shipping companies to reduce emissions. Consequently, adopting the shortest sailing distance for carbon emission calculations, represented by $h^* = 0$, is not only consistent with the goal of reducing carbon emissions, but also enables the government to issue policies and manage them easily.

2.7 Conclusions

In this study, we develop several carbon allocation methods per TEU per od pair from a governmental perspective. These methods take into account the traveling distance and the shortest sailing distance per od pair, as well as a convex combination of these distances, aiming to equitably consider the interests of three key stakeholders: the government, who focuses on boosting social welfare; shipping companies, who prioritize profit maximization; and customers, who are interested in shipping cost reductions. To address these concerns, we introduce a bi-level programming model and subsequently linearize the model to make it solvable. Furthermore, we design an algorithm to obtain the approximate optimal solutions efficiently.

Through the detailed case study with rigorous robustness tests, we obtain the following managerial insights. First, our findings highlight the significant advantage of using the shortest sailing distance ($h = 0$) to allocate carbon emissions per TEU per od pair. This approach not only maximizes social benefits but also enables shipping companies to formulate more rational operating strategies. In our analysis, there are instances where the harmonic factor h is not zero. However, these do not affect the shipping company's operating strategies, resulting in carbon emissions consistent with those calculated using the shortest sailing distance. As the harmonic factor ranges between 0 and 1, using the harmonic distance can be more challenging to implement compared to using only the shortest sailing distance. Consequently, we recommend using the shortest sailing distance for calculating carbon emission allocations. Second, this method of carbon allocation proves to be fairer to customers than those currently employed by leading shipping companies. This allocation method also allows government agencies to accurately monitor the carbon footprint of each route, facilitating the timely adjustment of policy measures such as CEAs. Third, this approach could be extended to control other types of emissions, such as sulfides, nitrides, and methane. A reasonable and well-considered allocation method aids the government in monitoring and setting reduction goals and is easy to implement since it takes into account the interests of various stakeholders.

Chapter 3

Optimizing Carbon Allocation for Liner Shipping Companies

3.1 Introduction

Maritime shipping, which accounts for 90% of global trade, plays a central role in facilitating international trade. It is widely regarded as the most energy-efficient mode for transporting cargoes (Useche, 2023). However, the sector remains heavily dependent on fossil fuels (Lee et al., 2013), contributing approximately 3% of global annual carbon dioxide emissions (IMO, 2020). This contribution exceeds the entire emissions of Japan, the world's fifth-largest carbon emitter (Tay and Konovessis, 2023). In response, there have been growing calls for effective measures to mitigate the environmental impact of maritime shipping. On May 16, 2023, the EU ETS adopted an agreement requiring ship operators to report their emissions and surrender allowances for every ton of CO_2 they emit.[1] Under this system, for every ton of reported CO_2, one EU Allowance (EUA) must be purchased and submitted to the EU annually (Wang et al., 2015). This requirement applies to all shipping companies, which are responsible for purchasing the EUAs. In response, major liner shipping companies, such as Maersk, introduced new surcharges in 2024 to pass the cost of carbon emissions onto their customers. However, these companies' surcharges per twenty-foot equivalent unit (TEU) container are mostly calculated based on individual trades, which typically encompass multiple od pairs within a region (e.g., from the Far East to Northern Europe). This surcharge structure fails to account for variations in distance between different od pairs within the same trade, resulting in a lack of precision in carbon emission allocation.

To provide customers with more equitable carbon emission surcharge structures, facilitate governmental regulation of carbon footprints, and promote overall reductions in carbon emissions, Tian et al. (2024) proposed three carbon emission allocation methods, specifically focusing on the perspective of the *government*. These methods allocate carbon emissions for each TEU based on either the traveling distance, which may vary between routes, the shortest sailing distance, determined by the relative positions of the origin and destination, or a combination of both. The government's primary objective is to minimize total social costs, which include the operating costs of shipping companies, the penalty costs of unshipped cargoes due to the increased shipping price, and the costs of carbon emissions. Notably, minimizing total social costs simultaneously minimizes the

[1] `https://www.maersk.com/news/articles/2023/09/15/eu-emissions-trading-system-ets`

corresponding total carbon emissions. Tian et al. (2024) demonstrated that carbon emission allocation based on the shortest sailing distance is sufficient for achieving this objective when considering a single route. However, while this approach effectively supports the government's environmental goals, it does not necessarily maximize the profits of shipping companies. In other words, the government prioritizes environmental objectives over industry profitability when formulating allocation strategies. Additionally, Tian et al. (2024) has overlooked the complexity of real-world shipping networks, which often involve multiple routes and opportunities for cargo transshipment between routes. As a result, allocation based on the shortest sailing distance may not fully align with the operational interests of shipping companies in certain cases.

Building on the three distance-based allocation methods proposed in Tian et al. (2024), this study shifts the perspective from the government to *shipping companies*, aiming to determine the optimal carbon emission allocation policy. Shipping companies operate complex shipping networks comprising multiple routes, with their primary objective being to maximize the total profit. The profit is calculated as the revenue generated from accepted cargoes minus the total operational costs of shipping routes. This involves determining the optimal cargo volume between each od pair and efficiently managing cargo flows across the network. The accepted cargoes for each od pair must not exceed the demand between the respective origin and destination. This demand is influenced by the carbon emission allocation, as higher allocations increase the carbon emission surcharge, thereby reducing demand. Furthermore, carbon emission allocation is shaped by the company's chosen emission allocation policy. As a result, the chosen policy in turn influences the final revenue of the shipping company.

The contributions of this study are threefold. First, from the perspective of liner shipping companies, this study proposes a carbon emission allocation method that maximizes their profits, calculated per TEU for each od pair. This method not only enhances the traceability of carbon footprints but also provides a more effective and precise basis for carbon emission surcharges. Second, the proposed carbon emission allocation method is not limited to a single route but is applicable to shipping networks comprising multiple routes. To account for different operational scenarios, this study considers networks both with and without transshipment options. This allows for the exploration of optimal carbon emission allocation methods and the corresponding flows of cargoes across the whole shipping network. Third, the study validates the carbon emission allocation method using both actual and synthetic shipping networks. By adjusting parameters such as the maximum carbon emission allocation acceptable to customers and the capacity of the shipping network, it identifies the strategies that liner shipping companies should adopt under varying circumstances. In particular, the study emphasizes the conditions under which fundamental distances, such as the shortest sailing distance or traveling distance, are inadequate, and demonstrates how consideration of the harmonic distance can yield higher profits. These findings provide valuable insights for practical decision making in the shipping industry.

The remainder of this chapter is organized as follows. Section 3.2 reviews the related literature. Section 3.3 outlines the problem, including the definitions of the augmented shipping network and the carbon emission allocation method. Section 3.4 develops the carbon emission allocation models with and without transshipment. Section 3.5 presents the tailored solution approach. Section 3.6 evaluates the proposed model and method using a real shipping network. Section 3.7

performs robustness tests on a synthetic shipping network to examine the optimal carbon emission allocation method under different conditions. Finally, Section 3.8 concludes this study.

3.2 Literature Review

Research has generally argued that to effectively control emissions, international carbon allowances should be allocated according to the actual carbon emissions of shipping companies (Heitmann and Khalilian, 2011; Selin et al., 2021). Hu et al. (2023) proposed that a more equitable approach to carbon emission allocation is to distribute carbon allowances based on the proportion of business conducted on specific shipping routes by each company. While current carbon allowances are accurately allocated to shipping companies, the carbon tariffs imposed by leading companies are primarily trade-based, often encompassing multiple od pairs within a region (e.g., from the Far East to Northern Europe). This approach overlooks crucial factors, such as the variability in carbon emission allocation results between routes and the differing distances associated with the od pairs included within the same trade. As a result, it fails to offer customers a more detailed and effective carbon emission allocation method, ultimately falling short of providing transparent and convincing pricing standards for carbon emissions.

From the perspective of shipping companies, studies have shown that with the allocation of carbon emission allowances, companies' emissions have been decreasing annually, but at the cost of a year-on-year decline in economic benefits for both shipping companies and society (Zhu et al., 2023; Goyal and Llop, 2024). To address this issue, some researchers have proposed operational strategies for shipping companies under these allowances, such as route selection and ship deployment (Wang and Chen, 2017; Dai et al., 2018; Ma et al., 2022; Sun et al., 2024). Additionally, several studies have explored more favorable mechanisms under different carbon emission allocation policies. For instance, Zhang et al. (2024) examined optimal pricing and revenue decision making in the supply chains of shipping logistics services, while Jin et al. (2024) proposed a cooperative emission reduction policy between shipping companies and ports, focusing on achieving mutual benefits. Despite these advancements, research on how shipping companies can allocate carbon emissions rationally and efficiently remains scarce. For example, Sun et al. (2022) examined the allocation of carbon emissions to specific routes in liner shipping but focused solely on identifying the routes, neglecting the effects of od pairs. Meanwhile, in the context of carbon emission allocation, both Kellner (2016), who focused on road transportation, and Tian et al. (2024), who examined shipping, demonstrated that distance-based carbon emission allocation strategies can effectively track carbon footprints and provide meaningful carbon emission surcharges. Therefore, this study focuses on allocating carbon emissions to od pairs based on routes from the perspective of liner shipping companies. It accounts for the complexities of shipping networks and incorporates the variations in distance between different od pairs to establish a more rational and effective carbon emission allocation framework.

Specifically, this study considers the case of a shipping company with a network that consists of multiple routes. To model this network, the augmented shipping network construction method proposed by Wang et al. (2013a) is adopted. Based on this network, we employ an od-link-based model, first introduced by Agarwal and Ergun (2008) and later applied to container routing by Bell et al.

(2011). In the od-link-based model, the decision variables represent the flow of containers on each link. Containers on each link can also be differentiated by their od pairs. This model has been increasingly used as the basis of studies on liner shipping networks, including research on shipping network design (Dong et al., 2015; Zheng et al., 2015), service-oriented container slot allocation (Liang et al., 2023), multiperiod heterogeneous fleet deployment problems (Wu et al., 2023), and the impact of the ETS on short-term fleet deployment (Chua et al., 2023). Therefore, this study establishes an augmented shipping network for the focal shipping company (Wang et al., 2013a) and develops an od-link-based model specific to liner shipping (Agarwal and Ergun, 2008; Bell et al., 2011). This approach enables a comprehensive and integrated consideration of carbon emission allocation across the entire shipping network.

3.3 Problem Description

In this section, we first construct an augmented shipping network based on an existing shipping network. Next, we provide a detailed definition of the carbon emission allocation method employed in the model. Finally, using a simple example, we illustrate that from the perspective of a liner shipping company, neither the shortest sailing distance nor the traveling distance necessarily maximizes profitability.

3.3.1 Shipping network

This problem is based on a shipping network for a shipping company. We define the set of physical ports as **P**. The set of origin nodes is denoted by **O**, and the set of destination nodes by $\mathbf{D}$, where $\mathbf{O} \subseteq \mathbf{P}$ and $\mathbf{D} \subseteq \mathbf{P}$. For physical ports $\hat{o} \in \mathbf{O}$, $\hat{d} \in \mathbf{D}$, the set of od pairs $(\hat{o}, \hat{d})$ is denoted by $\hat{\mathbf{W}}$, where $\hat{\mathbf{W}} \subseteq \mathbf{O} \times \mathbf{D}$. The shipping network is predetermined, and a single physical port may be visited multiple times across various shipping routes.

Example 3.1 *As illustrated in Figure 3.1, there are two shipping routes, each serving three physical ports $p \in \mathbf{P}$, with ports 1 and 4 being called twice.*

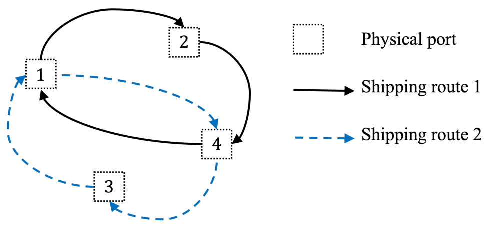

Figure 3.1: Original shipping routes.

Cargoes on an od pair can be transported through several shipping routes connecting the pair. When several routes call at the same physical port within an existing network, it becomes unclear which specific shipping route is being used when cargoes on the od pair pass through a physical port. To address this ambiguity, we construct a new shipping network based on physical ports. In this network, each original physical port is divided into multiple ports of call (nodes), corresponding to the number of times it is visited by different shipping routes.

Example 3.2 *As illustrated in Figure 3.2, physical ports 2 and 3 are each called once, so they are duplicated. Ports 1 and 4 are called twice, and thus both are split into two distinct ports of call.*

The set of shipping routes is denoted by as $\mathbf{R}$. In the new shipping network, the set of nodes (ports of call) for each route $r \in \mathbf{R}$ is denoted by $\mathbf{N}^r$, while the

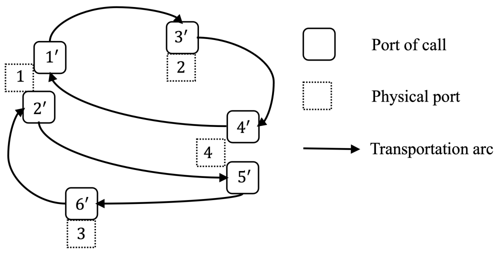

Figure 3.2: New shipping routes based on splitting nodes.

set of arcs (shipping legs, which connect consecutive ports of call) for each route $r \in \mathbf{R}$ is denoted by $\mathbf{A}^r$. When we partition a physical port into multiple nodes based on the times called, the original origin nodes $\hat{o} \in \mathbf{O}$ and destination nodes $\hat{d} \in \mathbf{D}$ are transformed. This replication of physical ports into multiple ports of call introduces various representations of the origin and destination nodes into the updated shipping network, thereby creating ambiguity in the network. To address this, we introduce source nodes $\mathbf{N}^{\text{src}}$ and sink nodes $\mathbf{N}^{\text{sink}}$ to replace the original origin and destination nodes, respectively. Each origin node $\hat{o} \in \mathbf{O}$ is represented by a corresponding source node $n_{\hat{o}}^{\text{src}} \in \mathbf{N}^{\text{src}}$, and each destination node $\hat{d} \in \mathbf{D}$ is represented by a corresponding sink node $n_{\hat{d}}^{\text{sink}} \in \mathbf{N}^{\text{sink}}$. The set of arcs that connect the source nodes $\mathbf{N}^{\text{src}}$ with their child ports of call is denoted by $\mathbf{A}^{\text{src}}$. Similarly, the set of arcs that connect the sink nodes $\mathbf{N}^{\text{sink}}$ with their child ports of call is denoted by $\mathbf{A}^{\text{sink}}$.

Example 3.3 *As illustrated in Figure 3.3, in the shipping network, the original physical port 1 is split into two nodes (ports of call),* $1'$ *and* $2'$*, and physical port 4 is similarly split into* $4'$ *and* $5'$*. Considering od pair* $(1, 4)$ *for cargo transportation from physical port 1 to 4 (although there are also demands for other od pairs), the new shipping network introduces four possible od pairs:* $(1', 4'), (2', 4'), (1', 5')$ *and* $(2', 5')$*. Consequently, we introduce two new nodes—source node* $7'$ *and sink* *node $8'$—to replace the original origin node (port 1) and destination node (port 4), respectively. In the new augmented network, the original od pair $(1, 4)$ is uniquely mapped to $(7', 8')$. The source node $7'$ is then connected to the corresponding ports of call $1'$ and $2'$, while the sink node $8'$ is connected to the corresponding ports of call $4'$ and $5'$, forming the respective source and sink arcs.*

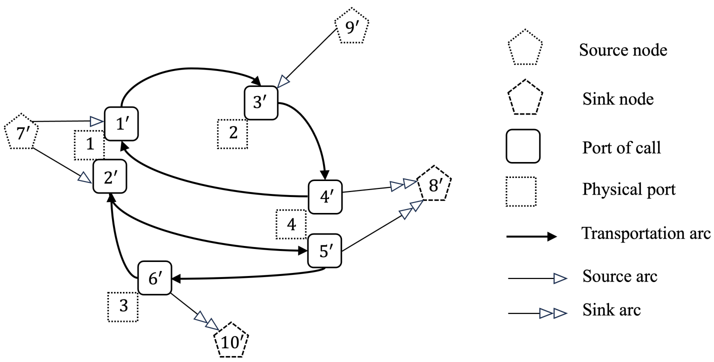

Figure 3.3: The augmented shipping network with source and sink nodes.

The origin nodes $\hat{o} \in \mathbf{O}$ and the destination nodes $\hat{d} \in \mathbf{D}$ correspond to the physical ports. In the augmented shipping network, we replace the original origin and destination nodes with newly introduced source nodes $n \in \mathbf{N}^{\text{src}}$ and sink nodes $n \in \mathbf{N}^{\text{sink}}$. Thus, in the augmented shipping network, each original $(\hat{o}, \hat{d})$ pair is replaced by a pair of newly introduced source and sink nodes. The set of these source and sink pairs is defined as

$$\mathbf{W} = \{(n_{\hat{o}}^{\text{src}}, n_{\hat{d}}^{\text{sink}}) | (\hat{o}, \hat{d}) \in \hat{\mathbf{W}}\} \subseteq \mathbf{N}^{\text{src}} \times \mathbf{N}^{\text{sink}}. \tag{3.1}$$

We now define the augmented shipping network $\mathbf{G} = (\mathbf{N}, \mathbf{A})$, where $\mathbf{N} = \mathbf{N}^{\text{src}} \cup \mathbf{N}^{\text{sink}} \cup_{r \in \mathbf{R}} \mathbf{N}^r$ and $\mathbf{A} = \mathbf{A}^{\text{src}} \cup \mathbf{A}^{\text{sink}} \cup_{r \in \mathbf{R}} \mathbf{A}^r$.

When the impact of carbon emission allocation on customer demand is not considered, the demand for $(\hat{o}, \hat{d}) \in \hat{\mathbf{W}}$ is represented by $q_{\hat{o}\hat{d}}$, and the demand between the corresponding source and sink nodes $(n_{\hat{o}}^{\text{src}}, n_{\hat{d}}^{\text{sink}}) \in \mathbf{W}$ is represented by

$$q_{n_{\hat{o}}^{\text{src}} n_{\hat{d}}^{\text{sink}}} = q_{\hat{o}\hat{d}}. \tag{3.2}$$

For source and sink node pairs where there is no demand ($n_1 \in \mathbf{N}^{\text{src}}, n_2 \in \mathbf{N}^{\text{sink}}, (n_1, n_2) \notin \mathbf{W}$), it is represented by

$$q_{n_1 n_2} = 0. \tag{3.3}$$

We define a mapping function g_n to associate each node $n \in \mathbf{N}$ with its corresponding physical port $p \in \mathbf{P}$. Additionally, we define a mapping function h_n to associate each node $n \in \cup_{r \in \mathbf{R}} \mathbf{N}^r$ with its corresponding shipping route $r \in \mathbf{R}$.

Example 3.4 *As shown in Figure 3.3, physical port 1 is split into nodes* $1', 2'$ *and a source node* $7'$ *in the augmented shipping network, so that* $g_{1'} = g_{2'} = g_{7'} = 1$. *Similarly, for physical port 4, we have* $g_{4'} = g_{5'} = g_{8'} = 4$. *We denote the route "*$1' \to 3' \to 4' \to 1'$*" as route 1, and the route "*$2' \to 5' \to 6' \to 2'$*" as route 2. Thus, we have* $h_{1'} = h_{3'} = h_{4'} = 1$*, and* $h_{2'} = h_{5'} = h_{6'} = 2$.

The capacity of each arc $(m, n) \in \mathbf{A}$ is denoted by V_{mn}. We assume that the ships operating on any given route are homogeneous, meaning that the capacity is identical for all arcs on that route. Specifically, for arcs $(m, n) \in \mathbf{A}^r$ for a specific route $r \in \mathbf{R}$, the capacity V_{mn} is determined by the capacity of the ships on the route. For arcs $(m, n) \in \mathbf{A}^{\text{src}} \cup \mathbf{A}^{\text{sink}}$, the capacity V_{mn} is set to ∞.

3.3.2 Carbon emission allocation method

This study focuses on container shipping, with costs calculated on a weekly basis. The transportation revenue per unit TEU for each $(o, d) \in \mathbf{W}$ is denoted by r_{od} (USD/TEU). The operational costs for each route $r \in \mathbf{R}$ are considered fixed and are represented by C^r (USD). Similarly, the carbon emissions for each route $r \in \mathbf{R}$ are assumed to be fixed and are denoted by δ^r (tons).

The allocation policy considers two fundamental types of distance: the shortest sailing distance for each $(o, d) \in \mathbf{W}$, denoted by l'_{od}, which is determined by the relative geographical positions of the origin and destination ports; and the traveling distance for each $(o, d) \in \mathbf{W}$ on route $r \in \mathbf{R}$, denoted by l^r_{od}, which may differ between routes.

Example 3.5 *As illustrated in Figure 3.4, suppose there is only one shipping route, denoted as route $r = 1$. This route begins at port of call 1, proceeds to port of call 2, continues to port of call 3, and finally returns to port of call 1. Ports of call 1 and 2 are located on the Land, while port of call 3 is located on the Island. Due to the narrow channel between the Land and the Island, the direction of movement is one-way only: from port of call 1 to port of call 2, and then to port of call 3. When cargo is transported from port of call 2 to port of call 1, the ships must follow the direction of the designated shipping route. The distances between the ports are provided in Figure 3.4. Notably, the distance from port of call 3 back to port of call 1 is significantly longer than the distance from port of call 1 to port of call 3 (100 nm > 20 nm). Consequently, even though the shortest sailing distance is $l'_{21} = 10$ nm, the traveling distance becomes $l^1_{21} = 10 + 100 = 110$ nm.*

To determine the optimal carbon emission allocation policy, we use the har-

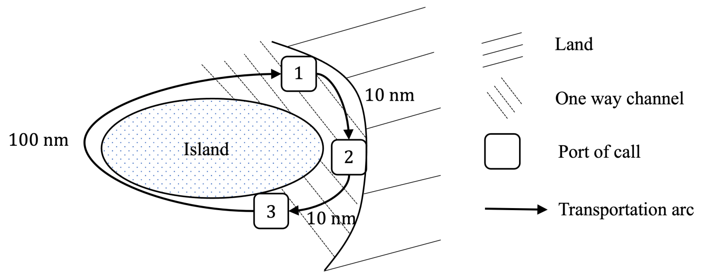

Figure 3.4: An example of the shortest sailing distance and the traveling distance.

monic factor h ($0 \leq h \leq 1$) to combine the shortest sailing distance l'_{od} and the traveling distances l^r_{od} across all routes $r \in \mathbf{R}$ for each $(o, d) \in \mathbf{W}$. This combination yields the harmonic distance for each $(o, d) \in \mathbf{W}$, denoted by $\hat{l}_{od}$ (the explicit formulation is provided in Formulas (3.14) and (3.30) in Section 3.4). The set of harmonic factors is denoted by $\mathbf{H}$, with $h \in \mathbf{H}$. We introduce a binary decision variable ω_h to indicate whether the policy (harmonic factor) h is selected, where $\omega_h = 1$ if policy h is selected, and $\omega_h = 0$ otherwise.

Not all demands are served, and the demands (in TEU) that are actually served and transported are represented as $y_{od}, (o, d) \in \mathbf{W}$. We use a binary variable z^r to denote whether shipping route $r \in \mathbf{R}$ will be used, and the total carbon emissions are represented by $\sum_{r \in \mathbf{R}} \delta^r z^r$. The carbon emission allocation per TEU for $(o, d) \in \mathbf{W}$ is denoted by x_{od}, where

$$x_{od} = \hat{l}_{od} \times \frac{\sum_{r \in \mathbf{R}} \delta^r z^r}{\sum_{(o',d') \in \mathbf{W}} y_{o'd'} \hat{l}_{o'd'}}. \tag{3.4}$$

Example 3.6 *As illustrated in Figure 3.4, for route $r = 1$, the total carbon emissions are predetermined and assumed to be $\delta^1 = 13$ tons. When cargo is transported from port of call 1 to 3, and from port of call 2 to 1, $z^1 = 1$, the carbon* *emission allocation for each* (o, d) *is represented by*

$$x_{od} = \frac{13}{\hat{l}_{13} y_{13} + \hat{l}_{21} y_{21}} \hat{l}_{od}, (o, d) \in \{(1, 3), (2, 1)\}, \tag{3.5}$$

where $\hat{l}_{od} = l'_{od}$ *when calculated using the shortest sailing distance, and* $\hat{l}_{od} = l^1_{od}$ *when calculated using the traveling distance.*

We use $x^{\max}_{od}$ ($(o, d) \in \mathbf{W}$) to denote the maximum carbon emission allocation that customers are willing to accept. When carbon emission allocation is not considered and $x^{\max}_{od}$ approaches to infinity, the demand for $(o, d) \in \mathbf{W}$ is represented by q_{od}. It is assumed that demand decreases as the carbon emission allocation increases. Specifically, this relationship is assumed to be linear, and the actual demand for each $(o, d) \in \mathbf{W}$ can be expressed as follows:

$$q_{od} - \frac{q_{od}}{x^{\max}_{od}} x_{od}. \tag{3.6}$$

3.3.3 Illustrative Example

In this section, we illustrate by an example, showing that from the shipping company's perspective, the harmonic factor h may yield increased profitability when it is set to a value other than 0 (shortest sailing distance) or 1 (traveling distance).

Following Example 3.6, in the absence of carbon emission allocation considerations, it is assumed that the demand from port of call 1 to 3 and from port of call 2 to 1 is $q_{13} = q_{21} = 10$ TEUs. Additionally, it is assumed that the maximum carbon emission allocation acceptable to customers is $x^{\max}_{13} = x^{\max}_{21} = 4.5$ tons. Thus, the transported cargoes y_{od} and the demand are governed by the following relationship:

$$y_{od} \leq 10 - \frac{10}{4.5} x_{od}, (o, d) \in \{(1, 3), (2, 1)\}. \tag{3.7}$$

Both the cargo flows from port of call 1 to 3 and from port of call 2 to 1 share the leg from port of call 2 to 3. Therefore, when the shipping route's capacity is limited—for example, to 10 TEUs—the total accepted cargoes from port of call 1 to 3 and from port of call 2 to 1 must not exceed this capacity, i.e.,

$$y_{13} + y_{21} \leq 10. \tag{3.8}$$

Thus, we can formulate a simplified optimization problem that disregards costs, with the objective of maximizing overall revenue. In this example, the shipping company's profits are equivalent to the overall revenue.

$$\max r_{13} y_{13} + r_{21} y_{21} \tag{3.9}$$

subject to Constraints (3.5), (3.7), (3.8), and

$$\hat{l}_{od}, x_{od}, y_{od} \geq 0, (o, d) \in \{(1, 3), (2, 1)\}. \tag{3.10}$$

Here, the number of containers is treated as a continuous variable, as it can be reasonably approximated as such in real-world scenarios involving a large volume of containers.

We vary h from 0 to 1 in increments of 0.1 and calculate the corresponding harmonic distance for each value of h:

$$\hat{l}_{od}(h) = h \times l_{od}^1 + (1-h) \times l'_{od}, (o,d) \in \{(1,3),(2,1)\}. \tag{3.11}$$

For instance, when $h = 0.4$, the harmonic distances are computed as

$$\hat{l}_{13}(0.4) = 0.4 \times 20 + (1-0.4) \times 20 = 20 \tag{3.12}$$

$$\hat{l}_{21}(0.4) = 0.4 \times 110 + (1-0.4) \times 10 = 50. \tag{3.13}$$

After assigning h, the harmonic distances $\hat{l}_{od}$ are determined, leaving only two decision variables in the model: x_{od} and y_{od}. With the revenue $r_{13} = 30$ and $r_{21} = 10$, we solve the model above for each h. The results are presented in Figure 3.5. In this scenario, when $h = 0$, the shipping company uses the shortest sailing distance for carbon emission allocation, which results in the lowest revenue, as shown by the blue line. When $h = 1$, the company uses the traveling distance for carbon emission allocation, as represented by the green line. Although the traveling distance outperforms the shortest sailing distance, there are seven other harmonic distances that yield higher revenue than both. Among these, the highest revenue is achieved when $h = 0.8$.

From the perspective of liner shipping companies, as demonstrated in the example above, different strategies correspond to varying levels of profitability, and neither the shortest sailing distance nor the traveling distance necessarily represents the most profitable option. In such cases, the harmonic distance emerges as a more effective and profitable solution.

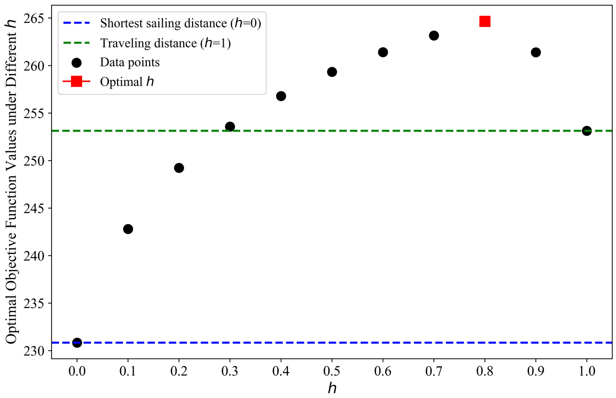

Figure 3.5: Optimal objective function values under different h.

3.4 Model Formulation

Based on the established augmented network and carbon emission allocation method described in Section 3.3, in this section, we formulate two carbon emission allocation models: one that does not consider transshipment and the other that incorporates transshipment.

3.4.1 Carbon allocation model without transshipment

In this model, we do not consider transshipment between different routes. Therefore, for each od pair, once the shipping company has selected specific routes for transport, the cargoes accepted for each route cannot be transferred to other routes.

We define the set of routes that can transport cargoes for $(o, d) \in \mathbf{W}$ as $\mathbf{R}^{od}$, where $\mathbf{R}^{od} \subseteq \mathbf{R}$. The demands for each $(o, d) \in \mathbf{W}$ transported by each route $r \in \mathbf{R}^{od}$ are represented by y^r_{od}, and $\sum_{r\in\mathbf{R}^{od}} y^r_{od} = y_{od}$. Additionally, we define the set of od pairs $(o, d) \in \mathbf{W}$ served by route $r \in \mathbf{R}$ as $\mathbf{W}^r \subseteq \mathbf{W}$.

Example 3.7 *As shown in Figure 3.3, the set of od pairs in the augmented net-*

work is $\{(7', 8'), (7', 10'), (9', 8'), (9', 10')\}$. *As transshipment is not allowed in this model, the demand for* $(9', 10')$ *cannot be transported. Consequently, the set of od pairs that can be transported by route 1 is represented as* $\mathbf{W}^1 = \{(7', 8'), (9', 8')\}$, *while the set of od pairs that can be transported by route 2 is represented as* $\mathbf{W}^2 = \{(7', 8'), (7', 10')\}$.

After introducing y^r_{od}, the harmonic distance $\hat{l}_{od}$ is calculated as

$$\hat{l}_{od} = \sum_{h \in \mathbf{H}} h\omega_h \times \sum_{r \in \mathbf{R}^{od}} l^r_{od} \frac{y^r_{od}}{y_{od}} + (1 - \sum_{h \in \mathbf{H}} h\omega_h) l'_{od}, (o, d) \in \mathbf{W}. \tag{3.14}$$

The decision variables for this model are shown below:

- x_{od}: The amount of carbon emissions allocated for each $(o, d) \in \mathbf{W}$.
- y_{od}: The volume of cargoes accepted for each $(o, d) \in \mathbf{W}$.
- $\hat{l}_{od}$: The harmonic distance for each $(o, d) \in \mathbf{W}$.
- y^r_{od}: The volume of cargoes accepted within route $r \in \mathbf{R}^{od}$ for each $(o, d) \in \mathbf{W}$.
- $f^{r,od}_{mn}$: The volume of cargoes transported on arc $(m, n) \in \mathbf{A}^r$ within route $r \in \mathbf{R}^{od}$ for each $(o, d) \in \mathbf{W}$.
- f^{md}_{mn}: The volume of cargoes transported on source arc $(m, n) \in \mathbf{A}^{\text{src}}$ for each $(m, d) \in \mathbf{W}^{h_n}$, which indicates that od pair (m, d) must be served by route $h_n \in \mathbf{R}$.
- f^{on}_{mn}: The volume of cargoes transported on sink arc $(m, n) \in \mathbf{A}^{\text{sink}}$ for each $(o, n) \in \mathbf{W}^{h_m}$, which indicates that od pair (o, n) must be served by route $h_m \in \mathbf{R}$.
- ω_h: A binary variable, where $\omega_h = 1$ indicates that policy $h \in \mathbf{H}$ is selected; otherwise, $\omega_h = 0$.

- z^r: A binary variable, where $z^r = 1$ indicates that shipping route $r \in \mathbf{R}$ is selected; otherwise, $z^r = 0$.

The objective of this model is to maximize the profit of the shipping company, which is calculated as the difference between revenue and costs. Revenue is derived from charges to customers, while costs vary for each shipping route. The model is outlined as follows:

$$\max \sum_{(o,d)\in\mathbf{W}} r_{od} y_{od} - \sum_{r\in\mathbf{R}} C^r z^r \tag{3.15}$$

subject to Constraints (3.4), (3.14) and

$$\sum_{h\in\mathbf{H}} \omega_h = 1 \tag{3.16}$$

$$y_{od} = \sum_{r\in\mathbf{R}^{od}} y_{od}^r, (o,d) \in \mathbf{W} \tag{3.17}$$

$$y_{od}^r = \sum_{n\in\mathbf{N}^r: g_n = g_o} f_{on}^{od}, r \in \mathbf{R}^{od}, (o,d) \in \mathbf{W} \tag{3.18}$$

$$\textstyle\sum_{(m,n)\in\mathbf{A}^r} f_{mn}^{r,od} - \sum_{(n,m)\in\mathbf{A}^r} f_{nm}^{r,od} = \begin{cases} -f_{on}^{od} & g_n = g_o \\ f_{nd}^{od} & g_n = g_d \\ 0 & \text{otherwise} \end{cases}, r \in \mathbf{R}^{od}, (o,d) \in \mathbf{W}, n \in \mathbf{N}^r \tag{3.19}$$

$$y_{od} \le q_{od} - \frac{q_{od}}{x_{od}^{\max}} x_{od}, (o,d) \in \mathbf{W} \tag{3.20}$$

$$\sum_{(o,d)\in\mathbf{W}^r} f_{mn}^{r,od} \le V_{mn} z^r, (m,n) \in \mathbf{A}^r, r \in \mathbf{R} \tag{3.21}$$

$$\omega_h \in \{0,1\}, h \in \mathbf{H} \tag{3.22}$$

$$z^r \in \{0,1\}, r \in \mathbf{R} \tag{3.23}$$

$$y_{od} \geq 0, (o,d) \in \mathbf{W} \tag{3.24}$$

$$y_{od}^r \geq 0, (o,d) \in \mathbf{W}, r \in \mathbf{R}^{od} \tag{3.25}$$

$$f_{mn}^{r,od} \geq 0, (o,d) \in \mathbf{W}, r \in \mathbf{R}^{od}, (m,n) \in \mathbf{A}^r \tag{3.26}$$

$$f_{mn}^{md} \geq 0, (m,n) \in \mathbf{A}^{\text{src}}, (m,d) \in \mathbf{W}^{h_n} \tag{3.27}$$

$$f_{mn}^{on} \geq 0, (m,n) \in \mathbf{A}^{\text{sink}}, (o,n) \in \mathbf{W}^{h_m} \tag{3.28}$$

$$x_{od} \geq 0, (o,d) \in \mathbf{W}. \tag{3.29}$$

Constraint (3.16) requires only one policy (harmonic factor) to be used in the shipping network. Constraints (3.17) require that for $(o,d) \in \mathbf{W}$, the sum of transported cargoes on each route $r \in \mathbf{R}^{od}$ equals to the total transported cargoes. Constraints (3.18) ensure that flows on shipping route $r \in \mathbf{R}$ are balanced with the corresponding outgoing (incoming) flows from the source (sink) nodes $\mathbf{N}^{\text{src}}$ ($\mathbf{N}^{\text{sink}}$). Constraints (3.19) require that inflows and outflows are balanced across the shipping network. Constraints (3.20) require that the carbon emission allocations and the demands of customers follow linear relationships. Constraints (3.21) require that the amount of cargoes transported on each route $r \in \mathbf{R}$ cannot exceed the capacity. Constraints (3.22)–(3.29) define the domains of the decision variables.

3.4.2 Carbon allocation model with transshipment

When considering transshipment in the network **G**, additional costs are incurred when cargo is transferred between different shipping routes. To model this, we introduce additional arcs, denoted as $(m, n) \in \mathbf{A}^{\mathrm{T}}$, where $g_m = g_n, m \in \mathbf{N}^r, n \in \mathbf{N}^{r'}, r, r' \in \mathbf{R}, r \neq r'$. This setup indicates that transshipment occurs at the same physical port between different ports of call associated with distinct routes.

Example 3.8 *As shown in Figure 3.6, transshipment arcs are added between ports of call $1'$ and $2'$, as well as between ports of call $4'$ and $5'$. These transshipment arcs enable cargoes to switch between shipping routes through physical ports 1 or 4, thereby increasing the overall flexibility of the shipping network. Specifically, when the demand is from physical port 2 to physical port 3 ($(\hat{o}, \hat{d}) = (2, 3)$), if transshipment is not allowed, the demand cannot be met. However, with transshipment, cargoes can be transported via route "$9' \to 3' \to 4' \to 5' \to 6' \to 10'$." Moreover, when the demand is from physical port 1 to physical port 3 ($(\hat{o}, \hat{d}) = (1, 3)$), without transshipment, cargoes can only be transported via "$7' \to 2' \to 5' \to 6' \to 10'$." If transshipment is allowed, an additional route is available: "$7' \to 1' \to 3' \to 4' \to 5' \to 6' \to 10'$."*

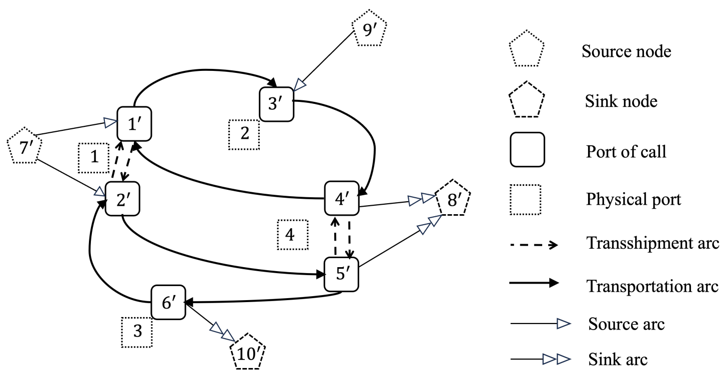

Figure 3.6: Additional arcs for transshipment.

Thus, the shipping network in this model is redefined as $\mathbf{G} = (\mathbf{N}, \mathbf{A})$, where $\mathbf{N} = \mathbf{N}^{\mathrm{src}} \cup \mathbf{N}^{\mathrm{sink}} \cup_{r \in \mathbf{R}} \mathbf{N}^r$, and $\mathbf{A} = \mathbf{A}^{\mathrm{src}} \cup \mathbf{A}^{\mathrm{sink}} \cup \mathbf{A}^{\mathrm{T}} \cup_{r \in \mathbf{R}} \mathbf{A}^r$. The distance for each arc $(m, n) \in \mathbf{A}$ is denoted by d_{mn}. The shortest sailing distance l'_{od} for each $(o, d) \in \mathbf{W}$ is the minimum value among the traveling distances l^r_{od} across all routes $r \in \mathbf{R}$ and is predetermined. For each transshipment arc $(m, n) \in \mathbf{A}^{\mathrm{T}}$, the distance is set to 0 nm, and the capacity is assumed to be ∞. Similarly, for each origin and destination arc $(m, n) \in \mathbf{A}^{\mathrm{src}} \cup \mathbf{A}^{\mathrm{sink}}$, the distance is also set to 0 nm. As carbon emissions from transshipment are covered by the port, and this study is conducted from the perspective of the shipping company, the carbon emissions generated during transshipment are ignored here. The transshipment cost per TEU for $(m, n) \in \mathbf{A}^{\mathrm{T}}$ is represented by c_{mn}.

The decision variables for this model are as follows:

- x_{od}: The amount of carbon emission allocated for each $(o, d) \in \mathbf{W}$.
- y_{od}: The volume of cargoes accepted for each $(o, d) \in \mathbf{W}$.
- $\hat{l}_{od}$: The harmonic distance for each $(o, d) \in \mathbf{W}$.
- f^{od}_{mn}: The volume of cargoes transported on arc $(m, n) \in \mathbf{A}$ for each $(o, d) \in \mathbf{W}$.
- z^r: A binary variable, where $z^r = 1$ indicates that shipping route $r \in \mathbf{R}$ is selected; otherwise, $z^r = 0$.
- ω_h: A binary variable, where $\omega_h = 1$ indicates that policy $h \in \mathbf{H}$ is selected; otherwise, $\omega_h = 0$.

Due to transshipment between different routes, the traveling distances for each $(o, d) \in \mathbf{W}$ are determined by the path over the arcs $(m, n) \in \mathbf{A}$, regardless of the specific routes. Thus, the harmonic distance $\hat{l}_{od}$ can be calculated as

$$\hat{l}_{od} = \sum_{h \in \mathbf{H}} h\omega_h \times \sum_{(m,n) \in \mathbf{A}} d_{mn} \frac{f^{od}_{mn}}{y_{od}} + (1 - \sum_{h \in \mathbf{H}} h\omega_h) l'_{od}, (o, d) \in \mathbf{W}. \tag{3.30}$$

Again, the objective of this model is to maximize the profits of the shipping company, i.e., the difference between revenue and costs. The revenue is derived from the charges levied on customers, while the costs encompass transshipment, among other expenses. The model is outlined as follows:

$$\max \sum_{(o,d)\in\mathbf{W}} r_{od}y_{od} - \sum_{r\in\mathbf{R}} C^r z^r - \sum_{(m,n)\in\mathbf{A}^{\mathrm{T}}} \sum_{(o,d)\in\mathbf{W}} c_{mn} f_{mn}^{od} \tag{3.31}$$

subject to Constraints (3.4), (3.16), (3.20), (3.22)–(3.24), (3.29)–(3.30), and

$$\sum_{(m,n)\in\mathbf{A}} f_{mn}^{od} - \sum_{(n,m)\in\mathbf{A}} f_{nm}^{od} = \begin{cases} -y_{od} & n = o \\ y_{od} & n = d \\ 0 & \text{otherwise} \end{cases}, (o,d) \in \mathbf{W}, n \in \mathbf{N} \tag{3.32}$$

$$\sum_{(o,d)\in\mathbf{W}} f_{mn}^{od} \leq V_{mn} z^r, (m,n) \in \mathbf{A}^r, r \in \mathbf{R} \tag{3.33}$$

$$f_{mn}^{od} \geq 0, (o,d) \in \mathbf{W}, (m,n) \in \mathbf{A}. \tag{3.34}$$

3.5 Solution Approach

The models in Section 3.4.1 and Section 3.4.2 involve several nonlinear terms (Constraints (3.4), (3.14), and (3.30)), primarily related to the calculation of harmonic distances and carbon emission allocation. In this section, we employ discretization and the Big-M technique to linearize these nonlinear terms. Subsequently, we perform necessary transformations and design the corresponding algorithm to solve the models efficiently.

3.5.1 Discretization of the volume of accepted cargoes

The nonlinear terms (Constraints (3.4), (3.14), and (3.30)) relate to the volume of cargoes accepted for each $(o, d) \in \mathbf{W}$, denoted by y_{od}, which specifically appears in the denominator. To linearize these terms, we transform each discretized decision variable y_{od} into multiple parameters. The domains of y_{od} are defined in (3.20) and (3.24); these domains depend on x_{od}, which is itself a decision variable. To facilitate computation, we extend the range of intervals for y_{od}, setting the interval as $[0, q_{od}], (o, d) \in \mathbf{W}$. We then uniformly discretize y_{od}, with the discretization precision denoted by θ. Based on θ, the discretized values of y_{od} are divided into J_{od} parts, where

$$J_{od} = \frac{q_{od}}{\theta}, (o, d) \in \mathbf{W}. \tag{3.35}$$

Here, we assume that q_{od} is an integer multiple of θ, ensuring that J_{od} is an integer. We denote the set of discretized values of y_{od} by $\mathbf{Y}_{od}$, defined as

$$\mathbf{Y}_{od} := \{y_{od}^0, y_{od}^1, ..., y_{od}^j, ..., y_{od}^{J_{od}}\}, (o, d) \in \mathbf{W}, \tag{3.36}$$

where $y_{od}^0 = 0$, $y_{od}^{J_{od}} = y_{od}$, and $y_{od}^j = y_{od}^0 + \theta j = \theta j, j \in \{1, ..., J_{od}\}$. We further introduce a binary decision variable z_{od}^j ($(o, d) \in \mathbf{W}, j \in \{0, ..., J_{od}\}$) to represent y_{od}. Thus, we have

$$y_{od} = \sum_{j=0}^{J_{od}} y_{od}^j z_{od}^j, (o, d) \in \mathbf{W} \tag{3.37}$$

$$\sum_{j=0}^{J_{od}} z_{od}^j = 1, (o, d) \in \mathbf{W} \tag{3.38}$$

$$z_{od}^j \in \{0, 1\}, (o, d) \in \mathbf{W}, j \in \{0, ..., J_{od}\}. \tag{3.39}$$

For each policy (harmonic factor) $h \in \mathbf{H}$, the nonlinear terms (Constraints (3.4), (3.14), (3.30)) can be replaced by the following three constraints, respectively:

$$\sum_{(o',d')\in\mathbf{W}}\sum_{j=0}^{J_{o'd'}} y^j_{o'd'} x_{od} z^j_{o'd'} \hat{l}_{o'd'} = \hat{l}_{od}\sum_{r\in\mathbf{R}} \delta^r z^r, (o,d) \in \mathbf{W} \tag{3.40}$$

$$\left[\hat{l}_{od} - (1-h)l'_{od}\right]\sum_{j=0}^{J_{od}} y^j_{od} z^j_{od} = h \times \sum_{r\in\mathbf{R}^{od}} l^r_{od} y^r_{od}, (o,d) \in \mathbf{W} \tag{3.41}$$

$$\left[\hat{l}_{od} - (1-h)l'_{od}\right]\sum_{j=0}^{J_{od}} y^j_{od} z^j_{od} = h \times \sum_{(m,n)\in\mathbf{A}} d_{mn} f^{od}_{mn}, (o,d) \in \mathbf{W}. \tag{3.42}$$

3.5.2 Big-M reformulation

After discretization, Constraints (3.40) also involve nonlinear terms $x_{od} z^j_{o'd'}$ ($(o,d) \in \mathbf{W}, (o',d') \in \mathbf{W}, j \in \{0, ..., J_{o'd'}\}$), which are the product of discrete variables $z^j_{o'd'}$ and continuous variables x_{od}. To address this, we employ the Big-M Formulation for further model transformation. Define $u^j_{od,o'd'} = x_{od} z^j_{o'd'}, (o,d), (o',d') \in \mathbf{W}, j \in \{0, ..., J_{o'd'}\}$. Constraints (3.40) can be replaced by

$$\sum_{(o',d')\in\mathbf{W}}\sum_{j=0}^{J_{o'd'}} y^j_{o'd'} u^j_{od,o'd'} \hat{l}_{o'd'} = \hat{l}_{od}\sum_{r\in\mathbf{R}} \delta^r z^r, (o,d) \in \mathbf{W} \tag{3.43}$$

$$u^j_{od,o'd'} \leq M z^j_{o'd'}, (o,d), (o',d') \in \mathbf{W}, j \in \{0, ..., J_{o'd'}\} \tag{3.44}$$

$$u^j_{od,o'd'} \leq x_{od}, (o,d), (o',d') \in \mathbf{W}, j \in \{0, ..., J_{o'd'}\} \tag{3.45}$$

$$u^j_{od,o'd'} \geq x_{od} - M(1 - z^j_{o'd'}), (o,d), (o',d') \in \mathbf{W}, j \in \{0, ..., J_{o'd'}\} \tag{3.46}$$

$$u^j_{od,o'd'} \geq 0, (o,d), (o',d') \in \mathbf{W}, j \in \{0, ..., J_{o'd'}\} \tag{3.47}$$

where M is a very large number, defined as $M = \max\{x_{od}^{\max}, (o,d) \in \mathbf{W}\}$. Based on the above transformation, for each policy $h \in \mathbf{H}$, we derive sub-models in Sections 3.5.3 and 3.5.4 corresponding to the models in Sections 3.4.1 and 3.4.2, respectively. Therefore, we solve the sub-models under each h and identify the optimal h that corresponds to the maximum objective function value.

3.5.3 Sub-model for the carbon emission allocation model without considering transshipment

Given a specific policy $h \in \mathbf{H}$, the decision variables are shown below:

- x_{od}: The amount of carbon emission allocated for each $(o,d) \in \mathbf{W}$.
- y_{od}^r: The volume of cargoes accepted within route $r \in \mathbf{R}^{od}$ for each $(o,d) \in \mathbf{W}$.
- y_{od}: The volume of cargoes accepted for each $(o,d) \in \mathbf{W}$.
- $f_{mn}^{r,od}$: The volume of cargoes transported on arc $(m,n) \in \mathbf{A}^r$ within route $r \in \mathbf{R}^{od}$ for each $(o,d) \in \mathbf{W}$.
- f_{mn}^{md}: The volume of cargoes transported on arc $(m,n) \in \mathbf{A}^{\text{src}}$ for each $(m,d) \in \mathbf{W}^{h_n}$, which indicates that od pair (m,d) must be served by route $h_n \in \mathbf{R}$.
- f_{mn}^{on}: The volume of cargoes transported on arc $(m,n) \in \mathbf{A}^{\text{sink}}$ for each $(o,n) \in \mathbf{W}^{h_m}$, which indicates that od pair (o,n) must be served by route $h_m \in \mathbf{R}$.
- z^r: A binary variable, where $z^r = 1$ indicates that the shipping route $r \in \mathbf{R}$ is selected; otherwise, $z^r = 0$.
- z_{od}^j: A binary variable, where $z_{od}^j = 1$ indicates that the volume of cargo

accepted, y_{od}^{j}, for $(o, d) \in \mathbf{W}$ in the $j \in \{0, ..., J_{od}\}$-th part is selected; otherwise, $z_{od}^{j} = 0$.

- $u_{od,o'd'}^{j}$: An auxiliary variable that represents the product of x_{od} and $z_{o'd'}^{j}$, where $(o, d), (o', d') \in \mathbf{W}, j \in \{0, ..., J_{o'd'}\}$.

Thus, the sub-model BM(h) can be reformulated as follows:

$$\text{BM}(h) = \max \sum_{(o,d)\in\mathbf{W}} r_{od} y_{od} - \sum_{r\in\mathbf{R}} C^r z^r \tag{3.48}$$

subject to (3.17)–(3.21), (3.23)–(3.29), (3.35), (3.38)–(3.39), (3.41), and (3.43)–(3.47).

3.5.4 Sub-model for the carbon emission allocation model considering transshipment

Given a specific policy $h \in \mathbf{H}$, the decision variables are shown below:

- x_{od}: The amount of carbon emissions allocated for each $(o, d) \in \mathbf{W}$.
- y_{od}: The volume of cargoes accepted for each $(o, d) \in \mathbf{W}$.
- f_{mn}^{od}: The volume of cargoes transported on arc $(m, n) \in \mathbf{A}$ for each $(o, d) \in \mathbf{W}$.
- z^r: A binary variable, where $z^r = 1$ indicates that shipping route $r \in \mathbf{R}$ is selected; otherwise $z^r = 0$.
- z_{od}^{j}: A binary variable, where $z_{od}^{j} = 1$ indicates that the volume of cargo accepted, y_{od}^{j}, for $(o, d) \in \mathbf{W}$ in the $j \in \{0, ..., J_{od}\}$-th part is selected; otherwise, $z_{od}^{j} = 0$.
- $u_{od,o'd'}^{j}$: An auxiliary variable that represents the product of x_{od} and $z_{o'd'}^{j}$,

where $(o,d),(o',d') \in \mathbf{W}, j \in \{0,...,J_{o'd'}\}$.

Thus, the sub-model TM(h) can be reformulated as follows:

$$\text{TM}(h) = \max \sum_{(o,d)\in\mathbf{W}} r_{od}y_{od} - \sum_{r\in\mathbf{R}} C^r z^r - \sum_{(m,n)\in\mathbf{A}^{\mathrm{T}}} \sum_{(o,d)\in\mathbf{W}} c_{mn} f_{mn}^{od} \tag{3.49}$$

subject to (3.20), (3.23)–(3.24), (3.29), (3.32)–(3.35), (3.38)–(3.39), and (3.43)–(3.47).

3.5.5 Algorithm

Based on the above sub-models, we can use Algorithm 3.1 to obtain the optimal solution and corresponding optimal cost for each model. We denote the set of optimal solutions by $\hat{\mathbf{x}}^*(\theta)$, where $\hat{\mathbf{x}}^*(\theta) = \{x_{od}^*, y_{od}^*, \hat{l}_{od}^*, y_{od}^{r*}, f_{mn}^{r,od*}, f_{mn}^{md*}, f_{mn}^{on*}, \omega_h^*, z^{r*} | (o,d) \in \mathbf{W}, (m,d) \in \mathbf{W}^{r_n}, (o,n) \in \mathbf{W}^{h_m}, r \in \mathbf{R}, (m,n) \in \mathbf{A}, h \in \mathbf{H}\}$ for the basic carbon emission allocation model, and $\hat{\mathbf{x}}^*(\theta) = \{x_{od}^*, y_{od}^*, \hat{l}_{od}^*, f_{mn}^{od*}, \omega_h^*, z^{r*} | (o,d) \in \mathbf{W}, r \in \mathbf{R}, (m,n) \in \mathbf{A}, h \in \mathbf{H}\}$ for the carbon emission allocation model considering transshipment.

Algorithm 3.1 Algorithm based on the sub-model

1: **Input parameters:** $r_{od}, q_{od}, x_{od}^{\max}, \mathbf{Y}_{od}, l'_{od}, l^r_{od}, C^r, \delta^r, c_{mn}, d_{mn}, V_{mn}, \theta$ $((o,d) \in \mathbf{W}, r \in \mathbf{R}, (m,n) \in \mathbf{A})$
2: Define the set of optimal solutions: $\hat{\mathbf{x}}^*(\theta)$
3: **Initialization:** The optimal cost is $C' = 10^{10}$
4: **for** $h \in \mathbf{H}$ **do**
5:     Solve the sub-model
6:     **if** the objective function value $C < C'$ **then**
7:         Update the $\hat{\mathbf{x}}^*(\theta)$, and $C' = C$.
8:     **end if**
9: **end for**

3.6 Case Study

In this section, we evaluate the models and corresponding algorithms proposed in Sections 3.4 and 3.5 using a real-world shipping network.

3.6.1 Parameter settings

We select three routes—A3C, A3S, and A3X—from Northeast Asia to Australia, which are served by COSCO.[2] These routes are illustrated in Figure 3.7 and detailed in Table 4.1. Based on these values, the traveling distances l^r_{od} for each route $r \in \mathbf{R}$ can also be calculated. For the transportation revenue r_{od}, part of the data are sourced from publicly available websites,[3] while the remaining data, which are unavailable, can be estimated based on factors such as distances and the number of routes visiting a given port. For instance, among the nine ports under consideration, those with a larger number of route visits, such as Shanghai, Xiamen, Hong Kong, Brisbane, Sydney, and Melbourne, tend to have a lower average revenue per nm than less frequently visited ports such as Kaohsiung, Shekou and Ningbo. The demands q_{od} between these ports primarily originate from Northeast Asia and are directed to Australia, with minimal demand observed within Northeast Asia.

We assume a uniform vessel size, specifically a 5000-TEU container ship (Wang et al., 2023a) with an operational cost of $180,000$ USD per week (Wang and Wang, 2021). The sailing speed range for such vessels is [13, 18] knots (Lai et al., 2022), and the average sailing speed $\bar{v}$ is set at 16 knots. The operational cost for each

[2] `https://lines.coscoshipping.com/`
[3] `https://qm.cargorate.cn/`

route $r \in \mathbf{R}$ can be calculated as follows:

$$\frac{\sum_{(m,n)\in\mathbf{A}^r} d_{mn}}{16 \times 24 \times 7} \times 180,000, \tag{3.50}$$

where d_{mn} represents the traveling distance between arc $(m,n) \in \mathbf{A}^r$ on route r. Based on this formula, the operational costs are calculated as follows: 5.04 million USD for route A3C, 4.86 million USD for route A3S, and 4.68 million USD for route A3X.

The carbon emissions δ^r for each route $r \in \mathbf{R}$ are calculated using the following formula:

$$\delta^r = C_{\mathrm{o}} \sum_{(m,n)\in\mathbf{A}^r} d_{mn}\bar{v}^2 \tag{3.51}$$

where $\sum_{(m,n)\in\mathbf{A}^r} d_{mn}\bar{v}^2$ represents the fuel consumption, and C_{o} is the conversion factor between fuel consumption and carbon emissions, set at 0.00085 (**?**). Using this formula, the carbon emissions for the routes are calculated as follows: $2,324$ tons for route A3C, $2,257$ tons for route A3S, and $2,170$ tons for route A3X. In addition, the transshipment cost c_{mn} ($(m,n) \in \mathbf{A}^{\mathrm{T}}$) is set at 50 USD/TEU.

The maximum acceptable carbon emission allocation for customers $x_{od}^{\max}$ for each $(o,d) \in \mathbf{W}$ is determined based on the calculated carbon emissions x_{od}. Consider an extreme scenario where all three routes are utilized. The total carbon emissions are the sum of emissions produced by these three routes, i.e., $\sum_{r\in\mathbf{R}} \delta^r z^r = 6,769$. The average amount of cargoes transported on each route is relatively small, i.e., $y_{o'd'} = 500$. Therefore, $\sum_{(o',d')\in\mathbf{W}} y_{o'd'}\hat{l}_{o'd'} = 500 \times 31,109$. The maximum observed value of x_{od} can then be calculated as:

$$x_{od} = \hat{l}_{od} \times \frac{\sum_{r\in\mathbf{R}} \delta^r z^r}{\sum_{(o',d')\in\mathbf{W}} y_{o'd'}\hat{l}_{o'd'}} = 5,029 \times \frac{6,769}{500 \times 31,109} = 2.19. \qquad (3.52)$$

Assuming that customers have a high tolerance for carbon emissions, we set $x_{od}^{\max}$ to 100. Additionally, the discretization precision θ is set to 100.

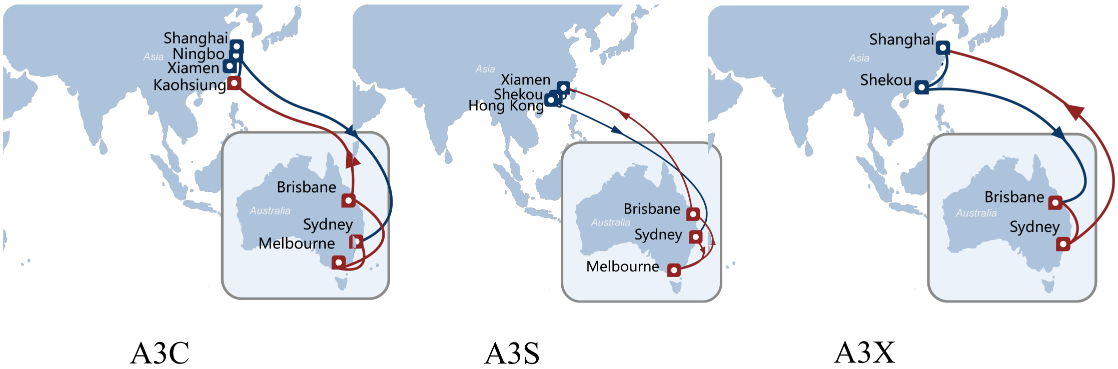

Figure 3.7: Visualization of COSCO shipping lines.

Table 3.1: Information of three COSCO Shipping lines.

Name	Physical port sequence
A3C	Xiamen $\rightarrow$ Shanghai $\rightarrow$ Ningbo $\rightarrow$ Sydney $\rightarrow$ Melbourne $\rightarrow$ Brisbane $\rightarrow$ Kaohsiung $\rightarrow$ Xiamen
A3S	Xiamen $\rightarrow$ HongKong $\rightarrow$ Shekou $\rightarrow$ Sydney $\rightarrow$ Melbourne $\rightarrow$ Brisbane $\rightarrow$ Xiamen
A3X	Shanghai $\rightarrow$ Shekou $\rightarrow$ Brisbane $\rightarrow$ Sydney $\rightarrow$ Shanghai

3.6.2 Results

Based on the given parameters, we first construct the augmented network. The relationship between physical ports and the nodes in the augmented network is presented in Table 3.2. For each physical port, the last two nodes represent the indices of origin o and destination d in the augmented network, respectively. For instance, a shipment from Ningbo to Shanghai is represented as (18, 21).

Table 3.2: Physical ports corresponding to nodes in the augmented shipping network.

Physical port	Nodes in augmented network
Ningbo	3, 18, 19
Shanghai	2, 14, 20, 21
Xiamen	1, 8, 22, 23
Kaohsiung	7, 24, 25
Hong Kong	9, 26, 27
Shekou	10, 15, 28, 29
Brisbane	6, 13, 16, 30, 31
Sydney	4, 11, 17, 32, 33
Melbourne	5, 12, 34, 35

When using Algorithm 3.1 to solve the model in Section 3.4.1 via the discretized sub-models in Section 3.5.3, the computation time is approximately 539 seconds. The optimal h is 0 and the corresponding objective function value is 76 million USD, selecting routes A3C and A3S for transportation. When using Algorithm 3.1 to solve the model in Section 3.4.2 via the discretized sub-models in Section 3.5.4, the computation time is approximately 666 seconds. The optimal h is again 0 and the corresponding objective function value is 77 million USD, again selecting routes A3C and A3S for transportation.

The model in Section 3.4.2, which allows transshipment, yields greater revenue (77 million USD $>$ 76 million USD) than the model in Section 3.4.1, which does not allow transshipment. This improvement arises primarily because certain demands, such as $(o, d) = (26, 19)$ (Hong Kong to Ningbo), cannot be directly satisfied by a single route and must rely on transshipment. Although transshipment incurs additional costs, it generates revenue as long as the costs remain manage-

Table 3.3: Comparison of solutions for models in Section 3.4.1 and Section 3.4.2

(o,d)	Demands (q_{od})	Solutions for model in Section 3.4.1			Solutions for model in Section 3.4.2		
		Cargoes accepted y_{od} (TEUs)	Carbon allocation x_{od} (tons)	Harmonic distance $\hat{l}_{od}$ (nm)	Cargoes accepted y_{od} (TEUs)	Carbon allocation x_{od} (tons)	Harmonic distance $\hat{l}_{od}$ (nm)
$(18,31)$	3,300	3,200	0.100	4,073	3,200	0.027	5,286.8
$(18,33)$	4,000	3,900	0.111	4,506	3,900	0.098	19,320.2
$(18,35)$	3,000	2,900	0.124	5,029	2,900	0.026	5,065.0
$(20,33)$	4,000	3,900	0.113	4,583	3,900	0.044	8,743.8
$(22,31)$	3,600	3,500	0.098	3,972	3,500	0.028	5,446.4
$(22,35)$	2,000	1,900	0.121	4,928	1,900	0.026	5,205.8
$(24,35)$	3,700	3,600	0.118	4,776	3,600	0.028	5,473.2
$(26,19)$	1,600	0	0.000	0	1,500	2.046	403,276.2
$(28,27)$	3,600	3,500	0.001	23	3,500	0.032	6,217.4
$(30,19)$	3,400	3,300	0.101	4,091	3,300	0.023	4,437.8
$(30,21)$	2,600	2,500	0.102	4,149	2,500	0.022	4,394.4
$(30,23)$	3,700	3,600	0.098	3,972	3,600	0.020	3,989.4
$(30,27)$	1,900	1,800	0.100	4,063	1,800	0.021	4,179.4
$(32,25)$	3,700	3,600	0.105	4,254	3,600	0.025	4,947.6
$(32,29)$	2,000	1,900	0.111	4,502	1,900	0.027	5,322.8
$(34,21)$	2,800	2,700	0.126	5,112	2,700	0.027	5,383.8

able. Moreover, transshipment increases the total volume of cargoes that can be accepted, i.e., for $(o, d) \in \mathbf{W} \setminus \{(26, 19)\}$, and dilutes the carbon emission allocation for other demands.

To investigate the effect of the value of $h \in \mathbf{H}$ on the sub-models, we record the objective function values for each sub-model under various h, as presented in Table 3.4. It is evident that in the model without transshipment (the model in Section 3.4.1), changes in h do not significantly affect the objective function value. This is because the shortest sailing distance l'_{od} and the traveling distance for each route l^r_{od} are identical for all $(o, d) \in \mathbf{W}$ in these routes. Similarly, in the model that considers transshipment (model in Section 3.4.2), the objective function values are similar for h ranging from 0 to 0.9, although they are significantly larger than the value at $h = 1$ (traveling distance).

Table 3.4: Objective function values for sub-models under different h

h	Objective function value for sub-model in Section 3.4.1 (1000 USD)	Objective function value for sub-model in Section 3.4.2 (1000 USD)
0	76,895	77,270
0.1	76,895	77,270
0.2	76,895	77,270
0.3	76,895	77,270
0.4	76,895	77,270
0.5	76,895	77,270
0.6	76,895	77,270
0.7	76,895	77,270
0.8	76,895	77,270
0.9	76,895	77,270
1	76,895	75,980

3.7 Robustness Tests

As the shortest sailing distance l'_{od} and the traveling distance l^r_{od} are essentially the same in real-world navigation in the absence of transshipment, the harmonic factor h does not affect the harmonic distance $\hat{l}_{od}$ in the model without transshipment (model in Section 3.4.1). As a result, the specific distance used for this model does not make a substantive difference. However, when transshipment is considered (model in Section 3.4.2), cargoes can be transferred between routes. While this incurs some transshipment costs, it also allows for the transportation of additional cargoes that would otherwise be unshippable, resulting in additional benefits. With transshipment, the traveling distance may differ from the shortest sailing distance, and in this context, the values of h correspond to different levels of profitability. To further explore the applicability of h in a shipping network, we design a synthetic shipping network in this section, primarily based on the model in Section 3.4.2, which considers transshipment.

3.7.1 Parameter settings for the synthetic shipping network

This synthetic shipping network consists of two routes, denoted 1 and 2, as illustrated in Figure 3.8. Route 1 follows the path $1 \to 2 \to 4 \to 1$, while route 2 follows the path $1 \to 4 \to 3 \to 1$. Based on the total distances for each route and the calculation outlined in Section 3.6.1, the costs C^r of operating routes 1 and 2 are set as 2.88 million USD and 7.20 million USD, respectively. The carbon emissions δ^r generated by routes 1 and 2 are 1,306 tons and 3,264 tons, respectively.

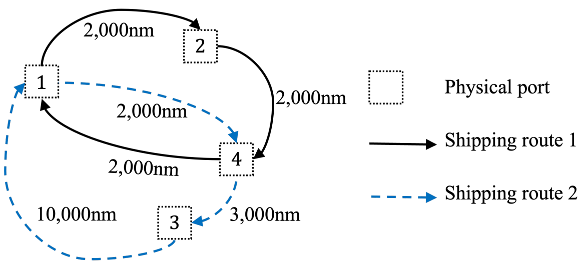

Figure 3.8: Synthetic shipping network.

In this section, we analyze the impact of varying demands q_{od} and the maximum acceptable carbon emission allocation for customers $x_{od}^{\max}$ on the optimal h. All other parameter settings remain consistent with those outlined in Section 3.6.1. Based on the demands provided in Table 3.5, we denote the demand from port 1 to port 4 as a, the demand from port 2 to port 3 as b, and the demand from port 3 to port 1 as c, with all other demands set to 0:

- a can be transported via either shipping route 1 or shipping route 2.
- b can only be transported through transshipment.

- c must be transported directly via shipping route 2.

Table 3.5: Demands q_{od} in synthetic network (TEUs)

	1	2	3	4
1	0	0	0	a
2	0	0	b	0
3	c	0	0	0
4	0	0	0	0

3.7.2 The impact of demand variations

While fixing the maximum acceptable carbon emission allocation at $x_{od}^{\max} = 100$, which reflects that customers have a high tolerance level, we vary the demands a, b, and c. The optimal h values are highlighted in bold in the table and indicated by the red boxes in the figure.

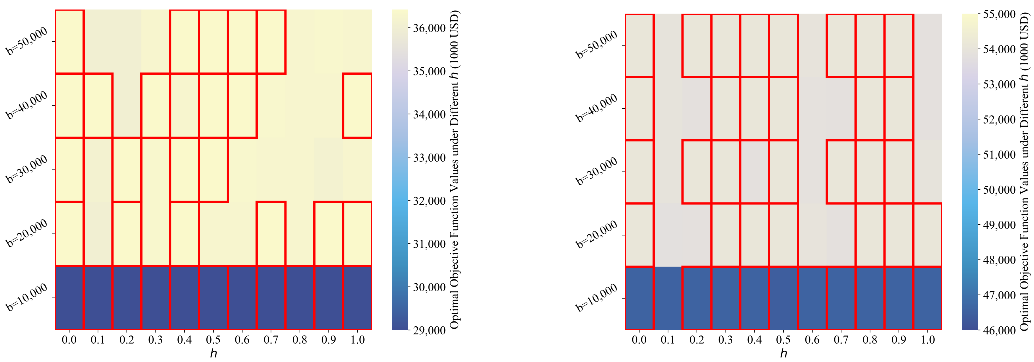

$a = c = 10,000$ $a = c = 20,000$

Figure 3.9: The impact of demand variation on the objective function value when $x_{od}^{\max} = 100$, where the red boxes indicate the optimal h for each line.

In addition, Figure 3.9 uses a color gradient to indicate the magnitude of the objective function values. Darker colors correspond to smaller objective function values, and vice versa. It is observed that as the demand increases, the objective function value also increases, indicated by the lighter colors. However, due to capacity constraints on the routes, the objective function value remains constant beyond a certain threshold value of demand.

We now analyze the impact of varying demand levels on the h. When most of the demand can be satisfied (e.g., $a = b = c = 10,000$), different h values all yield the same objective function value under the condition of a large maximum acceptable carbon emission allocation. However, when more demand remains unmet, not all h values optimize the objective function. Interestingly, under a large maximum acceptable carbon emission allocation, the shortest sailing distance ($h = 0$) consistently produces the optimal objective function values.

Therefore, when customers have a high tolerance for carbon emission allocation, the shortest sailing distance can be used as the basis for carbon emission allocation, regardless of whether the demand exceeds the capacity of the routes.

3.7.3 The impact of customers' maximum acceptable carbon emission allocation

While fixing the demands at $a = b = c = 10,000$, we vary the maximum acceptable carbon emission allocations for customers. The optimal h values are highlighted in bold in the table and indicated by the red boxes in the figure.

In Figure 3.10, a color gradient represents the magnitude of the objective function, with darker colors corresponding to smaller values. It is observed that as $x_{od}^{\max}$ decreases, the objective function value also decreases, as indicated by the darker colors.

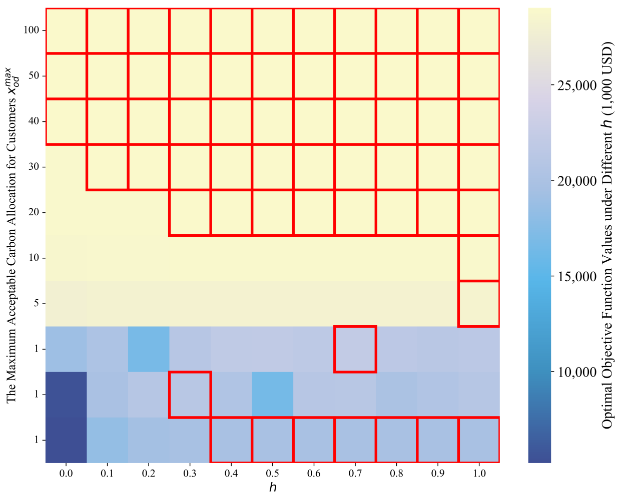

Figure 3.10: The impact of $x_{od}^{\max}$ on the objective function value when
$a = b = c = 10,000$,
where the red boxes indicate the optimal h for each line.

We now analyze the impact of $x_{od}^{\max}$ (customer tolerance for carbon emission allocation) on the h. When $x_{od}^{\max}$ is large, i.e., when customer tolerance for carbon emission allocation is high, varying the value of h does not impact the objective function value if most of the demand can be satisfied. This conclusion aligns with the observations in Section 3.7.2. However, as $x_{od}^{\max}$ becomes more restrictive—for example, when $x_{od}^{\max} \leq 30$ in this synthetic shipping network—not all h values in the sub-model maximize profits.

Notably, the optimal h does not follow a clear pattern under tighter carbon emission allocation constraints. This suggests that in such cases, liner shipping companies should systematically evaluate and select the optimal h as the basis for carbon emission allocation to maximize profitability.

3.8 Conclusions

This study investigates a feasible and efficient carbon emission allocation method from the perspective of liner shipping companies. The carbon surcharge methods currently employed by major liner shipping companies typically consider individual trades on a per-TEU basis, without accounting for variations in distance between different od pairs within the same trade. To address this gap, this study introduces a harmonic distance metric that combines the shortest sailing distance and the traveling distance. This metric serves as the basis for analyzing carbon emission allocation per od pair per TEU. Previous studies have highlighted the importance of precise carbon emission allocation down to the level of specific routes but have not provided corresponding methodologies. Leveraging the shipping network of a company, which includes multiple shipping routes, in this study models are developed for scenarios both without and with transshipment. These models aim to identify the optimal carbon emission allocation policy and cargo flows in the shipping network, with the objective of maximizing the shipping company's profits.

Chapter 4

Optimizing Dual-Fuel Ship Operations with Methane Slip

4.1 Introduction

Maritime shipping plays a crucial role in global trade, transporting approximately 90% of the volume of worldwide cargoes, and it is recognized as the most energy-efficient mode of mass transport (Zhen et al., 2019, 2024). Despite this, the shipping industry contributes significantly to pollution, accounting for 15% of nitrogen oxides emissions, 13% of sulfur dioxide emissions, and 2.7% of carbon dioxide emissions from human activities (Wang et al., 2022). To address these impacts, numerous initiatives have been launched. On January 1, 2015, the International Maritime Organization and regional authorities established four emission control areas to enforce stringent SO_X emission limits on ship exhaust. Within these ECAs established—the Baltic Sea, North Sea, North American, and US Caribbean ECAs—ships are required to use marine fuels with no more than 0.1% sulfur content or to implement equivalent emission-reducing measures (Wang et al., 2021). Building on this framework, the Mediterranean Sea will become the fifth ECA starting from May 1, 2025, where ships must also comply with the 0.10% sulfur limit in fuel oil used on board (IMO, 2022). In addition to regional measures, the IMO has globally reduced the maximum allowable sulfur content in marine fuels from 3.50% to 0.50% for ships operating outside ECAs. As a result, very low-sulfur fuel oil (VLSFO), which typically has a sulfur content of 0.45%–0.50%, is predominantly used outside ECAs (Tan et al., 2022). Furthermore, the EU has implemented the METS, effective from January 1, 2024, to regulate emissions from all large ships (5,000 gross tonnage and above) entering EU ports (European Commission, 2022). Under this system, 50% of CO_2 emissions are charged for shipping legs that begin or end outside the EU, while 100% of CO_2 emissions are charged for legs between two EU ports. Additionally, the EU has enacted a renewable fuel mandate, establishing a 2% sub-target for renewable fuels in marine applications. This mandate ensures that at least 2% of the fuel used in shipping comes from renewable sources (Wang et al., 2023a).

Despite the growing policy support for renewable fuels, it is impractical to replace all conventional fuels with them due to their higher costs and calorific value disparities and insufficient infrastructure developments. Consequently, some shipping companies, such as China Ocean Shipping Company (COSCO), are investing in dual-fuel ships in response to the regulatory environment and support for renewable fuels (Offshore Energy, 2022). Typically, these dual-fuel ships are equipped with bunkers for LNG as well as using conventional fuels such as VLSFO. This enables them to switch between fuel types depending on availability and regulatory requirements. For example, it is preferable for ships to use LNG within ECAs and VLSFO outside them. In addition, several ports now offer LNG bunkering services, enhancing LNG accessibility for ships (Maritime Page, 2025).

When measuring the impact of using LNG, we may consider the life cycle assessment (LCA) methodology. The LCA methodology involves assessing greenhouse gas emissions from fuel production to end-use by a ship, commonly referred to as the "Well-to-Wake" approach. This process consists of two main components: the "Well-to-Tank" part, which covers emissions from primary fuel production to the transport of fuel to the ship's tank (also known as upstream emissions), and the "Tank-to-Wake" part, which addresses emissions from the ship's fuel tank to the exhaust (also known as downstream emissions) (IMO, 2024). LNG has demonstrated significant environmental advantages over heavy fuel oil, reducing emissions of SO_X, NO_X, CO_2, and particulate matter by approximately 98%, 86%, 11%, and 96%, respectively, on a Tank-to-Wake basis (Elgohary et al., 2015). Given these benefits, the IMO and other organizations have introduced various regulations to promote the adoption of LNG in maritime operations, focusing on safety, technical standards, and operational protocols (IMO, 2023). While other environmentally friendly fuels, such as hydrogen and ammonia, are also available, this article focuses on the use of fuels for dual-fuel ships utilizing VLSFO and LNG.

However, the adoption of LNG as a marine fuel faces a significant hurdle due to "*methane slip*," a phenomenon whereby *unburned methane escapes from the engine's combustion chamber and other parts of the storage and transportation systems*. This leakage primarily occurs in low-pressure, dual-fuel four-stroke engines, with methane slip in exhaust plumes averaging 6.4% (Lloyd's List, 2024b). Methane, which makes up 85% to 95% of LNG, contributing significantly to its environmental impact (Environmental Defense Fund, 2022). When measured using global warming potential (GWP)—which is calculated based on the cumulative radiative forcing over a specified time horizon caused by a unit emission of a pollutant relative to an equivalent mass of CO_2—methane has 83 times the warming power of CO_2 over 20 years (Environmental Defense Fund, 2022; Lloyd's List, 2024a). Furthermore, the statistics mentioned above are primarily based on the Tank-to-Wake basis, which ignores emissions upstream of the well. When upstream emissions are accounted for—shifting from a Tank-to-Wake to a Well-to-Wake basis—the impact of LNG increases by approximately 30% (International Council on Clean Transportation, 2021). This phenomenon is concerning because methane, despite having a lower atmospheric concentration than CO_2, possesses a heat absorption capacity over 80 times greater than that of CO_2, and it therefore contributes significantly to global warming and ozone depletion (Mar et al., 2022). This issue is particularly acute in low-pressure gas engines, which exhibit high levels of methane slip at low operational loads of ships because of the suboptimal fuel utilization characterized by low fuel-air ratios (Ushakov et al., 2019).

Given this context, the aim of this study is to investigate the operations of dual-fuel ships with the consideration of the methane slip issue. Specifically, we consider the operational decisions of container shipping companies, including fleet composition, sailing speeds, and fuel usage strategies. The optimization objective is to minimize shipping companies' combined costs, including fuel expenses and carbon and methane slip taxes. The precision with which methane slip is characterized significantly influences the efficacy of the operational strategy. When describing methane slip, two primary characteristics must be considered:

- Methane slip peaks when ships operate at low speeds, typically under low load conditions, and decreases when ships operate at high speeds, which correspond to high load operations.

- Methane slip must not exceed fuel consumption; otherwise, the viability of LNG as a maritime fuel would be compromised.

The approximate fuel consumption f (in tons) for sailing one nautical mile (nm) at a certain speed v (in knots) can be represented by

$$f(v) = av^2, \tag{4.1}$$

where a is the fuel consumption coefficient (Wang and Meng, 2012; Wang et al., 2013a; Tian et al., 2024). Given the characteristics mentioned above, and referencing Formula (4.1), we formulate the approximate relationship between the amount of methane slip and sailing speed as follows:

$$f_{\mathrm{m}}(v) = bv^{\beta}, \tag{4.2}$$

where b denotes the methane slip coefficient, and β is a parameter controlling the rate of methane slip, where $0 < \beta < 2$.

This methane slip characterization captures all key features of the phenomenon. However, incorporating this characterization into the operational problem introduces nonlinear terms, as shown in Formula (4.2), potentially complicating the solvability of the model. Furthermore, methane slip occurs specifically in the context of using LNG, which is predominantly utilized in dual-fuel ships in ECAs (Wu et al., 2024). Consequently, the strategy for managing both fuel types, i.e., VLSFO and LNG, must be integrated into the model, adding another layer of complexity to the problem.

The contributions of this study are fourfold: First, we provide a precise characterization of the relationship between methane slip and sailing speed, consistent with observed behaviors where the methane slip rate peaks during the lowest load operations and is minimized during the highest load operations. The speed-reliant methane slip function derived from this characterization is adaptable to different sailing speeds, accommodating changes in the parameter β. Second, acknowledging that methane slip predominantly occurs in LNG-based dual-fuel ships—which presents a complex problem—this study develops a dual-fuel usage strategy applicable to such ships. We divide each shipping leg into several segments, considering the fuel usage within and outside ECAs, as well as the different sailing speed limits for port and sea regions. This strategy allows ships not only to switch fuel types between different segment types but also to adjust fuel types within a single type of segment. Third, the presence of several nonlinear terms in the problem increases the difficulty of solving it, with the complexity of the problem varying with different values of β. To address this, we introduce a tailored solution method that uses the sailing time within one nm as a proxy for the original speed. This approach discretizes the sailing time to effectively tackle the challenges posed by higher-power terms in the model. Rigorous mathematical proofs are developed to show the theoretical guarantees of the solution method. Fourth, we conduct numerical experiments using real-world data to test our proposed model and solution method for the considered problem. The results indicate that accounting for methane slip in the operational management of dual-fuel ships can help mitigate financial losses under certain conditions.

The remainder of this chapter is organized as follows. Section 4.2 reviews related literature and summarizes our contributions. The remainder of the paper is organized as follows. Section 4.3 describes the problem and formulates the benchmark nonlinear mixed-integer programming model, setting the context for subsequent analyses. Section 4.4 presents model transformations, proposes the dual-fuel usage strategy, and incorporates time discretization to address the problem, supported by rigorous theoretical validation. Section 4.5 reports the results of the computational experiments conducted on this problem and examines the performance of the proposed method. Section 4.6 concludes this study and proposes future research directions.

4.2 Literature Review

Our study contributes to the field of green shipping, which has garnered significant interest in recent scientific studies (Shangguan et al., 2024; Wang et al., 2023b; Zhen et al., 2020; He et al., 2017; Wan et al., 2016; Kontovas, 2014). Research on green shipping typically falls into one of three categories based on the perspectives adopted, namely research from the perspectives of port operators, shipping companies, and government regulatory bodies (Zhen et al., 2019). Our research is conducted for the operations management of shipping companies, a topic extensively reviewed by Meng et al. (2014). A significant contribution to this field is the study of Song et al. (2015), who introduced considerations of emission costs by addressing a joint tactical planning problem amid uncertainties of ship berthing times. However, optimizing for low bunker consumption often extends voyage durations, which increases the likelihood of schedule delays. To address this tradeoff, Zhang et al. (2022) integrated schedule reliability targets into the design of liner shipping timetables, aiming to simultaneously reduce bunker consumption and minimize schedule delays. Furthermore, He et al. (2024) reduced the operating costs and the carbon emissions by formulating a dual-objective mixed-integer nonlinear programming model. They employed an improved non-dominated sorting genetic algorithm II to solve this model.

In response to the recent introduction of environmental policies, an increasing number of studies have recognized that shipping companies must consider such policies in pursuing optimization. Studies from the perspectives of shipping companies have now incorporated these regulations to maximize profitability while optimizing operational strategies. For instance, some research has focused on the implications of a carbon tax (Gao et al., 2022; Sun et al., 2022; Zhuge et al., 2021; Liu et al., 2021; Wang et al., 2018). Other studies have focused on the requirements of ECAs where ships must use fuels emitting less sulfur, such as LNG. Chen et al. (2018) highlighted that the establishment of ECAs could lead ships to reroute around these areas, potentially causing excessive regional emissions under certain conditions. Tan et al. (2021) analyzed the evasion behavior adopted within ECAs to reduce total costs for shipping companies. In addition, several studies have explored solution methods for shipping companies that consider the impacts of ECAs. Zhen et al. (2018) investigated a mixed-integer programming model in ECAs to reschedule voyage plans and developed a solution method based on tabu search to solve the model effectively. Wang et al. (2021) addressed a comprehensive liner shipping service planning problem in ECAs and introduced a nesting algorithmic framework to address it. Zhou and Wang (2024) devised a nonlinear mixed-integer programming model incorporating nonconvex chance constraints in ECAs to manage demand uncertainties.

While these studies provide a foundation, none of them have considered the methane slip issue that has arisen with the emergence of dual-fuel ships. Given that LNG is preferred within ECAs and that the methane slip rate varies with regard to the sailing speed, a comprehensive understanding of this issue is crucial. Despite the wealth of discussion of fuel types and speeds within ECAs in the operations management, virtually all studies have overlooked the significant issue of methane slip when using LNG. Although some studies have advanced methods for the mitigation of methane slip from the perspectives of physical (Tavakoli et al., 2021; Zarrinkolah and Hosseini, 2023), chemical (Storrvik, 2016), and materials science (Winnes et al., 2020), its impact on the operations management of shipping companies has not been addressed. The real-world effectiveness of these strategies is reduced by their failure to account for the costs and environmental impacts of methane slip. To the best of our knowledge, the only study that has addressed methane slip reduction from an operations management perspective is by Wu et al. (2022b), who developed a nonlinear model for optimizing fleet deployment, ship refueling, and cruising speeds for dual-fuel ships. However, the model of Wu et al. (2022b) employed an averaged leakage rate, which simplifies the problem-solving process compared with using the speed-reliant methane slip function, resulting in a strategy that lacks the necessary precision for real-world applications.

4.3 Problem Formulation

We assume that a container shipping company operates a set of routes, denoted as $\mathbf{R}$. Each route, identified by $r \in \mathbf{R}$, comprises a set of shipping legs, $\mathbf{I}_r$ $(r \in \mathbf{R})$, with each leg $i \in \mathbf{I}_r$ connecting a pair of consecutive ports of call. The EU has implemented the METS, which imposes carbon emissions charges based on whether the origin or destination port is within the EU. However, there is a growing trend toward abolishing METS in favor of a uniform global carbon tax (Lloyd's List, 2024a). This approach not only enhances environmental protection but also simplifies the regulatory framework and eliminates potential tax avoidance, such as shipping lines bypassing EU ports. In this study, we thus consider adopting a uniform carbon tax rate for all shipping routes. Each shipping leg is further subdivided into segments based on two criteria: (i) intersection with ECAs, and (ii) proximity to port regions, which are subject to stricter speed limits than open sea regions. Here, we assume that port regions encompass the anchorage and docking areas of each port of call. Therefore, any shipping leg $i \in \mathbf{I}_r,\ r \in \mathbf{R}$, consists of a set of up to four segment types, denoted by $\mathbf{K} = \{1, 2, 3, 4\}$, where type-1 and type-2 segments are those that intersect with ECAs in port regions and sea regions, respectively, and type-3 and type-4 segments intersect with non-ECAs in port regions and sea regions, respectively. The length of leg i ($i \in \mathbf{I}_r$) is denoted by L_i (nm), and the length of a specific type of segment $k (k \in \mathbf{K})$ for leg i is denoted by L_i^k (nm), where $L_i = \sum_{k \in \mathbf{K}} L_i^k$. The basic assumptions of this research are as follows:

Assumption 1 *All ships considered in this study are equipped with dual-fuel capabilities, allowing them to switch between VLSFO and LNG across different shipping legs. In addition, the fleet consists of a uniform type of ships.*

Assumption 2 *Within ECAs, ships are required to use LNG in compliance with emission regulations. Specifically, within the type-1 and type-2 segments, which intersect with ECAs, ships can only use LNG, whereas within type-3 and type-4* *segments, which intersect with non-ECAs, ships can use both types of fuel (LNG and VLSFO).*

Assumption 3 *This study primarily focuses on container shipping services, which typically visit each port of call on a weekly basis (Meng et al., 2014). The model presented in this paper is versatile and can be adapted to other types of shipping services.*

We denote the set of fuel types by **F** ($f \in \mathbf{F}$), where $\mathbf{F} = \{\mathrm{O}, \mathrm{G}\}$; O denotes fuel type VLSFO, and G denotes LNG. We define decision variable m_r ($r \in \mathbf{R}$) to represent the number of ships allocated to route r. For each type of segment k ($k \in \mathbf{K}$) on leg i ($i \in \mathbf{I}_r, r \in \mathbf{R}$), we define decision variable l_{ik}^{f} (nm) to represent the total distances sailed using type f fuel ($f \in \mathbf{F}$), and decision variable $v_{ik}^{f}(x_{ik}^{f})$ (knots) to describe the instant speed corresponding to the instant sailing distance x_{ik}^{f} nm (note that x_{ik}^{f} (nm) is a decision variable as well), where $0 \leq x_{ik}^{f} \leq l_{ik}^{f}$.

We denote the fuel consumption coefficients be $a^f (f \in \mathbf{F})$, which characterize the relationship between the consumption of VLSFO and LNG within the traveling distance of one nm at a given speed. Following Formula (4.1), the fuel consumption for ships sailing at instant x_{ik}^{f} can be expressed as $a^f \left[v_{ik}^{f}(x_{ik}^{f})\right]^2 x_{ik}^{f}$ ($f \in \mathbf{F}, k \in \mathbf{K}, i \in \mathbf{I}_r, r \in \mathbf{R}$). Thus, the VLSFO consumption for sailing a distance of l_{ik}^{O} can be expressed as $a^{\mathrm{O}} \int_0^{l_{ik}^{\mathrm{O}}} \left[v_{ik}^{\mathrm{O}}(x_{ik}^{\mathrm{O}})\right]^2 dx_{ik}^{\mathrm{O}}$ ($k \in \{3,4\}, i \in \mathbf{I}_r, r \in \mathbf{R}$), and the LNG consumption for sailing a distance of l_{ik}^{G} can be expressed as $a^{\mathrm{G}} \int_0^{l_{ik}^{\mathrm{G}}} \left[v_{ik}^{\mathrm{G}}(x_{ik}^{\mathrm{G}})\right]^2 dx_{ik}^{\mathrm{G}}$ ($k \in \mathbf{K}, i \in \mathbf{I}_r, r \in \mathbf{R}$).

In the context of LNG usage, it is essential to factor in methane slip, i.e., unburnt methane emissions. By varying the ship's speed, operators can influence engine loads and consequently the methane slip rate. We use $\hat{a}$ to denote the methane slip conversion rate of a ship using LNG and sailing 1 nm at a given speed. Because the methane slip rate of a ship is higher at lower engine loads when the ship sails at a lower speed, and lower at higher engine loads when the ship sails at a higher speed, the instant methane slip when a ship sails x_{ik}^{G} at instant speed $v_{ik}^{\mathrm{G}}(x_{ik}^{\mathrm{G}})$ in a type-k segment of leg i can be formulated by $\hat{a}\left[v_{ik}^{\mathrm{G}}(x_{ik}^{\mathrm{G}})\right]^{\beta} x_{ik}^{\mathrm{G}}$ $(k \in \mathbf{K}, i \in \mathbf{I}_r, r \in \mathbf{R})$. Here, we assume that $0 < \beta < 2$ because the methane slip amount must be lower than the LNG consumption; otherwise, LNG would have no practical significance. Therefore, the cumulative methane slip amount for sailing a distance of l_{ik}^{G} can be denoted by $\hat{a}\int_0^{l_{ik}^{\mathrm{G}}}\left[v_{ik}^{\mathrm{G}}(x_{ik}^{\mathrm{G}})\right]^{\beta} dx_{ik}^{\mathrm{G}}$.

Before formulating the benchmark model, referred to as M1, we define the following additional parameters: V denotes the number of available ships, p_{o} denotes the weekly operating costs (\$) of a ship, p_{c} denotes the carbon tax (\$/ton), and p_{m} denotes the methane slip tax (\$/ton). Given that the GWP of methane is 83 times the warming power of CO_2 over a 20-year period and 30 times the warming power of CO_2 over a 100-year period, we select the 100-year GWP as the indicator. If the GWP over a 100-year period is significant, the impact over 20 years will be even more pronounced (Environmental Defense Fund, 2022). Accordingly, we use the 100-year GWP to convert p_{m}, resulting in $p_{\mathrm{m}} = 30p_{\mathrm{c}}$. The carbon emission coefficients γ^f $(f \in \mathbf{F})$ correspond to the fuel-to-emission conversion rates. α^f $(f \in \mathbf{F})$ denotes the unit price for fuel f (\$/ton), and T_r $(r \in \mathbf{R})$ indicates the total berthing time for ships on route r (hours). The objective of the model is to minimize the container shipping company's total costs, which consist of operating costs, environmental taxes, and fuel costs, shown as follows:

$$
\begin{aligned}
\min \quad & \underbrace{p_{\mathrm{o}} \sum_{r \in \mathbf{R}} m_r}_{\text{Total operating costs for all deployed ships}} \\
& + \underbrace{\sum_{r \in \mathbf{R}} \sum_{i \in \mathbf{I}_r} \sum_{k \in \{1,2\}} \alpha^{\mathrm{G}} \left[\underbrace{a^{\mathrm{G}} \int_0^{l_{ik}^{\mathrm{G}}} \left[v_{ik}^{\mathrm{G}}(x_{ik}^{\mathrm{G}}) \right]^2 dx_{ik}^{\mathrm{G}}}_{\text{Fuel consumption for sailing}} + \underbrace{\hat{a} \int_0^{l_{ik}^{\mathrm{G}}} \left[v_{ik}^{\mathrm{G}}(x_{ik}^{\mathrm{G}}) \right]^{\beta} dx_{ik}^{\mathrm{G}}}_{\text{Fuel consumption by methane slip}} \right]}_{\text{Overall fuel costs for type-1 and -2 segments}} \\
& + \underbrace{\sum_{r \in \mathbf{R}} \sum_{i \in \mathbf{I}_r} \sum_{k \in \{3,4\}} \left[\sum_{f \in \mathbf{F}} \underbrace{\alpha^f a^f \int_0^{l_{ik}^f} \left[v_{ik}^f(x_{ik}^f) \right]^2 dx_{ik}^f}_{\text{Fuel costs for sailing}} + \underbrace{\alpha^{\mathrm{G}} \hat{a} \int_0^{l_{ik}^{\mathrm{G}}} \left[v_{ik}^{\mathrm{G}}(x_{ik}^{\mathrm{G}}) \right]^{\beta} dx_{ik}^{\mathrm{G}}}_{\text{Fuel costs by methane slip}} \right]}_{\text{Overall fuel costs for type-3 and -4 segments}} \\
& + \underbrace{p_{\mathrm{c}} \sum_{r \in \mathbf{R}} \sum_{i \in \mathbf{I}_r} \left(\sum_{k \in \{1,2\}} \gamma^{\mathrm{G}} a^{\mathrm{G}} \int_0^{l_{ik}^{\mathrm{G}}} \left[v_{ik}^{\mathrm{G}}(x_{ik}^{\mathrm{G}}) \right]^2 dx_{ik}^{\mathrm{G}} + \sum_{k \in \{3,4\}} \sum_{f \in \mathbf{F}} \gamma^f a^f \int_0^{l_{ik}^f} \left[v_{ik}^f(x_{ik}^f) \right]^2 dx_{ik}^f \right)}_{\text{Overall carbon taxes incurred by } \mathrm{CO}_2 \text{ emissions}} \\
& + \underbrace{p_{\mathrm{m}} \hat{a} \sum_{r \in \mathbf{R}} \sum_{i \in \mathbf{I}_r} \left(\sum_{k \in \{1,2\}} \int_0^{l_{ik}^{\mathrm{G}}} \left[v_{ik}^{\mathrm{G}}(x_{ik}^{\mathrm{G}}) \right]^{\beta} dx_{ik}^{\mathrm{G}} + \sum_{k \in \{3,4\}} \int_0^{l_{ik}^{\mathrm{G}}} \left[v_{ik}^{\mathrm{G}}(x_{ik}^{\mathrm{G}}) \right]^{\beta} dx_{ik}^{\mathrm{G}} \right)}_{\text{Overall methane slip taxes}}.
\end{aligned} \tag{4.3}
$$

Next, we consider the following constraints:

The sum of all ships allocated to each route must not exceed the total number of ships available for deployment:

$$\sum_{r \in \mathbf{R}} m_r \leq V. \tag{4.4}$$

In this study, time parameters are measured in hours. Considering the weekly service requirement for each route, there are a total of 168 (7×24) hours in a week. The aggregate sailing time for all legs within the route, combined with the total docking time at all ports of call, must align with the availability determined by the number of ships deployed on that route:

$$\sum_{i\in\mathbf{I}_r}\left(\sum_{k\in\{1,2\}}\int_0^{l_{ik}^{\mathrm{G}}}\frac{x_{ik}^{\mathrm{G}}}{v_{ik}^{\mathrm{G}}(x_{ik}^{\mathrm{G}})}dx_{ik}^{\mathrm{G}}+\sum_{k\in\{3,4\}}\sum_{f\in\mathbf{F}}\int_0^{l_{ik}^{f}}\frac{x_{ik}^{f}}{v_{ik}^{f}(x_{ik}^{f})}dx_{ik}^{f}\right)+T_r\leq 168m_r, r\in\mathbf{R}. \tag{4.5}$$

For type-1 and -2 segments, which intersect with ECAs, ships can only use LNG for these segments, and the total distance using LNG must cover the entirety of ECA segment. For type-3 and -4 segments, ships can use both types of fuel (LNG and VLSFO), and the total distance sailed using both fuels must cover the entirety of each non-ECA segment.

$$l_{ik}^{\mathrm{G}}=L_i^k, r\in\mathbf{R}, i\in\mathbf{I}_r, k\in\{1,2\} \tag{4.6}$$

$$\sum_{f\in\mathbf{F}}l_{ik}^{f}=L_i^k, r\in\mathbf{R}, i\in\mathbf{I}_r, k\in\{3,4\}. \tag{4.7}$$

The operational speeds of ships must adhere to the designated minimum and maximum limits, which vary depending on whether the ship is navigating within port regions or open sea regions. We use $v_{\text{min}}^{\text{p}}$ and $v_{\text{max}}^{\text{p}}$ to denote the minimum and maximum speeds allowed within port regions, respectively, and $v_{\text{min}}^{\text{s}}$ and $v_{\text{max}}^{\text{s}}$ to denote the corresponding minimum and maximum speeds within sea regions, respectively. We have domains for the following decision variables:

$$v_{\text{min}}^{\text{p}}\leq v_{ik}^{\mathrm{G}}(x_{ik}^{\mathrm{G}})\leq v_{\text{max}}^{\text{p}}, r\in\mathbf{R},\ i\in\mathbf{I}_r, k\in\{1,3\} \tag{4.8}$$

$$v_{\text{min}}^{\text{p}}\leq v_{i3}^{\mathrm{O}}(x_{i3}^{\mathrm{O}})\leq v_{\text{max}}^{\text{p}}, r\in\mathbf{R},\ i\in\mathbf{I}_r \tag{4.9}$$

$$v^{\mathrm{s}}_{\min} \leq v^{\mathrm{G}}_{ik}(x^{\mathrm{G}}_{ik}) \leq v^{\mathrm{s}}_{\max}, r \in \mathbf{R},\ i \in \mathbf{I}_r, k \in \{2, 4\} \tag{4.10}$$

$$v^{\mathrm{s}}_{\min} \leq v^{\mathrm{O}}_{i4}(x^{\mathrm{O}}_{i4}) \leq v^{\mathrm{s}}_{\max}, r \in \mathbf{R},\ i \in \mathbf{I}_r. \tag{4.11}$$

The domains for the other decision variables are as follows:

$$l^{f}_{ik} \geq 0, f \in \mathbf{F}, r \in \mathbf{R},\ i \in \mathbf{I}_r, k \in \mathbf{K} \tag{4.12}$$

$$m_r \in \mathbb{Z}^{+}, r \in \mathbf{R}. \tag{4.13}$$

4.4 Solution Method

To address the primary complexity of the model, this section presents a series of model transformations. First, we introduce a preliminary model transformation to handle the complex integral expressions. Then, to manage the inverse power high-degree terms, we propose a dual-fuel usage strategy and incorporate time discretization to address the issue, supported by rigorous theoretical validation.

4.4.1 A preliminary model transformation

Model M1 features complex integral expressions such as $\int_0^{l^{\mathrm{G}}_{ik}} \left[v^{\mathrm{G}}_{ik}(x^{\mathrm{G}}_{ik})\right]^2 dx^{\mathrm{G}}_{ik}$ and $\int_0^{l^{\mathrm{G}}_{ik}} \left[v^{\mathrm{G}}_{ik}(x^{\mathrm{G}}_{ik})\right]^{\beta} dx^{\mathrm{G}}_{ik}$. These terms introduce an *infinite-dimensional* decision problem, making the model difficult to solve. However, we find that in any optimal solution and for each route, ships using the same type of fuel within segments of the same type will operate at a constant speed. This constancy simplifies the infinite-dimensional decision problem into a finite-dimensional one.

Proposition 1 *In any optimal solution, ships using the same type of fuel within segments of the same type for each route will operate at a constant speed.*

Model M1 presents an infinite-dimensional problem. In this model, we consider the type of fuel f ($f \in \mathbf{F}$) to be used for each segment type k ($k \in \mathbf{K}$) of each leg i ($i \in \mathbf{I}_r$) on each route r ($r \in \mathbf{R}$), as well as the corresponding speed and sailing distance. Thus, M1 can be regarded as a *shipping leg-wise* decision problem. However, according to Proposition 1, because ships operate at a constant speed when using the same type of fuel across segments of the same type on each route, this obviates the need to consider the decisions for each individual leg on each route. Because focusing solely on the four segment types is sufficient, the *shipping leg-wise* decision problem is transformed into a *segment type-wise* decision problem. Consequently, we develop an equivalent model, in which the decision variables are defined as follows:

- The speed of using each type of fuel for each type of segment in each route is represented by v_{rk}^{f} ($f \in \mathbf{F}, k \in \mathbf{K}, r \in \mathbf{R}$), which replaces $v_{ik}^{f}(x_{ik}^{f})$ ($f \in \mathbf{F}, k \in \mathbf{K}, i \in \mathbf{I}_r, r \in \mathbf{R}$) in model M1.
- The distance for which ships use each type of fuel for type-3 and type-4 segments on each route is denoted by l_{rk}^{f} ($k \in \{3, 4\}, f \in \mathbf{F}, r \in \mathbf{R}$), thereby avoiding the redundant use of x_{ik}^{f} ($f \in \mathbf{F}, k \in \{3, 4\}, i \in \mathbf{I}_r, r \in \mathbf{R}$) in model M1.

By establishing these two types of decision variables, we eliminate the need to consider the decisions for every shipping leg i ($i \in \mathbf{I}_r$) on each route r ($r \in \mathbf{R}$). This transformation effectively reduces the number of dimensions considered in the decision variables by one for each route. More importantly, by considering the *segment type-wise* characteristic, M1 is transformed into a finite-dimensional decision problem. In the transformed model, for each route r, the decision variables comprise m_r, v_{rk}^{G}, v_{rk}^{f}, and l_{rk}^{f}. We denote the total length of type-k segments on route r by $L'_{rk} = \sum_{i \in \mathbf{I}_r} L_i^k, k \in \mathbf{K}, r \in \mathbf{R}$. Additionally, to facilitate subsequent analyses, we use $t^f_{rk}(k \in \mathbf{K}, f \in \mathbf{F})$ to denote the time required to sail for 1 nm at speed v^f_{rk}, i.e., $t^f_{rk} = 1/v^f_{rk}$. Consequently, the transformed model M2 is as follows:

$$\begin{aligned}
\min p_{\text{o}} \sum_{r \in \mathbf{R}} m_r &+ \sum_{r \in \mathbf{R}} \sum_{k \in \{1,2\}} \alpha^{\text{G}} \left[a^{\text{G}} l^{\text{G}}_{rk} \left(t^{\text{G}}_{rk}\right)^{-2} + \hat{a} l^{\text{G}}_{rk} \left(t^{\text{G}}_{rk}\right)^{-\beta} \right] \\
&+ \sum_{r \in \mathbf{R}} \sum_{k \in \{3,4\}} \left[\sum_{f \in \mathbf{F}} \alpha^f a^f l^f_{rk} \left(t^f_{rk}\right)^{-2} + \alpha^{\text{G}} \hat{a} l^{\text{G}}_{rk} \left(t^{\text{G}}_{rk}\right)^{-\beta} \right] \\
&+ p_{\text{c}} \sum_{r \in \mathbf{R}} \left[\sum_{k \in \{1,2\}} \gamma^{\text{G}} a^{\text{G}} l^{\text{G}}_{rk} \left(t^{\text{G}}_{rk}\right)^{-2} + \sum_{k \in \{3,4\}} \sum_{f \in \mathbf{F}} \gamma^f a^f l^f_{rk} \left(t^f_{rk}\right)^{-2} \right] \\
&+ p_{\text{m}} \hat{a} \sum_{r \in \mathbf{R}} \left[\sum_{k \in \{1,2\}} l^{\text{G}}_{rk} \left(t^{\text{G}}_{rk}\right)^{-\beta} + \sum_{k \in \{3,4\}} l^{\text{G}}_{rk} \left(t^{\text{G}}_{rk}\right)^{-\beta} \right]
\end{aligned} \tag{4.14}$$

subject to Constraints (4.4), (4.13), and

$$\sum_{k \in \{1,2\}} l^{\text{G}}_{rk} t^{\text{G}}_{rk} + \sum_{k \in \{3,4\}} \sum_{f \in \mathbf{F}} l^f_{rk} t^f_{rk} + T_r \leq 168 m_r, r \in \mathbf{R} \tag{4.15}$$

$$l^{\text{G}}_{rk} = L'_{rk}, k \in \{1,2\}, r \in \mathbf{R} \tag{4.16}$$

$$\sum_{f \in \mathbf{F}} l^f_{rk} = L'_{rk}, k \in \{3,4\}, r \in \mathbf{R} \tag{4.17}$$

$$\frac{1}{v^{\text{p}}_{\max}} \leq t^{\text{G}}_{rk} \leq \frac{1}{v^{\text{p}}_{\min}}, k \in \{1,3\}, r \in \mathbf{R} \tag{4.18}$$

$$\frac{1}{v^{\text{p}}_{\max}} \leq t^{\text{O}}_{r3} \leq \frac{1}{v^{\text{p}}_{\min}}, r \in \mathbf{R} \tag{4.19}$$

$$\frac{1}{v^{\text{p}}_{\max}} \leq t^{\text{G}}_{rk} \leq \frac{1}{v^{\text{p}}_{\min}}, k \in \{2,4\}, r \in \mathbf{R} \tag{4.20}$$

$$\frac{1}{v^{\text{s}}_{\max}} \leq t^{\text{O}}_{r4} \leq \frac{1}{v^{\text{s}}_{\min}}, r \in \mathbf{R} \tag{4.21}$$

$$l^f_{rk} \geq 0, k \in \mathbf{K}, f \in \mathbf{F}, r \in \mathbf{R}. \tag{4.22}$$

4.4.2 An advanced model reformulation based on the duel-fuel usage strategy

Although model M2 is simpler than model M1, it incorporates some nonlinear terms, including the inverse power high-degree terms $\left(t_{rk}^{f}\right)^{-2}$ and $\left(t_{rk}^{\mathrm{G}}\right)^{-\beta}$, and the product of two decision variables $l_{rk}^{\mathrm{G}}\left(t_{rk}^{\mathrm{G}}\right)^{-\beta}$, all of which add complexity to the solution process. To tackle these complexities, we discretize the sailing time t_{rk}^{f} ($k \in \mathbf{K}, f \in \mathbf{F}, r \in \mathbf{R}$) in this study.

Notably, for type-1 and type-2 segments, which intersect with ECAs, it is mandatory for ships to solely use LNG throughout the segments. Thus, the decision variables are t_{rk}^{G} ($k \in \{1,2\}, r \in \mathbf{R}$). We further denote the total costs for sailing a duration of t_{rk}^{G} by $F^{\mathrm{G}}(t_{rk}^{\mathrm{G}})$. In contrast, for type-3 and type-4 segments, where ships can alternate between the two types of fuel, the decision variables include the sailing time for each type of fuel t_{rk}^{f} ($k \in \{3,4\}, f \in \mathbf{F}, r \in \mathbf{R}$) and the corresponding sailing distance l_{rk}^{f}, where $\sum_{f\in\mathbf{F}} l_{rk}^{f} = L_{rk}^{\prime}$. When we discretize the values of t_{rk}^{f} for type-3 and type-4 segments, solving for the distances l_{rk}^{f} still requires the use of an optimization solver, such as Gurobi.

In this section, to simplify the solving process for type-3 and type-4 segments, we introduce *a dual-fuel usage strategy*, which enables ships to switch fuel usage not only between different types of segments, but also within a single segment type. To this end, we define the total sailing time using two types of fuel for type-k segments within 1 nm on route r as t_{rk} ($k \in \{3,4\}, r \in \mathbf{R}$), where $t_{rk} = \sum_{f\in\mathbf{F}} l_{rk}^{f} t_{rk}^{f} / L_{rk}^{\prime}$. The corresponding costs when ships sail for a duration of t_{rk} are denoted by $F(t_{rk})$. This definition aids in determining the fuel usage strategy t_{rk}^{f} and l_{rk}^{f} ($k \in \{3,4\}, f \in \mathbf{F}, r \in \mathbf{R}$) and the total costs $F(t_{rk})$.

To facilitate a clearer analysis, we standardize the total distance of type-k ($k \in$

$\{3, 4\}$) segments on route r ($r \in \mathbf{R}$) as $L'_{rk} = 1$ nm, noting that the method and conclusions are also applicable to cases where $L'_{rk} > 1$ nm. In this standardized case, the definitions of t_{rk} and t^f_{rk} remain unchanged. However, we introduce a special consideration for l^f_{rk}, specifically, $\sum_{f\in\mathbf{F}} l^f_{rk} = 1$. The total costs for sailing 1 nm with different types of fuel within type-k segments on route r is represented as $F(t_{rk})$ ($k \in \{3, 4\}, r \in \mathbf{R}$). For notational brevity, we omit the subscript rk, and use t to represent the total sailing time when a ship travels 1 nm. Similarly, we use t^f ($f \in \mathbf{F}$) and l^f to represent the sailing time and sailing distance, respectively, using fuel type f within this 1-nm segment.

Before we introduce the dual-fuel strategy, it is instructive to consider a simpler scenario in which ships switch fuel usage only between different types of segments. For this scenario, we propose a single-fuel usage strategy. This strategy is considered a special case within the broader dual-fuel usage strategy framework.

(1) **Single-fuel usage strategy**

We begin by considering that ships utilize only one type of fuel (VLSFO or LNG) within any given segment type. In this scenario, the sailing time t_{rk} is simply denoted as t. For ships exclusively using VLSFO (or LNG), the costs for the duration of t are represented by $F^{\mathrm{O}}(t)$ (or $F^{\mathrm{G}}(t)$). The total costs of using VLSFO exclusively comprise two components, the fuel costs and carbon taxes, and can be calculated by

$$F^{\mathrm{O}}(t) = \left(\alpha^{\mathrm{O}} a^{\mathrm{O}} + p_{\mathrm{c}} \gamma^{\mathrm{O}} a^{\mathrm{O}}\right) t^{-2}. \tag{4.23}$$

In addition to fuel costs and carbon taxes, the total costs for LNG also encompass expenses related to methane slip, and can be represented by

$$F^{\mathrm{G}}(t) = \left(\alpha^{\mathrm{G}} a^{\mathrm{G}} + p_{\mathrm{c}} \gamma^{\mathrm{G}} a^{\mathrm{G}}\right) t^{-2} + \left(\alpha^{\mathrm{G}} \hat{a} + p_{\mathrm{m}} \hat{a}\right) t^{-\beta}. \tag{4.24}$$

Based on Equations (4.23) and (4.24), we further propose Assumption 4.

Assumption 4 *We use t to represent the sailing time for ships that utilize only one type of fuel (either VLSFO or LNG) to travel 1 nm. The costs corresponding to the duration of t for ships using VLSFO can be expressed as $F^O(t) = \left(\alpha^O a^O + p_c \gamma^O a^O\right) t^{-2}$, whereas the costs for LNG are given by*

$$F^G(t) = \left(\alpha^G a^G + p_c \gamma^G a^G\right) t^{-2} + \left(\alpha^G \hat{a} + p_m \hat{a}\right) t^{-\beta}, 0 < \beta < 2.$$

In most real-world scenarios, these two curves intersect at a single point.

To facilitate the analysis, in this section, we generalize these permissible speed ranges for type-3 segments $[v^{\mathrm{p}}_{\mathrm{min}}, v^{\mathrm{p}}_{\mathrm{max}}]$ and type-4 segments $[v^{\mathrm{s}}_{\mathrm{min}}, v^{\mathrm{s}}_{\mathrm{max}}]$ into a single speed range represented by $[v_{\mathrm{min}}, v_{\mathrm{max}}]$. Consequently, the corresponding time range required for a ship to sail 1 nm can be expressed as $[t_{\mathrm{min}}, t_{\mathrm{max}}]$, where $t_{\mathrm{min}} = 1/v_{\mathrm{max}}$ and $t_{\mathrm{max}} = 1/v_{\mathrm{min}}$. According to Assumption 4, the two curves must intersect at a point, as depicted in Figure 4.1. Let t^* represent the horizontal coordinate of the intersection point. In the initial analysis, we assume that $t^* \in [t_{\mathrm{min}}, t_{\mathrm{max}}]$. The intersection point can be calculated by

$$F^{\mathrm{O}}(t) = F^{\mathrm{G}}(t). \tag{4.25}$$

If a ship can only use one type of fuel within one segment type, to minimize the costs, our analysis dictates the following fuel usage strategy based on the value of t:

- When $t \in [t_{\mathrm{min}}, t^*]$, the total costs of using LNG do not exceed those of using VLSFO, and ships should use LNG.
- When $t \in (t^*, t_{\mathrm{max}}]$, the total costs of using LNG exceed those of using VLSFO, and ships should use VLSFO.

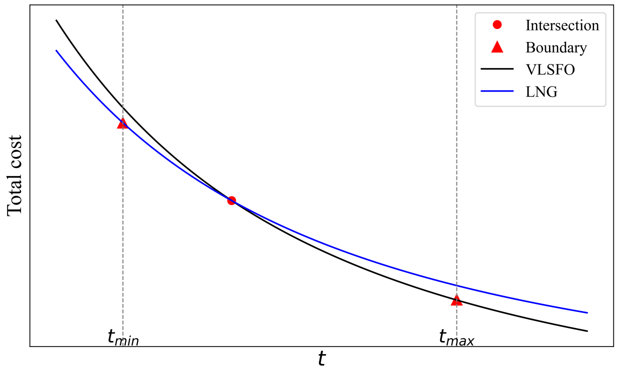

Figure 4.1: The relationship between total costs and the time sailing 1 nm for VLSFO and LNG two types of fuel.

(2) **Dual-fuel usage strategy**

We extend our analysis to the scenario where ships switch fuel types within a single segment type, developing a dual-fuel usage strategy. This approach potentially offers cost reductions compared with the single-fuel usage strategy. Under the dual-fuel usage strategy, once the total sailing time t with two types of fuel for 1 nm is established, we can directly determine the associated decision variables $t^{\mathrm{G}}, t^{\mathrm{O}}, l^{\mathrm{G}}$, and l^{O} within this 1-nm segment, and compute the corresponding total costs $F(t)$.

We demonstrate that the total cost functions for LNG and VLSFO are both convex and differentiable. The curves of these cost functions are decreasing and intersect at a single point, as shown in Figure 4.1. Thus, we can derive a tangent line that intersects the two cost curves simultaneously, yielding one tangent point for each curve, as shown in Figure 4.2. Each point on the tangent line segment represents a convex combination of the total costs associated with the two types of fuel usage.

To elaborate, the tangent points are represented by $(t_1, F^{\mathrm{G}}(t_1))$ and $(t_2, F^{\mathrm{O}}(t_2))$, where $F^{\mathrm{G}}(t_1)$ and $F^{\mathrm{O}}(t_2)$ signify the costs of ships sailing 1 nm at speeds $1/t_1$ and $1/t_2$ for LNG and VLSFO, respectively. The values of $(t_1, F^{\mathrm{G}}(t_1))$ and $(t_2, F^{\mathrm{O}}(t_2))$ can be analytically determined, and the function for the tangent line is defined as $y = (t - t_2)(F^{\mathrm{G}}(t_1) - F^{\mathrm{O}}(t_2))/(t_1 - t_2) + F^{\mathrm{O}}(t_2)$ for $t \in [t_1, t_2]$. Within this interval, the points on the tangent line indicate lower total costs when the ship alternates between LNG and VLSFO, irrespective of the relationship among t_{min}, t_{max}, t_1, and t_2. This finding supports the development of an effective dual-fuel usage strategy, as illustrated in Proposition 2.

Proposition 2 *Within the interval $[t_1, t_2]$, any point on this segment is represented as $(t', F(t'))$, where $F(t')$ denotes a convex combination of the costs of the tangent points $(t_1, F^G(t_1))$ and $(t_2, F^O(t_2))$. This point suggests an effective dual-fuel usage strategy wherein ships should use LNG to sail a distance of $(t_2 - t')/(t_2 - t_1)$ nm at speed $1/t_1$, and use VLSFO to sail $(t' - t_1)/(t_2 - t_1)$ nm at speed $1/t_2$. This strategic combination results in lower total costs compared with using a single type of fuel exclusively, which means that $F(t') \leq \min\{F^G(t_1), F^O(t_2)\}$.*

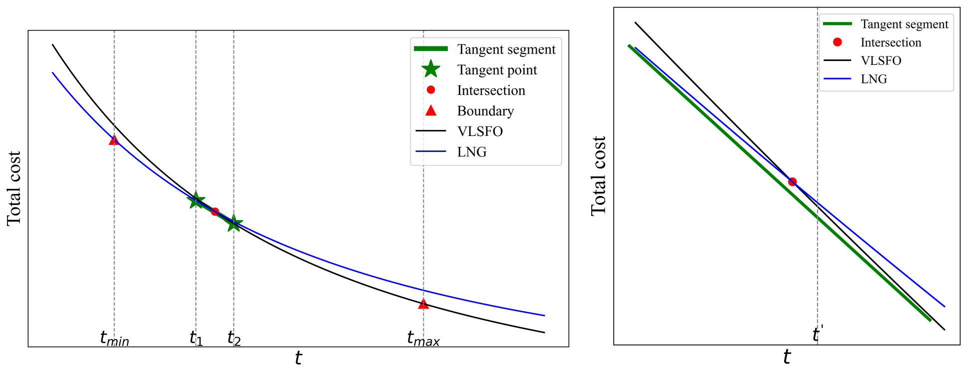

(a) Tangent segment

(b) Enlarged image of tangent segment

Figure 4.2: Tangent segment for costs of two types of fuel.

Proposition 2 demonstrates that within the interval $[t_1, t_2]$, any point on the tangent line signifies a dual-fuel usage strategy with lower total costs than other fuel usage strategies, regardless of the relative values of $t_{\min}$, $t_{\max}$, t_1, and t_2. We further explore various scenarios to consider the different relationships among $t_{\min}$, $t_{\max}$, t_1, and t_2, as shown in Figure 4.3, with full extensions of the dual-fuel usage strategy illustrated in Corollary 1.

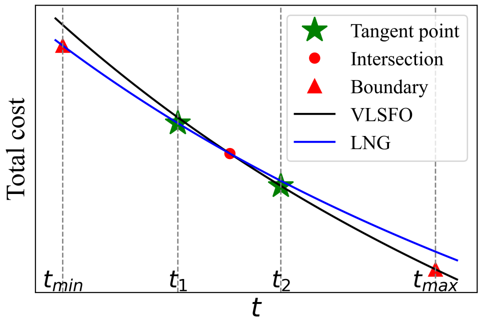

(a) Scenario 1: $t_{\min} \leq t_1 \leq t_2 \leq t_{\max}$

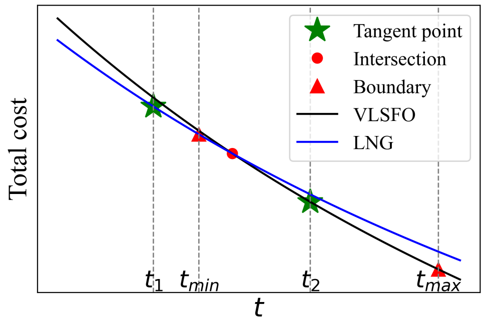

(b) Scenario 2: $t_1 \leq t_{\min} \leq t_2 \leq t_{\max}$

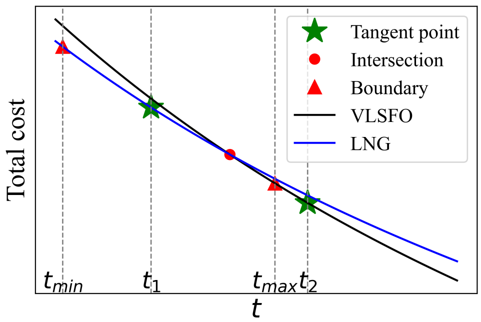

(c) Scenario 3: $t_{\min} \leq t_1 \leq t_{\max} \leq t_2$

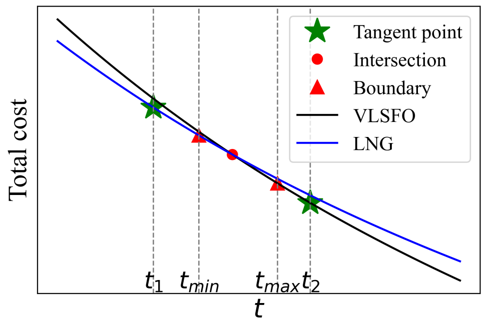

(d) Scenario 4: $t_1 \leq t_{\min} \leq t_{\max} \leq t_2$

Figure 4.3: Four possible relationships between $t_{\min}$, $t_{\max}$, t_1, and t_2.

Corollary 1 *By comparing the values of t_{min}, t_{max}, t_1, and t_2, we identify the following four scenarios along with the corresponding strategic responses within the 1-nm segment of the dual-fuel usage strategy:*

- *Scenario 1: $t_{min} \leq t_1 \leq t_2 \leq t_{max}$.*

- *When* $t \in [t_{min}, t_1]$, *ships should sail using LNG at speed* $1/t$ *for the whole 1 nm, and the corresponding costs are* $F^G(t)$.
- *When* $t \in (t_1, t_2]$, *the optimal strategy is to sail using LNG at speed* $t^G = 1/t_1$ *for length* $l^G = (t_2 - t)/(t_2 - t_1)$ *and sail using VLSFO at speed* $t^O = 1/t_2$ *for length* $l^O = (t - t_1)/(t_2 - t_1)$. *The corresponding costs are* $F(t) = (t - t_2)(F^G(t_1) - F^O(t_2))/(t_1 - t_2) + F^O(t_2)$.
- *When* $t \in (t_2, t_{max}]$, *ships should sail using VLSFO at speed* $1/t$ *for the whole 1 nm, and the corresponding costs are* $F^O(t)$.

• *Scenario 2:* $t_1 \leq t_{min} \leq t_2 \leq t_{max}$.

- *When* $t \in [t_{min}, t_2]$, *the optimal strategy is to sail using LNG at speed* $t^G = 1/t_{min}$ *for length* $l^G = (t_2 - t)/(t_2 - t_{min})$ *and sail using VLSFO at speed* $t^O = 1/t_2$ *for length* $l^O = (t - t_{min})/(t_2 - t_{min})$. *The corresponding costs are* $F(t) = (t - t_2)(F^G(t_{min}) - F^O(t_2))/(t_{min} - t_2) + F^O(t_2)$.
- *When* $t \in (t_2, t_{max}]$, *ships should sail using VLSFO at speed* $1/t$ *for the whole 1 nm, and the corresponding costs are* $F^O(t)$.

• *Scenario 3:* $t_{min} \leq t_1 \leq t_{max} \leq t_2$.

- *When* $t \in [t_{min}, t_1]$, *ships should sail using LNG at speed* $1/t$ *for the whole 1 nm, and the corresponding costs are* $F^G(t)$.
- *When* $t \in (t_1, t_{max}]$, *the optimal strategy is to sail using LNG at speed* $t^G = 1/t_1$ *for length* $l^G = (t_{max} - t)/(t_{max} - t_1)$ *and sail using VLSFO at speed* $t^O = 1/t_{max}$ *for length* $l^O = (t - t_1)/(t_{max} - t_1)$. *The corresponding costs are* $F(t) = (t - t_{max})(F^G(t_1) - F^O(t_{max}))/(t_1 - t_{max}) + F^O(t_{max})$.

• *Scenario 4:* $t_1 \leq t_{min} \leq t_{max} \leq t_2$.

- *For the whole region* $t \in [t_{min}, t_{max}]$, *the optimal strategy is to sail using LNG at speed* $t^G = 1/(t_{min})$ *for length* $l^G = (t_{max} - t)/(t_{max} - t_{min})$ *and sail using VLSFO at speed* $t^O = 1/t_{max}$ *for length* $l^O = (t - t_{min})/(t_{max} - t_{min})$. *The corresponding costs are* $F(t) = (t - t_{max})(F^G(t_{min}) - F^O(t_{max}))/(t_{min} - t_{max}) +$

$F^O(t_{max})$.

After specifying the parameters $p_{\mathrm{o}}, p_{\mathrm{c}}, p_{\mathrm{m}}, \alpha^{\mathrm{O}}, a^{\mathrm{O}}, \alpha^{\mathrm{G}}, a^{\mathrm{G}}, \hat{a}^{\mathrm{G}}, \gamma^{\mathrm{O}}$, and γ^{G}, we can formulate the total costs of using VLSFO and LNG exclusively, which are $F^{\mathrm{O}}(t)$ and $F^{\mathrm{G}}(t)$, respectively, for $k \in \{3,4\}$ and $r \in \mathbf{R}$ within 1 nm. Simultaneously, with given parameters $v^{\mathrm{p}}_{\max}, v^{\mathrm{p}}_{\min}, v^{\mathrm{s}}_{\max}$, and $v^{\mathrm{s}}_{\min}$, we can determine the range of 1-nm sailing time for type-1 and type-3 segments as $[1/v^{\mathrm{p}}_{\max}, 1/v^{\mathrm{p}}_{\min}]$, and the range of 1-nm sailing time for type-2 and type-4 segments as $[1/v^{\mathrm{s}}_{\max}, 1/v^{\mathrm{s}}_{\min}]$. Therefore, we define the range of sailing time for each type of segment as $[t^k_{\min}, t^k_{\min}]$, where

$$t^k_{\min}, t^k_{\max} = \begin{cases} t^{\mathrm{p}}_{\min}, t^{\mathrm{p}}_{\max} & \text{if } k \in \{1,3\} \\ t^{\mathrm{s}}_{\min}, t^{\mathrm{s}}_{\max} & \text{if } k \in \{2,4\}. \end{cases} \tag{4.26}$$

According to Proposition 2 and Corollary 1, once we determine the total sailing time t_{rk} of using two types of fuel for type-k segments within 1 nm on route r, we can also determine the resulting total costs and corresponding fuel usage strategies. Specifically, for type-3 and type-4 segments, the total costs are $F\left(t_{rk}\right)$ ($k \in \{3,4\}, r \in \mathbf{R}$), and the corresponding fuel usage strategies are $t^{\mathrm{G}}_{rk}, t^{\mathrm{O}}_{rk}, l^{\mathrm{G}}_{rk}$, and l^{O}_{rk}.

Given the above introduction, model M2 can be reformulated effectively into the following model, referred to as M3, shown as follows:

$$\min \quad p_{\mathrm{o}} \sum_{r \in \mathbf{R}} m_r + \sum_{r \in \mathbf{R}} \sum_{k \in \{1,2\}} L'_{rk} F^{\mathrm{G}}\left(t^{\mathrm{G}}_{rk}\right) + \sum_{r \in \mathbf{R}} \sum_{k \in \{3,4\}} L'_{rk} F\left(t_{rk}\right) \tag{4.27}$$

subject to Constraints (4.4), (4.13), (4.22), and

$$\sum_{k \in \{1,2\}} L'_{rk} t^{\mathrm{G}}_{rk} + \sum_{k \in \{3,4\}} L'_{rk} t_{rk} + T_r \leq 168 m_r, r \in \mathbf{R} \tag{4.28}$$

$$F^{\mathrm{O}}(t) = \left(\alpha^{\mathrm{O}} a^{\mathrm{O}} + p_{\mathrm{c}} \gamma^{\mathrm{O}} a^{\mathrm{O}}\right) t^{-2} \tag{4.29}$$

$$F^{\mathrm{G}}(t) = \left(\alpha^{\mathrm{G}} a^{\mathrm{G}} + p_{\mathrm{c}} \gamma^{\mathrm{G}} a^{\mathrm{G}}\right) t^{-2} + \left(\alpha^{\mathrm{G}} \hat{a} + p_{\mathrm{m}} \hat{a}\right) t^{-\beta} \tag{4.30}$$

$$t_{rk}^{\mathrm{G}}, l_{rk}^{\mathrm{G}} = \begin{cases} t_{rk}, L'_{rk} & \text{if } t_{\min}^k \le t_{rk} \le t_1 \\ 0, 0 & \text{if } t_2 \le t_{rk} \le t_{\max}^k \\ \dfrac{t_2 - t_{rk}}{t_2 - t_1} t_1, \dfrac{t_2 - t_{rk}}{t_2 - t_1} L'_{rk} & \text{if } t_{\min}^k \le t_1 \le t_{rk} \le t_2 \le t_{\max}^k \\ \dfrac{t_2 - t_{rk}}{t_2 - t_{\min}^k} t_{\min}^k, \dfrac{t_2 - t_{rk}}{t_2 - t_{\min}^k} L'_{rk} & \text{if } t_1 \le t_{\min}^k \le t_{rk} \le t_2 \le t_{\max}^k \\ \dfrac{t_{\max}^k - t_{rk}}{t_{\max}^k - t_1} t_1, \dfrac{t_{\max}^k - t_{rk}}{t_{\max}^k - t_1} L'_{rk} & \text{if } t_{\min}^k \le t_1 \le t_{rk} \le t_{\max}^k \le t_2 \\ \dfrac{t_{\max}^k - t_{rk}}{t_{\max}^k - t_{\min}^k} t_{\min}^k, \dfrac{t_{\max}^k - t_{rk}}{t_{\max}^k - t_{\min}^k} L'_{rk} & \text{if } t_1 \le t_{\min}^k \le t_{rk} \le t_{\max}^k \le t_2 \end{cases}, k \in \{3,4\}, r \in \mathbf{R} \tag{4.31}$$

$$t_{rk}^{\mathrm{O}}, l_{rk}^{\mathrm{O}} = \begin{cases} 0, 0 & \text{if } t_{\min}^k \le t_{rk} \le t_1 \\ t_{rk}, L'_{rk} & \text{if } t_2 \le t_{rk} \le t_{\max}^k \\ \dfrac{t_{rk} - t_1}{t_2 - t_1} t_2, \dfrac{t_{rk} - t_1}{t_2 - t_1} L'_{rk} & \text{if } t_{\min}^k \le t_1 \le t_{rk} \le t_2 \le t_{\max}^k \\ \dfrac{t_{rk} - t_{\min}^k}{t_2 - t_{\min}^k} t_2, \dfrac{t_{rk} - t_{\min}^k}{t_2 - t_{\min}^k} L'_{rk} & \text{if } t_1 \le t_{\min}^k \le t_{rk} \le t_2 \le t_{\max}^k \\ \dfrac{t_{rk} - t_1}{t_{\max}^k - t_1} t_{\max}^k, \dfrac{t_{rk} - t_1}{t_{\max}^k - t_1} L'_{rk} & \text{if } t_{\min}^k \le t_1 \le t_{rk} \le t_{\max}^k \le t_2 \\ \dfrac{t_{rk} - t_{\min}^k}{t_{\max}^k - t_{\min}^k} t_{\max}^k, \dfrac{t_{rk} - t_{\min}^k}{t_{\max}^k - t_{\min}^k} L'_{rk} & \text{if } t_1 \le t_{\min}^k \le t_{rk} \le t_{\max}^k \le t_2 \end{cases}, k \in \{3,4\}, r \in \mathbf{R} \tag{4.32}$$

$$F\left(t_{rk}\right) = \begin{cases} F^{\mathrm{G}}\left(t_{rk}\right) & \text{if } t_{\min}^k \le t_{rk} \le t_1 \\ F^{\mathrm{O}}\left(t_{rk}\right) & \text{if } t_2 \le t_{rk} \le t_{\max}^k \\ (t_{rk} - t_2)\dfrac{F^{\mathrm{G}}(t_1) - F^{\mathrm{O}}(t_2)}{t_1 - t_2} + F^{\mathrm{O}}(t_2) & \text{if } t_{\min}^k \le t_1 \le t_{rk} \le t_2 \le t_{\max}^k \\ (t_{rk} - t_2)\dfrac{F^{\mathrm{G}}(t_{\min}^k) - F^{\mathrm{O}}(t_2)}{t_{\min}^k - t_2} + F^{\mathrm{O}}(t_2) & \text{if } t_1 \le t_{\min}^k \le t_{rk} \le t_2 \le t_{\max}^k \\ (t_{rk} - t_{\max}^k)\dfrac{F^{\mathrm{G}}(t_1) - F^{\mathrm{O}}(t_{\max}^k)}{t_1 - t_{\max}^k} + F^{\mathrm{O}}(t_{\max}^k) & \text{if } t_{\min}^k \le t_1 \le t_{rk} \le t_{\max}^k \le t_2 \\ (t_{rk} - t_{\max}^k)\dfrac{F^{\mathrm{G}}(t_{\min}^k) - F^{\mathrm{O}}(t_{\max}^k)}{t_{\min}^k - t_{\max}^k} + F^{\mathrm{O}}(t_{\max}^k) & \text{if } t_1 \le t_{\min}^k \le t_{rk} \le t_{\max}^k \le t_2 \end{cases}, k \in \{3,4\}, r \in \mathbf{R} \tag{4.33}$$

$$t^k_{\text{min}} \le t^{\text{G}}_{rk} \le t^k_{\text{max}}, k \in \{1,2\}, r \in \mathbf{R} \tag{4.34}$$

$$t^k_{\text{min}} \le t^f_{rk} \le t^k_{\text{max}}, f \in \mathbf{F}, k \in \{3,4\}, r \in \mathbf{R} \tag{4.35}$$

$$t^k_{\text{min}} \le t_{rk} \le t^k_{\text{max}}, k \in \{3,4\}, r \in \mathbf{R}. \tag{4.36}$$

Based on the four scenarios in Corollary 1, we formulate Constraints (4.31)–(4.33). Given that t_{rk} ($k \in \{3,4\}, r \in$ **R**) is the convex combination of t^f_{rk} ($f \in$ **F**), and considering that t^f_{rk} for all $f \in$ **F** share the same domain as specified in Constraints (4.35), the decision variables t_{rk} and t^f_{rk} share identical domains, as illustrated in Constraints (4.36).

4.4.3 Time discretization

The introduction of the methane slip rate complicates our model considerably. Specifically, the model incorporates several nonlinear terms, including $\left(t^f_{rk}\right)^{-2}$, $\left(t^{\text{G}}_{rk}\right)^{-\beta}$, and $l^{\text{G}}_{rk}\left(t^{\text{G}}_{rk}\right)^{-\beta}$. These nonlinear terms make it challenging to obtain solutions in polynomial time using exact solution methods. Consequently, we employ discretization as a strategy to develop an approximate solution method.

We discretize the sailing time t^{G}_{rk} ($k \in \{1,2\}, r \in$ **R**) and t_{rk} ($k \in \{3,4\}, r \in$ **R**) in model M3. Let $N^{\text{p}} = (t^{\text{p}}_{\text{max}} - t^{\text{p}}_{\text{min}})/\theta$ and $N^{\text{s}} = (t^{\text{s}}_{\text{max}} - t^{\text{s}}_{\text{min}})/\theta$, where θ is the precision of the discretization. Thus, we introduce the following parameters after discretization:

- $t^{\text{G}}_{i_1,1,r} = t^{\text{p}}_{\text{min}} + i_1\theta, i_1 = 0, ..., N^{\text{p}}, r \in$ **R**;
- $t^{\text{G}}_{i_2,2,r} = t^{\text{s}}_{\text{min}} + i_2\theta, i_2 = 0, ..., N^{\text{s}}, r \in$ **R**;
- $t_{i_3,3,r} = t^{\text{p}}_{\text{min}} + i_3\theta, i_3 = 0, ..., N^{\text{p}}, r \in$ **R**;
- $t_{i_4,4,r} = t^{\text{s}}_{\text{min}} + i_4\theta, i_4 = 0, ..., N^{\text{s}}, r \in$ **R**.

We define the following new decision variables:

- $z^{\mathrm{G}}_{i_1,1,r}, i_1 = 0, ..., N^{\mathrm{p}}, r \in \mathbf{R}$: $z^{\mathrm{G}}_{i_1,1,r} = 1$ iff $t^{\mathrm{G}}_{r1} = t^{\mathrm{G}}_{i_1,1,r}$; otherwise, $z^{\mathrm{G}}_{i_1,1,r} = 0$;
- $z^{\mathrm{G}}_{i_2,2,r}, i_2 = 0, ..., N^{\mathrm{s}}, r \in \mathbf{R}$: $z^{\mathrm{G}}_{i_2,2,r} = 1$ iff $t^{\mathrm{G}}_{r2} = t^{\mathrm{G}}_{i_2,2,r}$; otherwise, $z^{\mathrm{G}}_{i_2,2,r} = 0$;
- $z_{i_3,3,r}, i_3 = 0, ..., N^{\mathrm{p}}, r \in \mathbf{R}$: $z_{i_3,3,r} = 1$ iff $t_{r3} = t_{i_3,3,r}$; otherwise, $z_{i_3,3,r} = 0$;
- $z_{i_4,4,r}, i_4 = 0, ..., N^{\mathrm{s}}, r \in \mathbf{R}$: $z_{i_4,4,r} = 1$ iff $t_{r4} = t_{i_4,4,r}$; otherwise, $z_{i_4,4,r} = 0$.

By discretizing the sailing time variables in model M3, we reformulate it into an approximate form, referred to as M4, as follows:

$$\min \quad p_{\mathrm{o}} \sum_{r \in \mathbf{R}} m_r + \sum_{r \in \mathbf{R}} \sum_{k \in \{1,2\}} L'_{rk} F^{\mathrm{G}} \left(t^{\mathrm{G}}_{rk} \right) + \sum_{r \in \mathbf{R}} \sum_{k \in \{3,4\}} L'_{rk} F \left(t_{rk} \right) \tag{4.37}$$

subject to Constraints (4.4), (4.13), (4.22), (4.28)–(4.33), and

$$t^{\mathrm{G}}_{r1} \in \{t^{\mathrm{G}}_{0,1,r}, ..., t^{\mathrm{G}}_{i_1,1,r}, ..., t^{\mathrm{G}}_{N^{\mathrm{p}},1,r}\}, r \in \mathbf{R} \tag{4.38}$$

$$t^{\mathrm{G}}_{r2} \in \{t^{\mathrm{G}}_{0,2,r}, ..., t^{\mathrm{G}}_{i_2,2,r}, ..., t^{\mathrm{G}}_{N^{\mathrm{s}},2,r}\}, r \in \mathbf{R} \tag{4.39}$$

$$t_{r3} \in \{t_{0,3,r}, ..., t_{i_3,3,r}, ..., t_{N^{\mathrm{p}},3,r}\}, r \in \mathbf{R} \tag{4.40}$$

$$t_{r4} \in \{t_{0,4,r}, ..., t_{i_4,4,r}, ..., t_{N^{\mathrm{s}},4,r}\}, r \in \mathbf{R}. \tag{4.41}$$

We denote an optimal solution for model M4 as

$$\hat{\mathbf{x}}^*(\theta) := (m^*_1, t^{\mathrm{G}*}_{11}, t^{\mathrm{G}*}_{12}, t^*_{13}, t^*_{14}, ..., m^*_{|\mathbf{R}|}, t^{\mathrm{G}*}_{|\mathbf{R}|1}, t^{\mathrm{G}*}_{|\mathbf{R}|2}, t^*_{|\mathbf{R}|3}, t^*_{|\mathbf{R}|4}).$$

Each t^*_{rk} ($r \in \mathbf{R}, k \in \{3,4\}$) corresponds to a particular implementation of the dual-fuel usage strategy, i.e., $\left(t^{\mathrm{G}*}_{rk}, l^{\mathrm{G}*}_{rk}, t^{\mathrm{O}*}_{rk}, l^{\mathrm{O}*}_{rk}, r \in \mathbf{R}, k \in \{3,4\}\right)$.

For each route $r \in \mathbf{R}$, the sailing time intervals for the port area $[t^{\mathrm{p}}_{\mathrm{min}}, t^{\mathrm{p}}_{\mathrm{max}}]$ and the sea area $[t^{\mathrm{s}}_{\mathrm{min}}, t^{\mathrm{s}}_{\mathrm{max}}]$ are determined by $v^{\mathrm{p}}_{\mathrm{min}}, v^{\mathrm{p}}_{\mathrm{max}}, v^{\mathrm{s}}_{\mathrm{min}}$, and $v^{\mathrm{s}}_{\mathrm{max}}$, which are constants. With the precision of the discretization θ, we define the sets of the discretization sailing time poits:

$$\mathbf{T}^{\mathrm{G}}_{r1} := \{t^{\mathrm{G}}_{0,1,r}, ..., t^{\mathrm{G}}_{i_1,1,r}, ..., t^{\mathrm{G}}_{N^{\mathrm{p}},1,r}\},$$

$$\mathbf{T}_{r2}^{\mathrm{G}} := \{t_{0,2,r}^{\mathrm{G}}, ..., t_{i_2,2,r}^{\mathrm{G}}, ..., t_{N^{\mathrm{s}},2,r}^{\mathrm{G}}\},$$

$$\mathbf{T}_{r3} := \{t_{0,3,r}, ..., t_{i_3,3,r}, ..., t_{N^{\mathrm{p}},3,r}\},$$

$$\mathbf{T}_{r4} := \{t_{0,4,r}, ..., t_{i_4,4,r}, ..., t_{N^{\mathrm{s}},4,r}\}.$$

For type-1 and type-2 segments, within each discretization set, specifically $t_{i_k,k,r}^{\mathrm{G}} \in \mathbf{T}_{rk}^{\mathrm{G}}, k \in \{1,2\}, r \in \mathbf{R}$, we can directly calculate the total costs $F^{\mathrm{G}}\left(t_{i_k,k,r}^{\mathrm{G}}\right)$ within 1 nm, where $F^{\mathrm{G}}\left(t_{i_k,k,r}^{\mathrm{G}}\right) = \left(\alpha^{\mathrm{G}}a^{\mathrm{G}} + p_{\mathrm{c}}\gamma^{\mathrm{G}}a^{\mathrm{G}}\right)\left(t_{i_k,k,r}^{\mathrm{G}}\right)^{-2} + \left(\alpha^{\mathrm{G}}\hat{a}^{\mathrm{G}} + p_{\mathrm{m}}\hat{a}^{\mathrm{G}}\right)\left(t_{i_k,k,r}^{\mathrm{G}}\right)^{-\beta}$. For type-3 and type-4 segments, we establish the relationships among $t_{\min}, t_{\max}, t_1, t_2$, and $t_{i_k,k,r}$ ($t_{i_k,k,r} \in \mathbf{T}_{rk}, k \in \{3,4\}, r \in \mathbf{R}$), based on the values of input parameters, i.e., $\alpha^{\mathrm{O}}, \alpha^{\mathrm{G}}, a^{\mathrm{O}}, a^{\mathrm{G}}, p_{\mathrm{c}}, \gamma^{\mathrm{O}}, \gamma^{\mathrm{G}}, v_{\max}^{\mathrm{s}}, v_{\min}^{\mathrm{s}}, v_{\max}^{\mathrm{p}}$, and $v_{\min}^{\mathrm{p}}$. The set of these relationships is denoted by $\mathbf{B} = \{b_1, b_2, b_3, b_4, b_5, b_6\}$, where

- b_1: $t_{\min}^k \leq t_{i_k,k,r} \leq t_1$;
- b_2: $t_2 \leq t_{i_k,k,r} \leq t_{\max}^k$;
- b_3: $t_{\min}^k \leq t_1 \leq t_{i_k,k,r} \leq t_2 \leq t_{\max}^k$;
- b_4: $t_1 \leq t_{\min}^k \leq t_{i_k,k,r} \leq t_2 \leq t_{\max}^k$;
- b_5: $t_{\min}^k \leq t_1 \leq t_{i_k,k,r} \leq t_{\max}^k \leq t_2$;
- b_6: $t_1 \leq t_{\min}^k \leq t_{i_k,k,r} \leq t_{\max}^k \leq t_2$.

To minimize the total costs, ships sailing within the type-3 and type-4 segments may use two types of fuel. According to the relationship b_j ($b_j \in \mathbf{B}$) and following Corollary 1, we can determine the optimal strategy for every $t_{i_k,k,r}$, including the sailing time using LNG and VLSFO within the 1-nm segment, i.e., $t_{i_k,k,r}^{\mathrm{G}}$ and $t_{i_k,k,r}^{\mathrm{O}}$, and the corresponding sailing distances, $l_{i_k,k,r}^{\mathrm{G}}$ and $l_{i_k,k,r}^{\mathrm{O}}$, respectively, and obtain the corresponding total costs $F(t_{i_k,k,r})$ for this 1-nm segment.

After discretization, the feasible solution set of model M4 is a proper subset of the solution set of model M3. Therefore, the optimal objective function value obtained from model M4 serves as an upper bound for that of model M3. Note that both models M3 and M4 may admit multiple optimal solutions. Let $\mathbf{X}^*$ and $\hat{\mathbf{X}}^*(\theta)$ be the sets of optimal solutions to models M3 and M4, respectively. For each $\mathbf{x}^* \in \mathbf{X}^*$, define $\mathbf{x}^* := (m_1^{*'}, t_{11}^{\mathrm{G}*'}, t_{12}^{\mathrm{G}*'}, t_{13}^{*'}, t_{14}^{*'}, ..., m_{|\mathbf{R}|}^{*'}, t_{|\mathbf{R}|1}^{\mathrm{G}*'}, t_{|\mathbf{R}|2}^{\mathrm{G}*'}, t_{|\mathbf{R}|3}^{*'}, t_{|\mathbf{R}|4}^{*'})$. We define the costs of implementing the decision $\mathbf{x}^* \in \mathbf{X}^*$ as $G(\mathbf{x}^*)$, i.e., $G(\mathbf{x}^*) = p_{\mathrm{o}} \sum_{r \in \mathbf{R}} m_r^{*'} + \sum_{r \in \mathbf{R}} \sum_{k \in \{1,2\}} L'_{rk} F^{\mathrm{G}} \left(t_{rk}^{\mathrm{G}*'}\right) + \sum_{r \in \mathbf{R}} \sum_{k \in \{3,4\}} L'_{rk} F \left(t_{rk}^{*'}\right)$. Next, we define the costs of implementing the decision $\hat{\mathbf{x}}^*(\theta) \in \hat{\mathbf{X}}^*(\theta)$ as $G(\hat{\mathbf{x}}^*(\theta))$, i.e., $G(\hat{\mathbf{x}}^*(\theta)) = p_{\mathrm{o}} \sum_{r \in \mathbf{R}} m_r^* + \sum_{r \in \mathbf{R}} \sum_{k \in \{1,2\}} L'_{rk} F^{\mathrm{G}} \left(t_{rk}^{\mathrm{G}*}\right) + \sum_{r \in \mathbf{R}} \sum_{k \in \{3,4\}} L'_{rk} F \left(t_{rk}^{*}\right)$.

4.4.4 Theoretical analysis for Model M4

Based on the formulated discretization model M4, we aim to provide theoretical guarantees of the solution method through the following propositions. In Proposition 3, we establish that the objective function G is Lipschitz continuous. Consequently, as θ approaches zero, the costs associated with the solution $\hat{\mathbf{x}}^*(\theta) \in \hat{\mathbf{X}}^*(\theta)$ converge to the optimal costs of model M3, as stated in Proposition 3.

Proposition 3 *As θ approaches zero, the costs of a solution $\hat{\mathbf{x}}^*(\theta) \in \hat{\mathbf{X}}^*(\theta)$ converge to the minimal costs of model M3 $G(\mathbf{x}^*), \mathbf{x}^* \in \mathbf{X}^*$. That is,* $\lim_{\theta \to 0} G(\hat{\mathbf{x}}^*(\theta)) = G(\mathbf{x}^*)$.

Although we demonstrate that the optimal objective function value of the discretization model M4 converges to that of model M3 as θ approaches zero, it is crucial to note that the set of optimal solutions to model M4, i.e., the sequence $\{\hat{\mathbf{x}}^*(\theta)\}$, may not be a singleton. Thus, the optimal solutions in $\{\hat{\mathbf{x}}^*(\theta)\}$ obtained by the discretization model M4 may not necessarily converge to the same solution. We substantiate this claim with a proof using a straightforward example, as stated in Proposition 4.

Proposition 4 *A sequence* $\{\hat{\mathbf{x}}^*(\theta)\}$ *of optimal solutions to discretization model M4, may not converge.*

Define subsequence $\{\hat{\mathbf{x}}^*(\theta_i)\}$ ($i \in [1, \infty)$) of sequence $\{\hat{\mathbf{x}}^*(\theta)\}$ as $\{\hat{\mathbf{x}}^*(\theta_i)\} = \Big\{\Big(m_1^*(\theta_i), t_{11}^{\mathrm{G}*}(\theta_i), t_{12}^{\mathrm{G}*}(\theta_i), t_{13}^*(\theta_i), t_{14}^*(\theta_i), ..., m_{|\mathbf{R}|}^*(\theta_i), t_{|\mathbf{R}|1}^{\mathrm{G}*}(\theta_i), t_{|\mathbf{R}|2}^{\mathrm{G}*}(\theta_i), t_{|\mathbf{R}|3}^*(\theta_i), t_{|\mathbf{R}|4}^*(\theta_i)\Big)\Big\}$. Based on Proposition 4, the optimal solutions in the sequence $\{\hat{\mathbf{x}}^*(\theta)\}$ may not converge. However, we find that the sequence $\{\hat{\mathbf{x}}^*(\theta)\}$ has a subsequence $\{\hat{\mathbf{x}}^*(\theta_i)\}$ that is convergent. Furthermore, each convergent subsequence $\{\hat{\mathbf{x}}^*(\theta_i)\}$ of sequence $\{\hat{\mathbf{x}}^*(\theta)\}$ converges to an optimal solution $\mathbf{x}^*$ for model M3, as illustrated in Propositions 5 and 6. These proofs collectively demonstrate that effective near-optimal solutions can indeed be identified using the discretization model M4.

Proposition 5 *Every sequence* $\{\hat{\mathbf{x}}^*(\theta)\}$ *has a subsequence that is convergent.*

Proposition 6 *Every convergent subsequence of sequence* $\{\hat{\mathbf{x}}^*(\theta)\}$ *converges to an optimal solution* $\mathbf{x}^*$ *for model M3.*

4.5 Computational Experiments

We conduct numerical experiments to examine the findings presented in this paper and provide managerial insights. The experiments are divided into two main parts. The first part involves solving a real-world case. In the second part, we adjust various parameters of the problem, such as the methane slip rate β, to evaluate the performance of the proposed discretization solution method, the effectiveness of the dual-fuel usage strategy, and the impact of the methane slip in operations management. These experiments are performed on a personal computer (Apple M2 Pro 16GB) programmed by Python with the solver Gurobi 10.0.3.

4.5.1 Experimental settings

The average prices α^{O} and α^{G} of VLSFO and LNG are $630/ton and $720/ton, respectively, and their energy densities are 41.6 MJ/kg (Ship&Bunker, 2020) and 55 MJ/kg (Rodrigue, 2017), respectively. Based on the energy density of the two types of fuel and the conversion rate of fuel consumption for a ship with a 5,000 twenty-feet equivalent unit (TEU) capacity (Wang and Meng, 2012), we set $a^{\mathrm{O}} = 0.0041$ and $a^{\mathrm{G}} = 0.0031$. The conversion rate of carbon emissions for VLSFO γ^{O} is about 3.17 kg/ton and that for LNG γ^{G} is about 2.70 kg/ton (Doudnikoff and Lacoste, 2014). Considering that the methane slip amount is much less than the fuel consumption amount, we set $\hat{a} = 0.0010$. According to the EU's emissions trading system allowance prices at close on March 28, 2024, the fee charged for carbon emissions p_{c} is about $100/ton. Furthermore, methane emission costs are calculated based on the GWP over a 100-year period, leading to the relation $p_{\mathrm{m}} = 30p_{\mathrm{c}}$.

We conduct our computational experiments using real-world data. Figure 4.4 shows two shipping lines within Europe, where all legs adopt a uniform carbon tax rate, provided by COSCO Shipping Lines (2025). Using the ports from these two shipping lines, we construct the shipping lines for this case study, including the original shipping routes (shipping lines 1 and 2) and four synthetically generated routes (shipping lines 4 to 6), as shown in Table 4.1. Detailed information about these shipping lines is provided in Table 4.2.

Furthermore, we assume that ships have a capacity of 5000 TEU, with weekly operating costs p_{o} of $115,400. The range of sailing speeds in the sea region is $[v^{\mathrm{s}}_{\mathrm{min}}, v^{\mathrm{s}}_{\mathrm{max}}] = [20, 26]$ knots (Wang and Meng, 2012). The range of sailing speeds

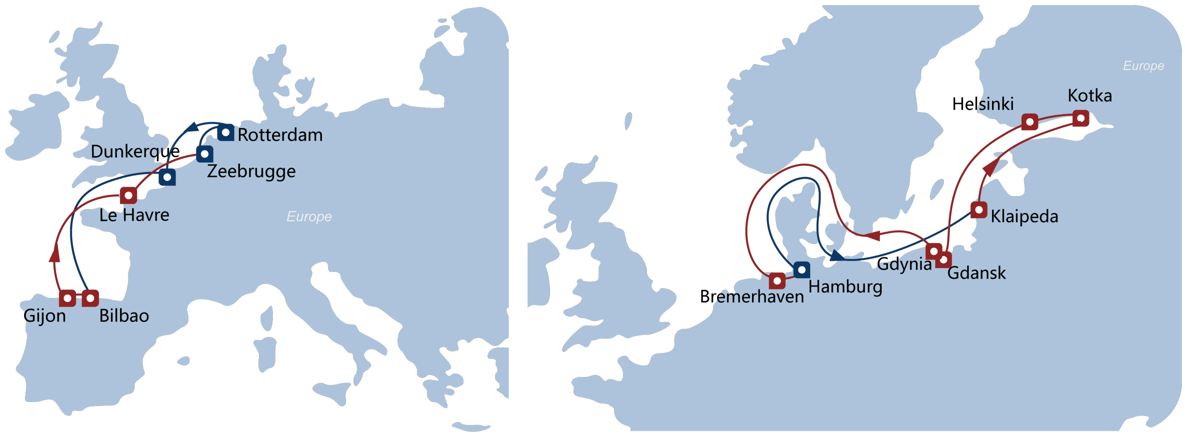

Figure 4.4: COSCO shipping lines.

Table 4.1: Ports of call of each shipping line.

No.	Shipping Lines
1	Zeebrugge → Rotterdam → Dunkerque → Bilbao → Gijon → Zeebrugge
2	Hamburg → Klaipeda → Kotka → Helsinki → Gdansk → Gdynia → Bremerhaven → Hamburg
3	Zeebrugge → Hamburg → Kotka → Helsinki → Gijon → Gdynia → Zeebrugge
4	Rotterdam → Klaipeda → Bilbao → Gdansk → Gijon → Rotterdam
5	Klaipeda → Kotka → Dunkerque → Gdansk → Gijon → Klaipeda
6	Hamburg → Klaipeda → Dunkerque → Bilbao → Hamburg

Table 4.2: Total lengths of four types of segments for each route (nm).

Route	Type-1	Type-2	Type-3	Type-4
1	122	1018	57	795
2	324	2375	0	0
3	439	5059	30	674
4	120	5087	148	1318
5	380	5151	52	652
6	350	2807	25	736

in the port region is based on the port information guides of various ports (Hamburg, 2021), and we set the range to $[v^{\mathrm{p}}_{\min}, v^{\mathrm{p}}_{\max}] = [0, 10]$ knots. We assume that the total docking time T_r ($r \in \mathbf{R}$) for each route is 7 days, and set the total number of ships V available for deployment at 20.

4.5.2 Results

Based on the parameters above, we set the initial discretization precision θ to 0.001 and the methane slip rate β to 0.8. The corresponding intersection speed is 7.1 knots. When using only one type of fuel, ships should use VLSFO when the optimal sailing speeds are lower than the intersection speed; otherwise, they should use LNG. The range of speeds where a dual-fuel usage strategy is advisable is between 6.9 and 7.2 knots, corresponding to sailing time points $[t_1, t_2] = [0.1400, 0.1389]$. Therefore, when the total sailing time t_{rk} ($r \in \mathbf{R}, k \in \{3, 4\}$) for using two types of fuel within 1 nm is within the interval $[0.1400, 0.1389]$, ships should employ the dual-fuel usage strategy.

The solution time is about 5.23 seconds, and the optimal objective value is \$2.67 million. The overall results are shown in Table 4.3. The sailing speeds for all four segment types fall within the required ranges. In type-3 segments, ships utilize both LNG and VLSFO, while in type-4 segments, LNG is used exclusively.

Table 4.3: Number of ships and sailing times (speeds) for four types of segments across all routes.

Route	Number of ships	Sailing speed (knots)				
		Type-1 segments	Type-2 segments	Type-3 segments		Type-4 segments using LNG
1	2	2.3	20.2	2.3	(VLSFO)	20.2
2	2	6.5	20.2	NA		NA
3	3	8.9	20.2	9.2	(LNG)	20.2
4	4	1.4	20.2	1.5	(VLSFO)	20.2
5	3	8.8	20.2	8.6	(LNG)	20.2
6	3	2.3	20.2	2.4	(VLSFO)	20.2

Note: "NA" indicates that there is no speed data for these segments, as their distances are zero.

4.5.3 Sensitivity analyses

(1) **Discretization precision** θ

We first change the discretization precision θ to determine the most suitable value for this case, as shown in Figure 4.5. The horizontal axis indicates the discretization precision from small to large values, and the vertical axes on the left and right represent the total objective function values and the solution time, respectively.

As the discretization precision θ increases, there is an approximate linear reduction in the solution time. Conversely, decreasing the discretization precision θ significantly enhances the objective function value, but only up to $\theta = 0.0005$. Although finer precisions below 0.0005 continue to improve the objective function values, the enhancements are marginal. Consequently, a discretization precision of 0.0005 is considered optimal for this case and is employed in subsequent experiments.

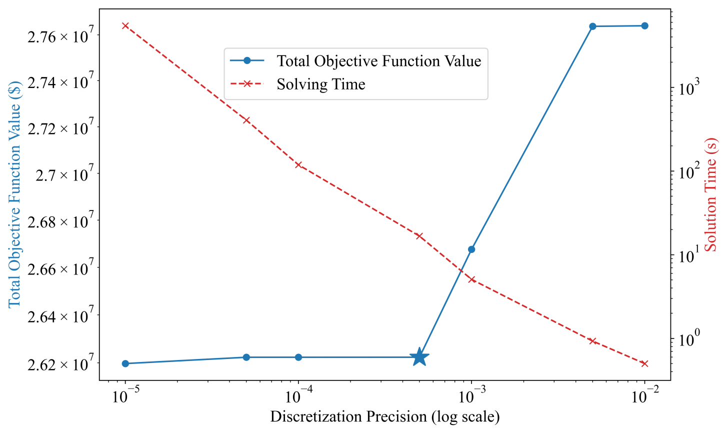

Figure 4.5: Total objective function values and solution times under different discretization precisions.

(2) **The number of available ships** V

Interestingly, in Table 4.3, the sailing speeds for type-2 and type-4 segments are nearly identical across all cases, except for shipping route 2, where the distance the type-4 segments is zero. Since the routes provided in Section 4.5.1 are shorter and require fewer ships, we have scaled up all distances in Table 4.2 by a factor of ten in this part to examine in detail the impact of fleet size on operational decisions. We first explore which option shipping companies prefer when they are presented with a choice between using fewer ships or reducing speeds to save costs. The type-2 and type-4 segments are within sea regions characterized by high-speed sailing, where the impact of methane slip is minor. In this context, ships can reduce their operational costs by adjusting their sailing speeds within the required speed range.

Subsequently, we modify the scale of ship availability, denoted by V, while other parameters remain fixed. In this analysis, we still focus on type-2 and type-4 segments, where ships operate at high speeds and the impact of methane slip is minor. The findings, presented in Table 4.4, show that columns 3 and 5 represent the average speed of ships traveling on all routes, which can be used to assess the effect of ship availability on speeds. Columns 4 and 6 indicate the absolute difference in the speeds of ships across all routes, reflecting variations in speed across different routes. We observe that when ship availability is limited, speed variations increase across routes, and shipping companies are compelled to raise speeds on type-2 and type-4 segments. In contrast, when ships are abundant, companies tend to reduce speeds until ships reach the minimum speed limit.

In Table 4.4, the objective function value when the number of ships is 110 is identical to that when the number is 120, indicating that the speed reaches the minimum speed limit when there are 110 ships. To further investigate the impact of the number of ships on the objective function and analyze the underlying reasons,

Table 4.4: Total objective function values and sailing speeds for type-2 and type-4 segments under different numbers of ships.

Number of ships	Total objective function value (million $)	Average sailing speed in type-2 segments (knots)	Absolute difference in the speeds of ships across all routes in type-2 segments (knots)	Average sailing speed in type-4 segments (knots)	Absolute difference in the speeds of ships across all routes in type-4 segments (knots)
90	28.72	21.3	2.0	22.0	0.9
100	25.43	20.0	0.0	20.0	0.0
110	25.39	20.0	0.0	20.0	0.0
120	25.39	20.0	0.0	20.0	0.0

we vary the number of ships from 90 to 110. The corresponding objective function values and detailed information are presented in Table 4.5. The second column shows the total objective function value, which decreases as the number of ships increases until the minimum speed limit is reached, aligning with the previous analysis. The fourth and seventh columns represent the percentage of the objective function value contributed by type-3 and type-4 segments, respectively. When the methane slip rate is 0.8, the corresponding intersection speed is 7.1 knots, and the recommended speed range for the dual-fuel usage strategy is between 6.9 and 7.2 knots. Although ships in type-4 segments can utilize both LNG and VLSFO, these segments correspond to sea regions where ships must operate within the speed range of $[20, 26]$ knots, which is entirely above the intersection speed and the optimal range for dual-fuel usage. As a result, in this case, the methane slip from LNG usage is minimal, and all ships in type-4 segments operate on LNG regardless of the fleet size.

The fifth and sixth columns present the percentage of sailing distances and total costs associated with LNG usage in type-3 segments. When the number of available ships is tightly constrained (90−95 ships), ships must maintain higher speeds—above the intersection speed and the optimal range for dual-fuel usage—which results in lower methane slip. To minimize costs under these conditions, all ships operate on LNG. However, as the fleet size gradually expands (96−101 ships), some vessels can reduce their speeds to achieve cost savings. This makes it more economical for some ships to switch to VLSFO. As the number of available ships increases further (102−110 ships), all ships eventually transition to VLSFO. At this stage, the primary source of additional cost savings comes from further speed reductions.

(3) **Fee charged for carbon emissions** p_{c}

In this study, we use GWP to convert methane emissions into carbon emission costs. Therefore, the fee charged for carbon emissions p_{c} plays a crucial role in the analysis. To assess the impact of variations in the carbon emission fee on the objective function value and ship speed, we vary the fee from 50 to 150. The corresponding results are presented in Table 4.6. The objective function value increases proportionally with the carbon emission fee, while speed remains unchanged. This is because, all costs—including those from carbon and methane emissions—are standardized using GWP. As long as this conversion relationship remains consistent, changes in the carbon emission fee do not influence ship speed.

4.5.4 The effect of methane slip

When shipping companies develop strategies without considering the methane slip issue, the costs associated with using VLSFO and LNG are illustrated in Figure 4.6. In this scenario, the costs of using LNG are always lower than those of using VLSFO, leading companies to solely use LNG. Thus, without considering

Table 4.5: Total objective function values and corresponding detailed information under different numbers of ships.

Number of ships	Total objective function value (million $)	Percentage of cost for type-1 and type-2 segments in total cost (%)	Percentage of cost for type-3 segments in total cost (%)	Percentage of sailing distances using LNG in type-3 segments (%)	Percentage of cost using LNG in type-3 segments (%)	Percentage of cost for type-4 segments in total cost (%)	Percentage of sailing distances using LNG in type-4 segments (%)
90	28.72	83.67	0.27	100.00	100.00	16.06	100.00
91	27.97	83.92	0.28	100.00	100.00	15.79	100.00
92	27.40	83.83	0.28	100.00	100.00	15.88	100.00
93	26.85	83.68	0.28	100.00	100.00	16.04	100.00
94	26.31	83.62	0.28	100.00	100.00	16.10	100.00
95	25.88	83.47	0.24	100.00	100.00	16.29	100.00
96	25.54	83.80	0.22	81.73	87.60	15.98	100.00
97	25.51	83.78	0.20	72.12	82.20	16.00	100.00
98	25.48	83.76	0.21	72.12	80.90	16.04	100.00
99	25.45	83.74	0.19	55.45	65.78	16.07	100.00
100	25.43	83.73	0.18	47.44	58.17	16.09	100.00
101	25.41	83.76	0.14	18.27	30.03	16.10	100.00
102	25.40	83.76	0.12	0.00	0.00	16.11	100.00
103	25.40	83.76	0.11	0.00	0.00	16.13	100.00
104	25.40	83.75	0.11	0.00	0.00	16.14	100.00
105	25.39	83.74	0.11	0.00	0.00	16.15	100.00
106	25.39	83.74	0.11	0.00	0.00	16.15	100.00
107	25.39	83.74	0.11	0.00	0.00	16.15	100.00
108	25.39	83.73	0.09	0.00	0.00	16.16	100.00
109	25.39	83.74	0.10	0.00	0.00	16.17	100.00
110	25.39	83.74	0.10	0.00	0.00	16.17	100.00

the methane slip problem, we formulate a new model. However, this strategy may incur higher costs compared to one that incorporates the methane slip issue.

To evaluate the impact, we solve this new model under different values of β, and then substitute the solution back into the objective function of model M4 to verify the effect of methane slip. Considering both the presence (reflected in model M4) and absence of the methane slip problem, we calculate the absolute and relative gaps between the objective function values, as shown in Table 4.7. As the value of β decreases, these gaps also decrease. This is because a smaller β value

Table 4.6: Impact of carbon emission fee on total objective function value and sailing speeds.

Carbon emission fee ($/ton)	Total objective function value (million $)	Average sailing speed in Type 1 segments (knots)	Average sailing speed in Type 2 segments (knots)	Average sailing speed in Type 3 segments (knots)	Average sailing speed in Type 4 segments (knots)
50	2.58	3.1	20.0	2.9	20.0
60	2.59	3.1	20.0	2.9	20.0
70	2.60	3.1	20.0	2.9	20.0
80	2.60	3.1	20.0	2.9	20.0
90	2.61	3.1	20.0	2.9	20.0
100	2.62	3.1	20.0	2.9	20.0
110	2.63	3.1	20.0	2.9	20.0
120	2.64	3.1	20.0	2.9	20.0
130	2.65	3.1	20.0	2.9	20.0
140	2.66	3.1	20.0	2.9	20.0
150	2.67	3.1	20.0	2.9	20.0

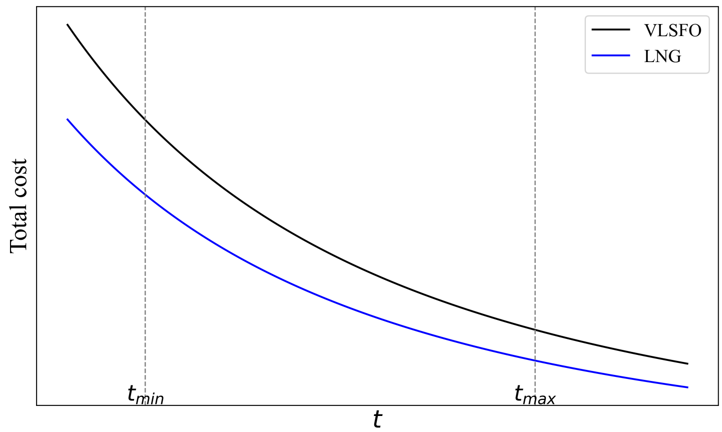

Figure 4.6: The costs of the two types of fuel ignoring the methane slip problem.

results in a lower intersection speed, which in turn reduces the usage of VLSFO.

The methane slip-related term in our model is $\left(\alpha^{\mathrm{G}}\hat{a} + p_{\mathrm{m}}\hat{a}\right) t^{-\beta}$, where $\alpha^{\mathrm{G}}\hat{a} + p_{\mathrm{m}}\hat{a}$ represents the whole methane slip coefficient. Notably, when $\beta = 1.28$, the relative gap reaches its highest value at 0.4601%. To examine the impact of this

Table 4.7: Impact of β on the optimal objective for the methane slip issue.

β	Between model M4 and model E.1		β	Between model M4 and model E.1	
	Absolute Gap ($)	Relative Gap (%)		Absolute Gap ($)	Relative Gap (%)
1.28	135 797.52	0.4601	1.00	1750.76	0.0065
1.27	114 442.28	0.3892	0.90	1180.07	0.0044
1.26	93 720.71	0.3199	0.80	1089.68	0.0042
1.25	73 607.58	0.2522	0.70	1007.33	0.0039
1.24	54 087.09	0.1859	0.60	932.61	0.0036
1.23	35 141.79	0.1212	0.50	862.87	0.0034
1.22	16 754.71	0.0580	0.40	798.19	0.0031
1.21	9216.70	0.0320	0.30	739.16	0.0029
1.20	3410.48	0.0119	0.20	685.25	0.0027
1.10	2497.79	0.0090	0.10	636.50	0.0025

coefficient on the objective function of model M4, we incrementally increase the coefficient by 10% to 50% under $\beta = 1.28$, as detailed in Table 4.8. The results indicate that as the coefficient increases, the corresponding relative gap also rises, reaching a maximum of 1.6285% when the coefficient is increased by 50%.

Table 4.8: Relative gaps between the objective function values of models M4 and E.1 under various values methane slip coefficient.

β	Increasing percent of the methane slip coefficient $\alpha^{\mathrm{G}}\hat{a} + p_{\mathrm{m}}\hat{a}$				
	10%	20%	30%	40%	50%
1.28	0.7034%	0.9428%	1.1764%	1.4043%	1.6285%

Table 4.8 shows that when $\beta = 1.28$, even with a 50% increase in the methane slip coefficient, the corresponding relative gap remains only 1.6285%. Therefore, under the conditions described in Section 4.5.1, methane slip has a relatively minor impact. This is because ships can switch fuel usage on both type-3 and type-4 segments, and as noted in Section 4.5.1, the distances of type-3 and type-4 segments constitute a small percentage of the total distance of each route, thereby minimizing the impact of methane slip.

To further examine the effect of methane slip, we reassign the distances of type-1, -2, -3, and -4 segments in Section 4.1 by swapping them: in the new setting, the distances of type-1 and -2 now correspond to the original distances of type-3 and -4, and vice versa. With $\beta = 1.28$, we again incrementally increase the coefficient from 10% to 50%, and the results are presented in Table 4.9. In this case, when the coefficient is increased by 50%, the corresponding relative gap reaches nearly 9%. At this point, methane slip becomes a significant factor that must be considered in practical operations.

Table 4.9: Relative gaps between the objective function values of models M4 and E.1 under various values of the methane slip coefficient after exchanging the distances between type-1 and type-2 segments with those of type-3 and type-4.

β	Increasing percent of the methane slip coefficient $\alpha^{\mathrm{G}}\hat{a} + p_{\mathrm{m}}\hat{a}$				
	10%	20%	30%	40%	50%
1.28	3.7825%	5.0726%	6.3562%	7.6334%	8.9044%

4.5.5 The Performance of the Proposed Solution Method

In this section, we attempt to solve the exact model M2 for a specified value of β, and evaluate the efficiency and effectiveness of the discretization solution method proposed in this study. In the original model M2, there are two types of nonlinear terms, specifically $(t^f_{rk})^{-2}$ ($f \in \mathbf{F}, r \in \mathbf{R}, k \in \mathbf{K}$) and $(t^{\mathrm{G}}_{rk})^{-\beta}$ ($r \in \mathbf{R}, k \in \mathbf{K}$). Initially, these terms can be converted into hyperbolic inequalities, which can be transformed subsequently into constraints suitable for second-order cone programming (SOCP) (Du et al., 2011).

We begin by transforming the terms $(t^f_{rk})^{-2}$ ($f \in \mathbf{F}, r \in \mathbf{R}, k \in \mathbf{K}$). We conduct similar transformations for terms $(t^{\mathrm{G}}_{rk})^{-\beta}$ by considering two specific scenarios of β: $\beta = 1$ and $\beta = 0.75$. When $\beta = 1$, we also conduct the transformation, allowing us to formulate a new model. When $\beta = 0.75$, the transformation and the new model is also made. Notably, the computational complexity for $\beta = 0.75$ is significantly higher than that for $\beta = 1$.

The transformed models above can be solved directly by Gurobi. Given the complexity of these models, we set both the Feasibility Tolerance and the Optimality Tolerance to their maximum allowable values (0.01). However, Gurobi fails to find the optimal solution for the aforementioned models within 3 hours. Consequently, we limit the maximum solution time to 3 hours. Next, we compare the objective function values achieved within this timeframe with the optimal objective function values determined by the method described in this study, as presented in Table 4.10.

Table 4.10: Comparison of the results of different solution methods.

β	The objective value (OB1) obtained by Gurobi within 3 hours (million \$)	The objective value (OB2) obtained by our solution method (million \$)	Absolute gap (OB1−OB2) (million \$)	Relative gap ((OB1−OB2)/OB2)	Solution time of our solution method (seconds)
1	2.68	2.67	0.0076	0.29%	13.36
0.75	2.59	2.55	0.0351	1.36%	13.42

It is evident that the objective function values obtained within 3 hours by models transformed under SOCP for $\beta = 1$ and $\beta = 0.75$ are inferior to those achieved by the solution method presented in this study. Moreover, our solution method delivers results in a remarkably short time, approximately 13 seconds. The transformation for $\beta = 0.75$ is notably more complex than that for $\beta = 1$ primarily due to the variability in β, which further decelerates the solution process. These observations underscore the difficulty of obtaining an exact optimal solution for the original model M2, and illustrate how the determination surrounding the value of β adds another layer of complexity to the problem.

4.5.6 The effectiveness of the dual-fuel usage strategy

The proposed dual-fuel usage strategy has been proved mathematically feasible (Proposition 2). In this section, we mainly alter the values of β to examine the effectiveness of the dual-fuel usage strategy.

Based on the various values of β, we can obtain the corresponding intersection speeds $1/t_1$ and $1/t_2$ and the range between them $1/t_2 - 1/t_1$, as shown in Figure 4.7. Here, we only show the cases where $\beta \leq 1.28$ because when $\beta = 1.28$, the intersection speed already exceeds the range of speeds, as shown in Figure 4.8. As the value of β increases, the intersection speed also increases, which means that when using only one type of fuel, ships will use VLSFO to minimize the costs induced by methane slip until the optimal sailing speed exceeds the intersection speed.

In the absence of a dual-fuel strategy, we develop a new model based on the single-fuel usage strategy. By solving this new model under various values of β, we obtain results consistent with those from the dual-fuel strategy, indicating that ships do not switch fuel types within the same type of segment. This outcome can be attributed to the very narrow range of $1/t_1$ and $1/t_2$, as indicated in Figure 4.7. Although the ranges between $1/t_1$ and $1/t_2$ expand slightly with the increasing β values, the overall impact remains minor.

Despite these findings, the dual-fuel usage strategy retains its value. Although the results from this model indicate that ships do not switch fuels within a segment type, we cannot disregard potential scenarios where fuel switching within a segment type may occur. Thus, the dual-fuel strategy remains a critical component of our study.

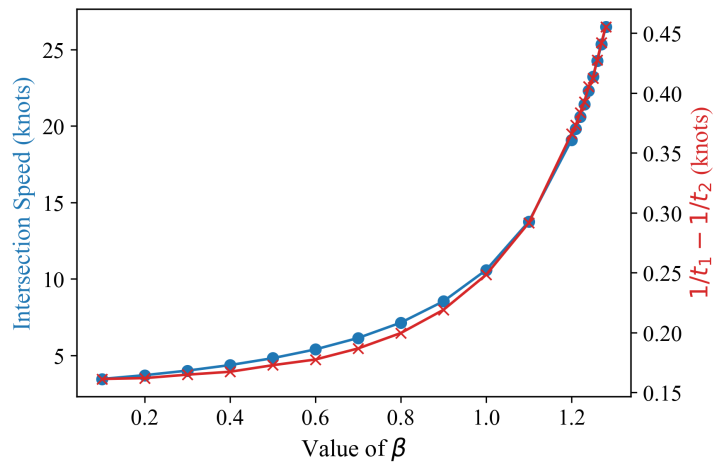

Figure 4.7: The intersection speed and the range between t_1 and t_2 under different values of β.

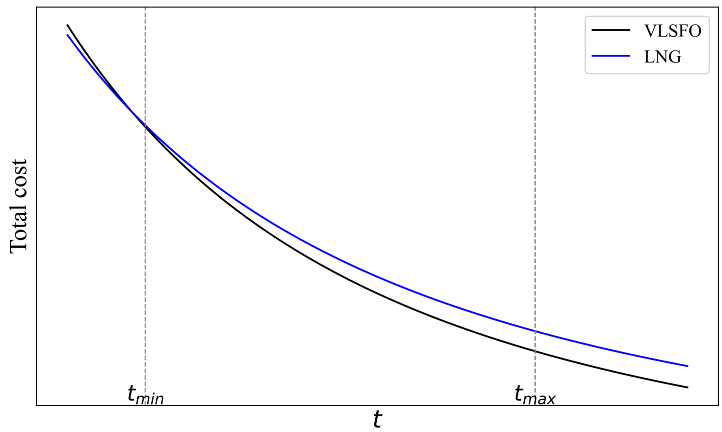

Figure 4.8: The costs of two types of fuel when $\beta = 1.28$.

4.6 Conclusions

Considering the phenomenon of methane slip when ships utilize LNG, this paper conducts a study on the optimal fuel usage strategy for shipping companies to minimize total costs. Recognizing that many ships are equipped with dual-fuel engines, this study compares the costs of VLSFO and LNG, proposing a dual-fuel usage strategy that encompasses a single-fuel usage strategy and allows ships to switch the fuel type within one type of segment. From the perspective of shipping companies, this study develops a model aimed at minimizing the total costs, which include operational costs, fuel expenses, and carbon emission and methane slip taxes. The model incorporates several nonlinear terms that make it difficult to solve, and the determination surrounding the methane slip rate β introduces additional complexity. Finding an exact solution within a short timeframe is challenging, as discussed in Section 4.5.5. Consequently, this paper proposes an effective solution method that substitutes sailing speed with sailing time and discretizes the latter to obtain an appropriate solution. This method shows theoretical guarantees. Finally, this paper validates the model and the proposed method through experiments based on real-world data. These experiments not only explore the impact of the discretization precision and scale of ship availability, but also indicate that accounting for methane slip in the operational management of dual-fuel ships can help mitigate financial losses under certain conditions.

From the perspective of characterizing the phenomenon of methane slip, to the best of our knowledge, this paper is the first to characterize the methane slip rate using a quantitative measure. The functions characterizing the methane slip issue are versatile and can be adapted to a wide range of real-world navigational scenarios. Currently, based on the methane slip phenomenon, our research further explores a dual-fuel usage strategy that is applicable to dual-fuel ships and encompasses all potential fuel switching scenarios. This strategy has been rigorously validated mathematically, enhancing its applicability and reliability in practical settings.

From the methodological perspective, this paper introduces a tailored solution method that addresses the challenges posed by the higher-power terms in the methane slip problem. This tailored method substitutes sailing speed with sailing time and then discretizes the transformed time to construct an approximate model. Rigorous mathematical proofs demonstrate that this approximate model can replicate the same outcomes as the original model, provided that the discretization precision is adequately fine. The experimental evidence detailed in this study further validates that, while the original model poses significant computational challenges, our proposed solution method effectively overcomes these issues and delivers superior results within a limited timeframe.

From a managerial perspective, we conduct numerical experiments using real-world data. The results indicate that considering methane slip is worthwhile for managers of shipping companies. As the coefficient of methane slip increases, its impact on the total costs rises, underscoring its necessity in operational and financial planning.

Chapter 5

Conclusions and Future Research Directions

5.1 Conclusions

This thesis has examined the modeling and optimization of green shipping systems from both governmental and industry perspectives. Through three interconnected studies, we analyze carbon emission allocation, carbon surcharge decision making under network dynamics, and dual-fuel operational strategies considering methane slip, offering comprehensive insights for sustainable maritime policy design and operational planning.

Chapter 2 investigates carbon emission allocation policies from the perspective of governmental regulation. To address the fairness and inefficiency concerns of current carbon surcharge practices, this study develops a bi-level programming model that captures the strategic interactions between regulatory authorities and liner shipping companies. Three carbon allocation measures—based on actual sailing distance, shortest sailing distance, and a convex combination known as harmonic distance—are introduced and evaluated. Numerical experiments and robustness analyses reveal that the allocation approach using the shortest sailing distance yields a socially optimal balance among government, industry, and consumer interests. This method also enhances emission transparency and provides a practical foundation for broader environmental regulation.

Chapter 3 shifts to the decision-making perspective of liner shipping companies and examines how carbon emission allocation influences operational strategies in networks with and without transshipment. A multi-route augmented network is constructed, and two optimization models are developed to determine optimal cargo flows and carbon surcharge policies. Results show that carbon allocation has minimal impact in networks without transshipment, while it plays a decisive role when transshipment is present. These findings highlight the importance of aligning carbon pricing structures with network topology to avoid unintended profit distortions and to support environmentally responsible yet economically sustainable operations.

Chapter 4 studies the optimal fuel usage strategy for dual-fuel ships operating with LNG, considering the phenomenon of methane slip, which increases at lower sailing speeds and poses significant climate risks. A nonlinear mixed-integer programming model is developed to jointly optimize fleet composition, sailing speed, and fuel switching strategies under carbon and methane taxation schemes. To overcome computational challenges, this chapter proposes a solution approach that substitutes sailing speed with discretized sailing time, supported by theoretical guarantees and validated through real-world data experiments. The results indicate that explicitly accounting for methane slip can guide shipping companies toward operational strategies that reduce both financial losses and environmental impacts.

Collectively, these studies demonstrate the importance of integrating environmental considerations with rigorous optimization modeling in maritime transportation. The proposed methodologies contribute to the design of more equitable and effective environmental policies while offering practical operational strategies that enable shipping companies to maintain profitability under tightening sustainability regulations. As the maritime sector continues its transition toward low-carbon and cleaner energy solutions, the insights presented in this thesis provide a timely and valuable foundation for both policy development and industry decision-making.

5.2 Future Research Directions

The first study develops carbon emission allocation policies per TEU per od pair from a governmental perspective, and several promising avenues for future research emerge. First, this study assumes a linear relationship between customer demand and carbon allocation; however, real-world demand is jointly shaped by freight rates, cargo characteristics, port efficiency, distance, and other operational factors. Future work may incorporate demand elasticity and heterogeneity to capture richer customer behavior. Second, the current model considers a single representative shipping company, whereas competitive interactions among multiple firms may significantly influence carbon pricing strategies. Extending the analysis to an oligopolistic market structure could reveal competitive dynamics in emission regulation. Third, the study focuses on a simplified route structure rather than a full-scale network, and future research could integrate complex shipping networks while developing efficient solution algorithms for large-scale bi-level policy design. Finally, future work could incorporate ship loading conditions, since cargo weight affects fuel consumption and emissions; doing so would yield more realistic and comprehensive carbon allocation guidelines. In addition, key parameters such as fuel prices, carbon tax rates, and operating costs are inherently uncertain and subject to market volatility. Incorporating stochastic or robust optimization frameworks would allow policymakers to design carbon allocation schemes that remain effective under parameter uncertainty, thereby improving the practical reliability of regulatory decisions. Finally, extending the static policy design framework to a dynamic, multi-period setting could enable the analysis of long-term policy impacts, such as how carbon taxes influence fleet composition, route structure, and infrastructure investment decisions over time.

The second study examines carbon emission allocation and cargo flow optimization from the perspective of liner shipping companies, particularly in networks with and without transshipment. While the proposed models are validated using real and synthetic network data, additional extensions remain. In transshipment networks, the flexibility to transfer cargo between multiple routes complicates the direct use of either the shortest sailing distance or the actual traveling distance as a universal allocation basis. Future research can systematically explore the conditions under which each carbon allocation policy is most effective, particularly when customer tolerance for carbon emissions varies or when capacity constraints limit feasible cargo flows. Moreover, developing adaptive or case-specific carbon allocation schemes that respond to changing demand, capacity, and regulatory conditions may offer greater robustness and managerial relevance. Building on the uncertainty considerations introduced in the first study, future work may further incorporate stochastic demand, volatile fuel prices, and fluctuating carbon charges into network flow optimization models, enabling shipping companies to derive operational strategies that are resilient to market uncertainty. In addition, adopting a dynamic, multi-period modeling framework would allow researchers to investigate how shipping companies and customers gradually adapt to carbon allocation policies, capturing the long-term effects of such policies on route stability, fleet deployment, transshipment patterns, and infrastructure utilization.

The third study investigates optimal fuel usage strategies for dual-fuel ships under methane slip considerations and suggests several avenues for further research. First, key parameters such as fuel prices, carbon emission taxes, and operating costs are subject to uncertainty. Incorporating stochastic programming approaches would allow future models to explicitly account for parameter variability and enhance solution robustness. Second, expanding the analysis from a "tank-to-wake" perspective to a "well-to-wake" life cycle assessment would enable a more complete evaluation of LNG's environmental performance by including upstream emissions. Third, variations in carbon pricing rules across different shipping legs under policy frameworks such as METS could be incorporated to further refine the operational decision model. In addition, a significant operational challenge for LNG dual-fuel ships arises from the limited and unevenly developed global LNG refueling infrastructure. Incorporating refueling availability and infrastructure constraints into the modeling framework would allow future studies to jointly consider fuel choice, route planning, and speed optimization decisions, thereby better reflecting practical operational conditions. Extending the current framework in these directions would provide a more comprehensive and realistic assessment of dual-fuel operational strategies in practice.

References

Agarwal, R., Ergun, Ö., 2008. Ship scheduling and network design for cargo routing in liner shipping. Transportation Science, 42(2), 175–196.

Alharbi, A., Wang, S., Davy, P., 2015. Schedule design for sustainable container supply chain networks with port time windows. Advanced Engineering Informatics, 29(3), 322–331.

Armstrong, V.N., 2013. Vessel optimization for low carbon shipping. Ocean Engineering, 73, 195–207.

Bell, M.G., Liu, X., Angeloudis, P., Fonzone, A., Hosseinloo, S.H., 2011. A frequency-based maritime container assignment model. Transportation Research Part B: Methodological, 45(8), 1152–1161.

Carratù, M., Chiarini, B., Piselli, P., 2020. Effects of European emission unit allowance auctions on corporate profitability. Energy Policy, 144, 111584.

Cheaitou, A., Cariou, P., 2019. Greening of maritime transportation: A multi-objective optimization approach. Annals of Operations Research, 273(1–2), 501–525.

Chen, L., Yip, T.L., Mou, J., 2018. Provision of emission control area and the impact on shipping route choice and ship emissions. Transportation Research Part D: Transport and Environment, 58, 280–291.

Chua, Y.J., Soudagar, I., Ng, S.H., Meng, Q., 2023. Impact analysis of environmental policies on shipping fleet planning under demand uncertainty. Transportation Research Part D: Transport and Environment, 120, 103744.

Clark, X., Dollar, D., Micco, A., 2004. Port efficiency, maritime transport costs, and bilateral trade. Journal of Development Economics, 75(2), 417–450.

COSCO Shipping Lines, 2025. Available at: `https://lines.coscoshipping.com`.

Cullinane, K., Cullinane, S., 2013. Atmospheric emissions from shipping: The need for regulation and approaches to compliance. Transport Reviews, 33(4), 377–401.

Dai, W.L., Fu, X., Yip, T.L., Hu, H., Wang, K., 2018. Emission charge and liner shipping network configuration–An economic investigation of the Asia–Europe route. Transportation Research Part A: Policy and Practice, 110, 291–305.

De Oliveira, G.F., 2014. Determinants of European freight rates: The role of market power and trade imbalance. Transportation Research Part E: Logistics and Transportation Review, 62, 23–33.

Dong, J.X., Lee, C.Y., Song, D.P., 2015. Joint service capacity planning and dynamic container routing in shipping network with uncertain demands. Transportation Research Part B: Methodological, 78, 404–421.

Doudnikoff, M., Lacoste, R., 2014. Effect of a speed reduction of containerships in response to higher energy costs in sulphur emission control areas. Transportation Research Part D: Transport and Environment, 28, 51–61.

Du, Y., Chen, Q., Quan, X., Long, L., Fung, R.Y., 2011. Berth allocation considering fuel consumption and vessel emissions. Transportation Research Part E: Logistics and Transportation Review, 47(6), 1021–1037.

Elgohary, M.M., Seddiek, I.S., Salem, A.M., 2015. Overview of alternative fuels with emphasis on the potential of liquefied natural gas as future marine fuel. Proceedings of the Institution of Mechanical Engineers, Part M: Journal of Engineering for the Maritime Environment, 229(4), 365–375.

Environmental Defense Fund, 2022. Global Warming Potentials (GWPs)/CO_2-equivalent (CO_{2e}) and the importance of time horizons. Available at: https://www.edf.org/sites/default/files/content/emission_equivalency_tool_documentation_methodology_23062022.pdf.

European Commission, 2022. Reducing emissions from the shipping sector. Available at: https://www.edf.org/sites/default/files/content/emission_equivalency_tool_documentation_methodology_23062022.pdfhttps://climate.ec.europa.eu/eu-action/transport/reducing-emissions-shipping-sector_en.

Gao, S., Xin, X., Li, C., Liu, Y., Chen, K., 2022. Container ocean shipping network design considering carbon tax and choice inertia of cargo owners. Ocean & Coastal Management, 216, 105986.

Garcia, B., Foerster, A., Lin, J., 2021. Net zero for the international shipping sector? An analysis of the implementation and regulatory challenges of the IMO strategy on reduction of GHG emissions. Journal of Environmental Law, 33, 85–112.

Gössling, S., Meyer-Habighorst, C., Humpe, A., 2021. A global review of marine air pollution policies, their scope and effectiveness. Ocean & Coastal Management, 212, 105824.

Guo, J., Kuang, H., Luo, J., 2020. A decision-making model of port carbon emission reduction investment under uncertainty. In IOP Conference Series: Earth and Environmental Science, 598(1), 012110.

Goyal, S., Llop, M., 2024. The shipping industry under the EU Green Deal: An Input–Output impact analysis. Transportation Research Part A: Policy and Practice, 182, 104035.

Hamburg, 2021. Port information guide. Available at: `https://www.hamburg-port-authority.de/fileadmin/user_upload/Port-Information-Guide_2021.pdf`.

He, Q., Zhang, X., Nip, K., 2017. Speed optimization over a path with heterogeneous arc costs. Transportation Research Part B: Methodological, 104, 198–214.

He, S., Xie, H., Feng, Y., 2024. The optimization of fleet deployment for container liner shipping under the carbon tax and energy efficiency operation indicator. ASCE–Journal of Risk and Uncertainty in Engineering Systems, Part A: Civil Engineering, 10(4), 04024056.

Heitmann, N., Khalilian, S., 2011. Accounting for carbon dioxide emissions from international shipping: Burden sharing under different UNFCCC allocation options and regime scenarios. Marine Policy, 35(5), 682–691.

HiFleet. Available at: `https://www.hifleet.com/`.

Hong, Z., Chu, C., Zhang, L.L., Yu, Y., 2017. Optimizing an emission trading scheme for local governments: A Stackelberg game model and hybrid algorithm. International Journal of Production Economics, 193, 172–182.

Huang, Z., Shi, X., Wu, J., Hu, H., Zhao, J., 2013. How will the marine emissions trading scheme influence the profit and CO_2 emissions of a containership. In Computational Logistics: 4th International Conference, ICCL 2013, Copenhagen, Denmark, September, pp. 25–27.

Hu, Z., Huang, Y., Sun, L., Qi, X., Pan, X., 2023. Study on international carbon emission quota allocation of shipping industry-based on fairness and efficiency. Frontiers in Marine Science, 10, 1269643.

IMO, 2020. Fourth IMO GHG Study 2020. International Maritime Organization (IMO), London, UK. Available at: `https://www.imo.org/en/OurWork/Environment/Pages/Fourth-IMO-Greenhouse-Gas-Study-2020.aspx`.

IMO, 2022. IMO progress on revised GHG strategy, Mediterranean ECA adopted. Available at: `https://www.imo.org/en/MediaCentre/PressBriefings/pages/MEPC-79.aspx`.

IMO, 2023. Alternative fuel use–regulatory status mapped. Available at: `https://www.imo.org/en/MediaCentre/Pages/WhatsNew-1841.aspx`.

IMO, 2024. IMO framework on life cycle GHG intensity of marine fuels (LCA). Available at: https://www.imo.org/en/OurWork/Environment/Pages/Lifecycle-GHG---carbon-intensity-guidelines.aspx.

International Council on Clean Transportation, 2021. Accounting for well-to-wake carbon dioxide equivalent emissions in maritime transportation climate policies. Available at: https://theicct.org/sites/default/files/publications/Well-to-wake-co2-mar2021-2.pdf.

Jin, J., Meng, L., Wang, X., He, J., 2024. Carbon emission reduction strategy in shipping industry: A joint mechanism. Advanced Engineering Informatics, 62, 102728.

Jugović, A., Komadina, N., Perić Hadžić, A., 2015. Factors influencing the formation of freight rates on maritime shipping markets. Pomorstvo, 29(1), 23–29.

Kellner, F., 2016. Allocating greenhouse gas emissions to shipments in road freight transportation: Suggestions for a global carbon accounting standard. Energy Policy, 98, 565–575.

Kim, J.G., Kim, H.J., Lee, P.T.W., 2014. Optimizing ship speed to minimize fuel consumption. Transportation Letters, 6(3), 109–117.

Kontovas, C.A., 2014. The green ship routing and scheduling problem (GSRSP): A conceptual approach. Transportation Research Part D: Transport and Environment, 31, 61–69.

Lai, X., Wu, L., Wang, K., Wang, F., 2022. Robust ship fleet deployment with shipping revenue management. Transportation Research Part B: Methodological, 161, 169–196.

Law, L.C., Foscoli, B., Mastorakos, E., Evans, S., 2021. A comparison of alternative fuels for shipping in terms of lifecycle energy & cost. Energies, 14(24), 8502.

Lee, T.C., Chang, Y.T., Lee, P.T., 2013. Economy-wide impact analysis of a carbon tax on international container shipping. Transportation Research Part A: Policy and Practice, 58, 87–102.

Li, L., Pan, Y., Gao, S., Yang, W., 2022. An innovative model to design extreme emission control areas (ECAs) by considering ship's evasion strategy. Ocean & Coastal Management, 227, 106289.

Liao, Z., Zhu, X., Shi, J., 2015. Case study on initial allocation of Shanghai carbon emission trading based on Shapley value. Journal of Cleaner Production, 103, 338–344.

Liang, J., Li, L., Zheng, J., Tan, Z., 2023. Service-oriented container slot allocation policy under stochastic demand. Transportation Research Part B: Methodological, 176, 102799.

Liu, Y., Xin, X., Yang, Z., Chen, K., Li, C., 2021. Liner shipping network–transaction mechanism joint design model considering carbon tax and liner alliance. Ocean & Coastal Management, 212, 105817.

Liu, J., Xu, H., Lyu, Y., 2023. Emission reduction technologies for shipping supply chains under carbon tax with knowledge sharing. Ocean & Coastal Management, 246, 106869.

Lloyd's List, 2024a. Regulation: Shipping will get a global carbon price. Available at: https://www.lloydslist.com/LL1151779/Regulation-Shipping-will-get-a-global-carbon-price.

Lloyd's List, 2024b. LNG engines emit more methane slip than shipping regulators assume, argues study. Available at: https://www.lloydslist.com/LL1148048/LNG-engines-emit-more-methane-slip-than-shipping-regulators-assume-argues-study.

Ma, W., Zhang, J., Han, Y., Zheng, H., Ma, D., Chen, M., 2022. A chaos-coupled multi-objective scheduling decision method for liner shipping based on the NSGA-III algorithm. Computers & Industrial Engineering, 174, 108732.

Maersk, 2023a. EU Emissions Trading System (ETS) effective January 1, 2024. Available at: https://www.maersk.com/news/articles/2023/09/15/eu-emissions-trading-system-ets.

Maersk, 2023b. Rate Announcement–Far East to North Europe. Available at: https://www.maersk.com/news/articles/2023/07/03/rate-announcement-far-east-to-north-europe.

Mao, Z., Ma, A., Zhang, Z., 2024. Towards carbon neutrality in shipping: Impact of European Union's emissions trading system for shipping and China's response. Ocean & Coastal Management, 249, 107006.

Mar, K.A., Unger, C., Walderdorff, L., Butler, T., 2022. Beyond CO_2 equivalence:

The impacts of methane on climate, ecosystems, and health. Environmental Science and Policy, 134, 127–136.

Maritime Page, 2025. What is a dual-fuel engine in a ship: An overview. Available at: `https://maritimepage.com/what-is-a-dual-fuel-engine-in-a-ship/`.

Meng, Q., Wang, S., 2011. Liner shipping service network design with empty container repositioning. Transportation Research Part E: Logistics and Transportation Review, 47(5), 695–708.

Meng, Q., Wang, S., Andersson, H., Thun, K., 2014. Containership routing and scheduling in liner shipping: Overview and future research directions. Transportation Science, 48(2), 265–280.

Mulder, J., Dekker, R., 2014. Methods for strategic liner shipping network design. European Journal of Operational Research, 235(2), 367–377.

Offshore Energy, 2022. COSCO: "World's first" LNG dual-fuel VLCC delivered in China. Available at: `https://www.offshore-energy.biz/cosco-worlds-first-lng-dual-fuel-vlcc-delivered-in-china/`.

Rodrigue, J.P., 2017. *The Geography of Transport Systems*. Routledge, New York.

Romano, A., Yang, Z., 2021. Decarbonisation of shipping: A state of the art survey for 2000–2020. Ocean & Coastal Management, 214, 105936.

Selin, H., Zhang, Y., Dunn, R., Selin, N.E., Lau, A.K., 2021. Mitigation of CO_2 emissions from international shipping through national allocation. Environmental Research Letters, 16(4), 045009.

Shangguan, Y., Tian, X., Pang, K.W., Ruan, Q., Jin, Y., Wang, S., 2024. Navigating the green shipping: Stochastic hydrogen hub deployment in inland waterways. Transportation Research Part D: Transport and Environment, 129, 104126.

Ship&Bunker, 2020. Integr8: VLSFO calorific value, pour point and competitiveness with LSMGO. Available at: `https://shipandbunker.com/news/world/662089-integr8-vVLSFO-calorific-value-pour-point-and-competitiveness-with-lsmgo`.

Ship&Bunker, 2024. Bunker prices. Available at: `https://shipandbunker.com/prices/emea/nwe/nl-rtm-rotterdam#LNG`.

Song, D.P., Li, D., Drake, P., 2015. Multi-objective optimization for planning liner shipping service with uncertain port times. Transportation Research Part E: Logistics and Transportation Review, 84, 1–22.

Stavins, R.N., 1995. Transaction costs and tradeable permits. Journal of Environmental Economics and Management, 29(2), 133–148.

Storrvik, H.M., 2016. Catalysis for Control of Methane Slip in Marine Machinery–Using Platinum-Based Catalysts. Master thesis. Trondheim: Norwegian University of Science and Technology.

Sun, Y., Zheng, J., Han, J., Liu, H., Zhao, Z., 2022. Allocation and reallocation of ship emission permits for liner shipping. Ocean Engineering, 266, 112976.

Sun, Y., Zheng, J., Yang, L., Li, X., 2024. Allocation and trading schemes of the maritime emissions trading system: Liner shipping route choice and carbon emissions. Transport Policy, 148, 60–78.

Tan, Z., Liu, H., Shao, S., Liu, J., Chen, J., 2021. Efficiency of Chinese ECA policy on the coastal emission with evasion behavior of ships. Ocean & Coastal Management, 208, 105635.

Tan, Z., Zhang, M., Shao, S., Liang, J., Sheng, D., 2022. Evasion strategy for a coastal cargo ship with unpunctual arrival penalty under sulfur emission regulation. Transportation Research Part E: Logistics and Transportation Review, 164, 102818.

Tavakoli, S., Schramm, J., Pedersen, E., 2021. Strategies on methane slip mitigation of spark-ignition natural gas engine during transient motion. SAE Technical Paper, 26, 128–140.

Tay, Z.Y., Konovessis, D., 2023. Sustainable energy propulsion system for sea transport to achieve United Nations sustainable development goals: A review. Discover Sustainability, 4(1), 20.

Tian, X., Shangguan, Y., Pang, K.W., Guo, Y., Lyu, M., Wang, S., Huang, G.Q., 2024. Carbon emission allocation policy making in liner shipping: A novel approach toward equitable and efficient maritime sustainability. Ocean & Coastal Management, 256, 107270.

Useche, M.I.I.J., 2023. Maritime shipping in international trade. Doctoral dissertation, Purdue University.

Ushakov, S., Stenersen, D., Einang, P.M., 2019. Methane slip from gas fuelled ships: a comprehensive summary based on measurement data. Journal of Marine Science and Technology, 24(4), 1308–1325.

Wagenborg, 2023. EU Emissions Trading System (ETS) in practice. Available at: `https://www.wagenborg.com/sustainability/wagenborg-is-committed-to-achieve-a-better-climate-and-environment`.

Wan, Z., Zhu, M., Chen, S., Sperling, D., 2016. Pollution: Three steps to a green shipping industry. Nature, 530(7590), 275–277.

Wan, Z., El Makhloufi, A., Chen, Y., Tang, J., 2018. Decarbonizing the international shipping industry: Solutions and policy recommendations. Marine Pollution Bulletin, 126, 428–435.

Wang, C., Chen, J., 2017. Strategies of refueling, sailing speed and ship deployment of containerships in the low-carbon background. Computers & Industrial Engineering, 114, 142–150.

Wang, H., Guo, J., 2024. Research on the impact mechanism of multiple environmental regulations on carbon emissions under the perspective of carbon peaking pressure: A case study of China's coastal regions. Ocean & Coastal Management, 249, 106985.

Wang, S., Meng, Q., 2012. Sailing speed optimization for container ships in a container shipping network. Transportation Research Part E: Logistics and Transportation Review, 48(3), 701–714.

Wang, S., Meng, Q., Sun, Z., 2013. Container routing in liner shipping. Transportation Research Part E: Logistics and Transportation Review, 49(1), 1–7.

Wang, T., Meng, Q., Wang, S., Tan, Z., 2013. Risk management in liner ship fleet deployment: A joint chance constrained programming model. Transportation Research Part E: Logistics and Transportation Review, 60, 1–12.

Wang, K., Fu, X., Luo, M., 2015. Modeling the impacts of alternative emission trading schemes on international shipping. Transportation Research Part A: Policy and Practice, 77, 35–49.

Wang, T., Wang, X., Meng, Q., 2018. Joint berth allocation and quay crane assignment under different carbon taxation policies. Transportation Research Part B: Methodological, 117, 18–36.

Wang, S., Zhuge, D., Zhen, L., Lee, C.Y., 2021. Liner shipping service planning under sulfur emission regulations. Transportation Science, 55(2), 491–509.

Wang, S., Qi, J., Laporte, G., 2022. Governmental subsidy plan modeling and optimization for liquefied natural gas as fuel for maritime transportation. Transportation Research Part B: Methodological, 155, 304–321.

Wang, H, Liu, Y., Wang, S., Zhen, L., 2023. Optimal ship deployment and sailing speed under alternative fuels. Journal of Marine Science and Engineering, 11(9), 1809.

Wang, H., Yan, R., Au, M.H., Wang, S., Jin, Y.J., 2023. Federated learning for green shipping optimization and management. Advanced Engineering Informatics, 56, 101994.

Wang, Y., Wang, S., 2021. Deploying, scheduling, and sequencing heterogeneous vessels in a liner container shipping route. Transportation Research Part E: Logistics and Transportation Review, 151, 102365.

Winnes, H., Fridell, E., Ellis, J., Forsman, B., Ramsay, W., Westermark, H., 2020. Aftertreatment of methane slip from marine gas engines. Lighthouse Swedish Maritime Competence Centre.

Wu, M., Li, K.X., Xiao, Y., Yuen, K.F., 2022. Carbon emission trading scheme in the shipping sector: Drivers, challenges, and impacts. Marine Policy, 138, 104989.

Wu, Y., Huang, Y., Wang, H., Zhen, L., 2022. Joint planning of fleet deployment, ship refueling, and speed optimization for dual-fuel ships considering methane slip. Journal of Marine Science and Engineering, 10(11), 1690.

Wu, Y., Wang, S., Zhen, L., Laporte, G., Tan, Z., Wang, K., 2023. How to operate ship fleets under uncertainty. Production and Operations Management, 32(10), 3043–3061.

Wu, Y., Guo, H., Qi, J., Wang, S., Zhen, L., 2024. Ship refueling optimization for dual-fuel ships considering carbon intensity indicator rating limit and uncertain fuel prices. Multimodal Transportation, 3(3), 100138.

Xin, X., Wang, X., Tian, X., Chen, Z., Chen, K., 2019. Green scheduling model of shuttle tanker fleet considering carbon tax and variable speed factor. Journal of Cleaner Production, 234, 1134–1143.

Xue, Y., Lai, K.H., Wang, C., 2024. How to invest decarbonization technology in shipping operations? Evidence from a game-theoretic investigation. Ocean & Coastal Management, 251, 107076.

Zarrinkolah, M.T., Hosseini, V., 2023. Methane slip reduction of conventional dual-fuel natural gas diesel engine using direct fuel injection management and alternative combustion modes. Fuel, 331, 125775.

Zhang, A., Zheng, Z., Teo, C.P., 2022. Schedule reliability in liner shipping timetable design: A convex programming approach. Transportation Research Part B: Methodological, 155, 499–525.

Zhang, G., Xu, J., Zhang, Z., Chen, W., 2024. Optimal decision making and coordination of the shipping logistics service supply chain cooperation mode under the carbon quota and trading mechanism. Ocean & Coastal Management, 255, 107240.

Zhen, L., Li, M., Hu, Z., Lv, W., Zhao, X., 2018. The effects of emission control area regulations on cruise shipping. Transportation Research Part D: Transport and Environment, 62, 47–63.

Zhen, L., Hu, Y., Wang, S., Laporte, G., Wu, Y., 2019. Fleet deployment and demand fulfillment for container shipping liners. Transportation Research Part B: Methodological, 120, 15–32.

Zhen, L., Zhuge, D., Murong, L., Yan, R., Wang, S., 2019. Operation management of green ports and shipping networks: overview and research opportunities. Frontiers of Engineering Management, 6(2), 152–162.

Zhen, L., Wu, Y., Wang, S., Laporte, G., 2020. Green technology adoption for fleet deployment in a shipping network. Transportation Research Part B: Methodological, 139, 388–410.

Zhen, L., Zhuge, D., Zhang, S., Wang, S., Psaraftis, H.N., 2024. Optimizing sulfur emission control areas for shipping. Transportation Science, 5(3), 614–638.

Zheng, J., Gao, Z., Yang, D., Sun, Z., 2015. Network design and capacity exchange for liner alliances with fixed and variable container demands. Transportation Science, 49(4), 886–899.

Zhonggu Logistics. Available at: `https://www.zhonggu56.com`.

Zhou, X., Dai, L., Hu, H., Zhang, M., 2024. An environmental and economic investigation of shipping network configuration considering the maritime emission trading scheme. Ocean & Coastal Management, 249, 107013.

Zhou, Y., Wang, C., 2024. Decisions on ship route, refueling, and sailing speed considering ECA regulation and demand uncertainty. Journal of the Operational Research Society, 1–20.

Zhu, M., Chen, M., Kristal, M., 2018. Modelling the impacts of uncertain carbon tax policy on maritime fleet mix strategy and carbon mitigation. Transport, 33(3), 707–717.

Zhu, M., Shen, S., Shi, W., 2023. Carbon emission allowance allocation based on a bi-level multi-objective model in maritime shipping. Ocean & Coastal Management, 241, 106665.

Zhuge, D., Wang, S., Wang, D.Z., 2021. A joint liner ship path, speed and deployment problem under emission reduction measures. Transportation Research Part B: Methodological, 144, 155–173.